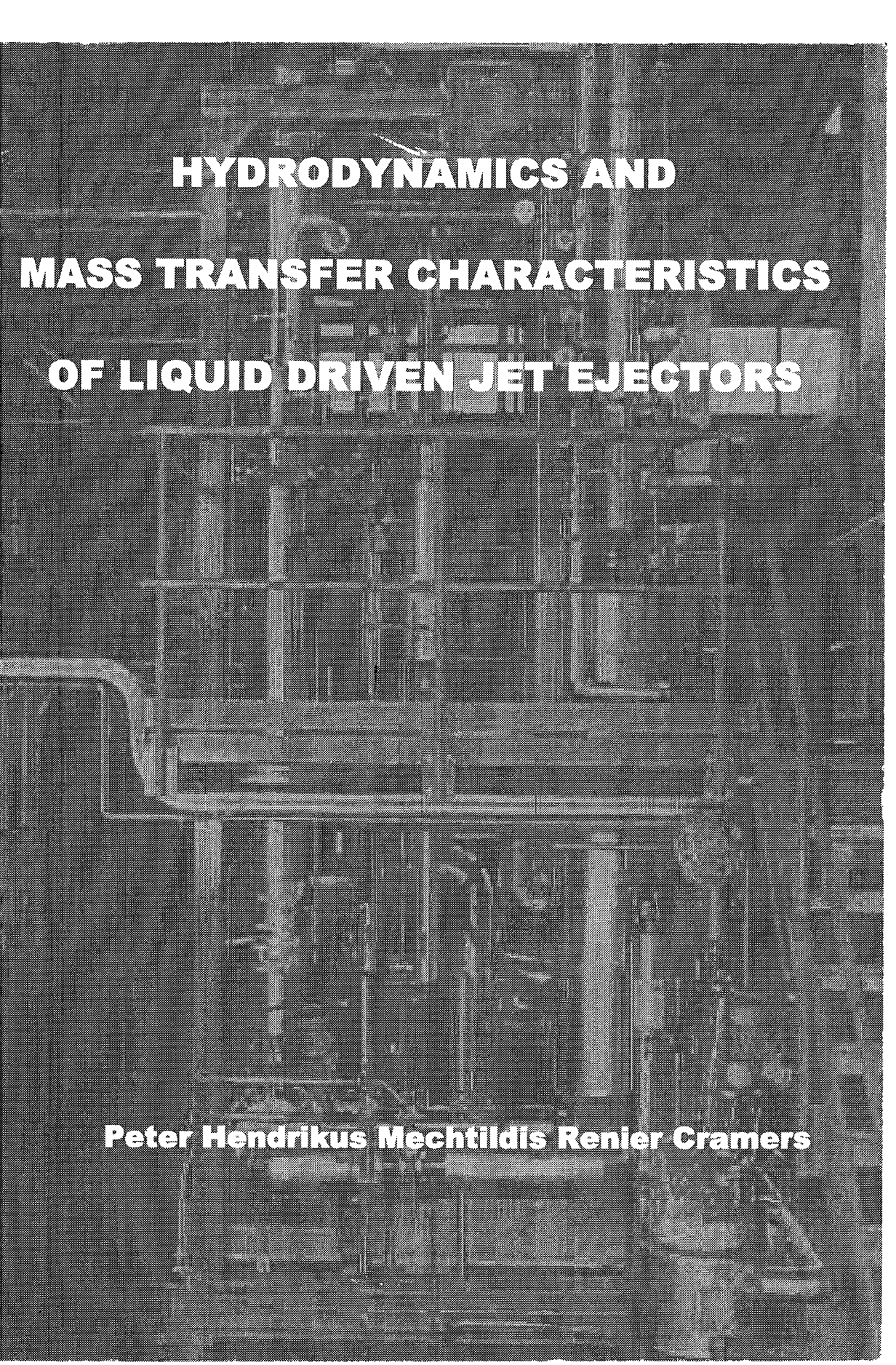
HYDRODYNAMICS AND
MASS TRANSFER CHARACTERISTICS
OF LIQUID DRIVEN JET EJECTORS
Peter Hendrikus Mechtildis Renier Cramers

Promotoren : Prof. dr. ir. L.P.B.M. Janssen
Prof. dr. ir. A.A.C.M. Beenackers ✞

Beoordelingscommissie: Prof. dr. J.A. Moulijn
Prof. dr. ir. G. F. Versteeg
Prof. ir. M. W. M. Boesten

The author is indebted to Davy Process Technology (Switzerland) AG (former Buss AG), Pratteln, Switzerland and DSM Research, Geleen, The Netherlands for financially supporting this work.

aan mijn kinderen Stan & Mitch

Summary

In many chemical processes, requiring gas-liquid- (solid) reactors, gas-liquid interfacial mass transfer frequently limits the overall production rate. High shear rates induced by appropriate disperser configurations can enhance mass transfer by generating very small bubbles. Therefore, the efficient dispersion of gases is of considerable importance in many water treatments, petrochemical, biochemical, pharmaceutical and fine chemical and other chemical engineering processes.

The most frequently used gas-liquid contactors are bubble columns, mechanically agitated reactors and trickle bed reactors. During the last decades there has been an increased interest in the development of more efficient and compact gas-liquid contactors (process intensification). In order to improve the mass transfer rates within bubble columns, special internals were proposed such as baffles, perforated screen plates, motionless mixers and various types of gas distributors. The most common used gas distributors are: spargers, perforated plates and porous plates. Recently, various types of venturi's and/or gas-liquid ejectors were proposed as gas distributors. These special types of gas distributors induce very high shear rates, thereby generating very small bubbles and hence improving the gas-liquid interfacial mass transfer rate of the entire system.

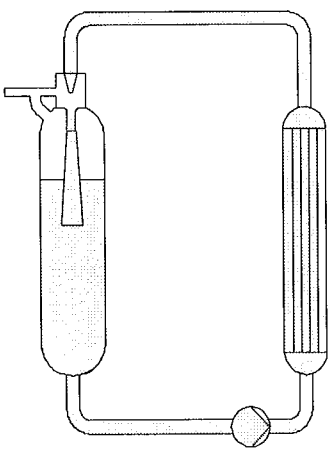

Schematic representation of a commercial Buss Loop Reactor (BLR).

Gas-liquid contactors with ejector type of gas distributors (Loop-Venturi Reactors) have been recommended for processes where gas-liquid interfacial mass transfer is the rate controlling step of the process (Leuteritz, 1976; Nagel et al., 1976; Otake et al., 1981; Ogawa et al., 1983; Radharkrishnan and Mitra, 1984; Rylek and Zahradnik, 1984; Zahradnik et al., 1981; Dutta and Raghavan, 1987; Dirix and van der Wiele, 1990 and Cramers et al., 1992). The most versatile design of a commercial Loop Reactor (BLR) is

claimed to be that developed by Buss AG in Pratteln, Switzerland (Leuteritz, 1976; Malone, 1982). A schematic representation of the BLR is shown in the diagram above.

The Buss Loop Reactor consists of an autoclave, an external forced liquid loop (including centrifugal pump and heat exchanger) and a mixer (gas-liquid ejector) fitted at the top of the autoclave. The reaction mixture, including heterogeneous catalyst, is continuously pumped from the bottom of the autoclave, through the heat exchanger, back into the top of the autoclave through the ejector. In this ejector, through which the reaction suspension travels at a high velocity, the gas is sucked in from the headspace of the autoclave. A zone of high shear mixing is created in the ejector locally, resulting in the formation of small gas bubbles.
The major amount of gas, which has not reacted, disengages in the reaction autoclave and returns to the headspace of the autoclave, where it is re-entrained again into the reaction mixer. The reactor is simple in design and requires no external compression device for dispersing the gas, since the gas phase is sucked in and dispersed by the ejector.

The liquid, which is pumped continuously from the bottom of the autoclave through the external loop, enters the nozzle of the ejector. Due to the reduced cross-sectional area at the outlet of the nozzle, the liquid stream is accelerated. Due to this acceleration, a high velocity jet discharges from the nozzle into the ejector. This high velocity jet causes entrainment (suction) of gas from the gaseous headspace of the autoclave. Inside the reaction mixer the gas phase is dispersed very finely in an intense turbulent field (the so-called mixing shock zone). Thereafter, both phases flow homogeneously through the diffuser and the remaining volume of the ejector. Due to the high velocity inside the ejector, a two-phase jet discharges from the ejector into the autoclave, where further reaction (and gas-liquid separation) takes place. Nearly all the commercial BLR's are slurry reactors and operate at elevated pressures and temperatures (up to 100 barg and 300 °C, respectively).

For the design and scale-up of gas-liquid ejectors, reliable data are required which describe the gas suction rates and mass transfer characteristics as a function of the gas- and liquid physical properties; geometrical design and process related parameters. However, until now a systematic study concerning the influence of the above-mentioned parameters has not been published yet. Therefore, the main objective of this thesis is to get more physical insight in the mechanisms of gas entrainment and gas dispersion within ejectors. Further, in order to obtain reliable design and scale rules/criteria, relations have to be formulated describing the gas entrainment rate and mass transfer rates of gas-liquid ejectors as a function of the gas- and liquid physical properties, the geometrical design parameters and the operating parameters.

Structure of the thesis

This thesis is mainly focused on the ejector as a stand-alone device. In order to understand the physical phenomena occurring in ejectors, first the gas entrainment mechanism of liquid jets has to be studied. Therefore, Chapter 2 deals with the gas entrainment mechanism and rate of high velocity jets. A review is given of previous experimental and theoretical research. Further, the influence of the gas density on the gas entrainment rate and mechanism is studied both experimentally and theoretically. The results of this chapter give a physical explanation on how the gas entrainment rate and mechanism are influenced by the gas density.

Chapter 3 deals with the gas suction rate of ejectors at elevated pressures and on how changes in the gas density affect the gas suction rate. Further the influence of the operating parameters (like the jet velocity and the gas phase pressure difference) and some geometrical parameters are studied. The influence of the liquid physical properties is discussed theoretically and is validated with data from the literature.

The second part of this thesis deals with the mass transfer characteristics of ejectors. Since commercial loop reactors are operated at elevated pressures, Chapter 4 deals with the influence of the gas density on the bubble stability. A relation from the literature is shown to be valid (Levich, 1962) and could be extended to predict the maximum stable bubble size present in an isotropic turbulent flow field. The extended relation is validated using data from the literature. This relation forms the basis for the mass transfer correlations applied in the following chapters. In Chapter 5, the mass transfer characteristics of ejectors are studied in more detail. The influences of geometrical parameters (like the nozzle and the ejector configuration) are studied experimentally. The influence of the gas density is also considered. In this chapter, design relations are presented for designing ejectors, independent of scale. This chapter indicates that each ejector configuration requires its own characteristic relation and that the mass transfer characteristics of ejectors should be studied in more detail. The final chapter (Chapter 6) of this thesis is concerned with the modelling of the mass transfer characteristics of ejectors and on how the effects of the ejector configuration and of operating parameters can be explained theoretically. A model has been developed, which is tested with experimental data. The results show that the model is able to predict the experimental data qualitatively. The main conclusion is that the ejector has to be considered as a "reactor system" of two reactor units in series and that the local phenomena occurring in the mixing shock region should be studied in much more detail.

Samenvatting

In veel chemische reactoren wordt de omzettingssnelheid (en dus de produktiecapaciteit) bepaald door stofoverdrachtslimiteringen in gas/vloeistof reactoren. "High shear rates" veroorzaakt door efficiente gasverdeelorganen kunnen gas/vloeistof stofoverdrachts processen versnellen, doordat zij kleine gasbellen creëren. Daarom is het van groot belang dat in industriële processen zoals in de afvalwaterzuivering, petrochemie, biochemie, pharma en fijnchemie een efficiente gasdispersie wordt gecreëerd om deze stofoverdrachtslimiteringen tot een minimum te beperken.
Bellenzuilen en mechanisch geroerde reactoren zijn tot heden toe de meest bekende en toegepaste batch gas/vloeistof reactoren in de industrie. Gedurende de laatste jaren is er vanuit de chemische industrie groeiende belangstelling getoond in het ontwikkelen van meer efficiente/kompactere gas/vloeistof reactoren (process intensificatie).
Om de stofoverdrachts karakteristieken in bellenzuilen te verbeteren, zijn speciale internals ontwikkeld zoals baffles, geperforeerde platen, statische mengers en vele andere typen van gasverdeelorganen. De meest gebruikte gasverdeelorganen zijn gasverdeelringen en geperforeerde of poreuse platen. Gedurende de laatste jaren zijn verschillende typen van venturies of gas/vloeistof ejecteurs voorgesteld als gasverdeelorgaan. Deze speciale gasverdeelorganen veroorzaken lokaal extreem hoge "shear rates" en creëren daardoor zeer kleine gasbellen en dus een duidelijke verbetering van het gas-vloeistof contact oppervlak van het gehele systeem.

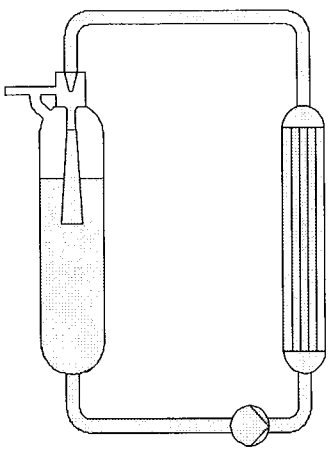

Schematische weergave van een commerciele Buss Loop Reactor (BLR).

Zoals reeds eerder is vermeld zijn bellenzuilen en mechanisch geroerde reactoren zijn meest bekend, maar er is een groeiende belangstelling voor reactoren met omloopsystemen en voor gasfase gedispergering met behulp van gas/vloeistof ejecteurs wanneer

de omzettingssnelheid van een reactie wordt bepaald door de grootte van het gas/vloeistof contactoppervlak (Leuteritz, 1976; Nagel et al., 1976; Otake et al., 1981; Ogawa et al., 1983; Radharkrishnan en Mitra, 1984; Rylek en Zahradnik, 1984; Zahradnik et al., 1981; Dutta en Raghavan, 1987; Dirix en van der Wiele, 1990 en Cramers et al., 1992).
De meest bekende commerciële venturiereactor is ontwikkeld door de firma Buss AG in Pratteln, Zwitserland (Leuteritz, 1976; Malone, 1982). Een schematische voorstelling van deze door Leuteritz voorgestelde venturiereactor is getoond in Figuur 1.

De Buss-Loop-Reaktor (BLR) bestaat uit een reactievat in de vorm van een slanke kolom met een extern vloeistofcirculatiessysteem, waarin achtereenvolgens een circulatie pomp, een warmtewisselaar en een gas/vloeistof ejecteur zijn opgenomen. In de ejecteur wordt de door de pomp in de vloeistofstraal geïntroduceerde kinetische energie benut om de gasfase uit het reactievat aan te zuigen en te dispergeren. In de ejecteur wordt lokaal veel energie gedissipeert (de zogenaamde mengschok), welke resulteert in het ontstaan van zeer kleine gasbellen. Na deze mengschok stromen het gedispergeerde gas en vloeistof met een hoge snelheid door het resterende volume van de ejecteur en wordt vervolgens de tweefasen dispersie met hoge snelheid in het reactievat geinjecteert, waar de verdere reactie (en gas/vloeistof separering) plaats vindt. Het reactiegas, dat niet heeft gereageerd, wordt gescheiden in het reactievat en gaat terug naar de gasfase van het reactievat, waar het weer door de gas/vloeistof ejecteur wordt aangezogen en gedispergeerd.
Integenstelling tot bellenzuilen en geroerde reactoren is de venturiereactor eenvoudig in ontwerp en benodigt de BLR geen extra gas compressor om het gas te dispergeren, omdat de gas fase weer intern aangezogen wordt door de ejecteur. Bijna alle industiële BLR's welke worden toegepast in de chemische industrie zijn slurry-fase reactoren met reactor volumina tot 100 m^3 en worden meestal bedreven onder verhoogde druk (tot 100 barg) en bij hogere temperaturen (tot 300 °C).

Voor het ontwerp en opschaling van gas/vloeistof ejecteurs zijn betrouwbare data benodigd om de hoeveelheid aangezogen gas en stofoverdrachtskarakteristieken van ejecteurs correct te beshrijven. Helaas heeft er tot heden geen systematisch onderzoek plaats gevonden welke de invloed van bovengenoemde parameters beschrijft en is de voornaamste doelstelling van dit promotieonderzoek ook om meer fysisch inzicht te verkrijgen in het mechanisme van gasaanzuiging en gasdispersie welke plaats vinden in de ejecteur. Om betrouwbare opschalings regels/criteria te verkrijgen moeten er formules/correlaties worden gedefinieerd welke de gasaanzuigsnelheid en stofoverdrachtskarakteristieken van gas/vloeistof ejecteurs beschrijven als funktie van de fysische eigenschappen van de gas- en vloeistoffase, geometrische ontwerpregels en proces parameters.

Opbouw van het proefschrift.

Dit proefschrift is voornamelijk gericht op gas/vloeistof ejecteurs als alleenstaand apparaat. Om de lokale fenomenen te begrijpen die plaats vinden in ejecteurs moet allereerst het mechanisme worden bestudeerd hoe vloeistofstralen gas meesleuren en dispergeren. Daarom wordt in het tweede hoofdstuk een literatuuroverzicht gegeven van het mechanisme van gas transport en wordt vervolgens de invloed van de gasdichtheid op het mechanisme en de hoeveelheid meegesleurd gas experimenteel geverificiëerd en verklaard. In hoodstuk 3 wordt behandeld hoeveel gas door ejecteurs wordt aangezogen en welk effect de gasdichtheid heeft of de volumetrisch hoveelheid aangezogen gas. Verder worden de bedrijfsparameters (zoals vloeistofstraal snelheid, drukverschal van de gasfase over de ejecteur) en andere geometrische ontwerp parameters bestudeerd. De invloed van de fysische vloeistofeigenschappen wordt theoretisch behandeld aan de hand van literatuur data.

In het tweede gedeelte van dit proefschrift worden de stofoverdrachts karakteristieken van gas/vloeistof ejecteurs behandeld. Door het feit dat industriële venturiereactoren meestal worden bedreven onder verhoogde druk, behandelt hoofdstuk 4 de invloed van de gasdichtheid (drukinvloed) op belgrootte and instabiliteit. M.b.v. Levich's theoriën (1962) en enige modificaties is een theoretische correlatie ontwikkeld die de maximaal stabiele belgrootte beschrijft in een isotroop turbulent veld. Deze correlatie is gevalideerd met behulp van literatuur data. Deze nieuwe correlatie is de basis voor de stofoverdrachts correlaties zoals gebruikt in de verdere hoofdstukken. De stofoverdrachts karakteristieken van ejecteurs wordt in meer detail beschreven in hoofdstuk 5. De invloed van de geometrische ontwerpparameters (zoals nozzle diameter en de ejecteurconfiguratie) op de stofoverdrachtsparameters wordt experimenteel gemeten. De invloed van de gasdischtheid wordt ook experimenteel geverificeerd. In hoofdstuk 5 worden relaties gedefineerd voor het ontwerpen van gas/vloeistof ejecteurs, onafhankelijk van de schaalgrootte. Verder wordt aangetoond dat iedere ejecteurconfiguratie zijn eigen karakteristieke correlatie behoeft en dat de lokale stofoverdrachtsfenomenen, welke plaats vinden in gas/vloeistof ejecteurs, nog meer in detail bestudeerd moeten worden. In het laatste hoofdstuk (hoofdstuk 6) van dit proefschrift wordt getracht de stofoverdrachts-karakteristieken van ejecteurs te modelleren en hoe de invloed van de ejecteurgeometrie en de bedrijfsparameters theoretisch kunnen worden beschreven en verklaard. Een theoretisch model is ontwikkelt welke wordt getest m.b.v. experimentele data. Het theoretische model beschrijft de experimentele data kwalitatief zeer goed, maar zolang de "echte vloeistofstraal diameter" op het moment dat de vloeistofstraal in de mengzone "penetreert" niet bekend is, is het bijna onmogelijk om kwantitatieve berekeningen uit te voeren. Om ejecteurs te modelleren /correleren moeten de lokale stofoverdrachtskarakteristieken van een gas/vloeistof ejecteur

beschreven worden als twee reactoren in serie en zullen de lokale fenomenen die optreden op het moment dat de vloeistofstraal in de mengzone penetreert verder bestudeerd moeten worden ten aanzien van een verfijning van het model.

Publications

1. Cramers P.H.M.R., van Dierendonck L.L. and Beenackers A.A.C.M. (1992), ***Influence of the gas density on the gas entrainment rate and gas hold-up in loop venturi reactors***, Chem. Eng. Sci., 47, 2251-2256.

2. Cramers P.H.M.R., Beenackers A.A.C.M. and van Dierendonck L.L. (1992), ***Hydrodynamics and mass transfer characteristics of a loop venturi reactor with a down-flow jet ejector***,Chem. Eng. Sci., 47, 3557-3564.

3. Cramers P.H.M.R., Leuteritz G., van Dierendonck L.L. and Beenackers A.A.C.M. (1993), ***Hydrodynamics and local mass transfer characteristics of gas-liquid ejectors***, Chem. Eng. J., 53, 67-73.

4. Cramers P.H.M.R., van Dierendonck L.L. and Beenackers A.A.C.M. (1993), ***Venturireactor dispergeert gas efficiënter***, Poly Technisch tijdschrift, 2, 42-45.

5. Cramers P.H.M.R,.Beenackers A.A.C.M. and van Dierendonck L.L. (1994), ***Process Intensification with Buss Loop Reactors***, Catalysis in Multiphase Reactors European Symposium, Lyon, France, 7-9 December, Paper C-III-4.

6. Cramers P.H.M.R., Beenackers A.A.C.M. and Dierendonck van L.L. (1996), ***Prediction of the mass transfer characteristics of gas-liquid ejectors***, The 5th World Congress of Chemical Engineering, San Diego, USA, July 14-18, Vol. 3, 202-207.

7. Cramers P.H.M.R and Reichelt K. (1997), ***The "Advanced" Buss Loop Reactor Technology***, Achema 1997, Frankfurt, Germany

8. Cramers P.H.M.R and Reichelt K. (2000), ***Continuous Operation using High Performance Slurry Phase Reactors***, Achema 2000, Frankfurt, Germany

9. Cramers P.H.M.R. and Beenackers A.A.C.M. (2001), ***Influence of the ejector configuration, scale and the gas density on the mass transfer characteristics of gas-liquid ejectors***, Chem. Eng. J., 3770, 1-11

10. Cramers P. and Selinger C. (2002) ***Advanced Hydrogenation Technology for Fine Chemical and Pharmaceutical Applications***, Pharma Chem June 2002

11. Cramers P.H.M.R. (2003), ***High Performance Gas-Liquid Ejector Technology,*** Achema 2003, Frankfurt, Germany

12. Cramers P., Juvet J. (2003), ***High Performance Gas-Liquid Ejector Technology for intensified Oxidation Processes,*** 5th International Conference on Process Intensification for the Chemical Industry, Maastricht, The Netherlands, 13-15 October

CONTENTS

Chapter 1
General introduction

1.1. INTRODUCTION

In many chemical processes, requiring gas-liquid- (solid) reactors, gas-liquid interfacial mass transfer frequently limits the overall production rate. High shear rates induced by appropriate disperser configurations can enhance mass transfer by generating very small bubbles. Therefore, the efficient dispersion of gases is of considerable importance in many water treatment, biochemical and chemical engineering processes.

Gas-liquid contactors with ejector type of gas distributors (Buss Loop Reactors) have been recommended for processes where gas-liquid interfacial mass transfer is the rate-controlling step of the process (Leuteritz, 1976; Nagel et al., 1976; Otake et al., 1981; Ogawa et al., 1983; Radharkrishnan and Mitra, 1984; Rylek and Zahradnik, 1984; Zahradnik et al., 1982; Dutta and Raghavan, 1987; Dirix and van der Wiele, 1990 and Cramers et al., 1992). The most versatile design of a commercial Loop Reactor (BLR) is claimed to be that developed by Buss AG in Pratteln, Switzerland (Leuteritz, 1976; Malone, 1982).

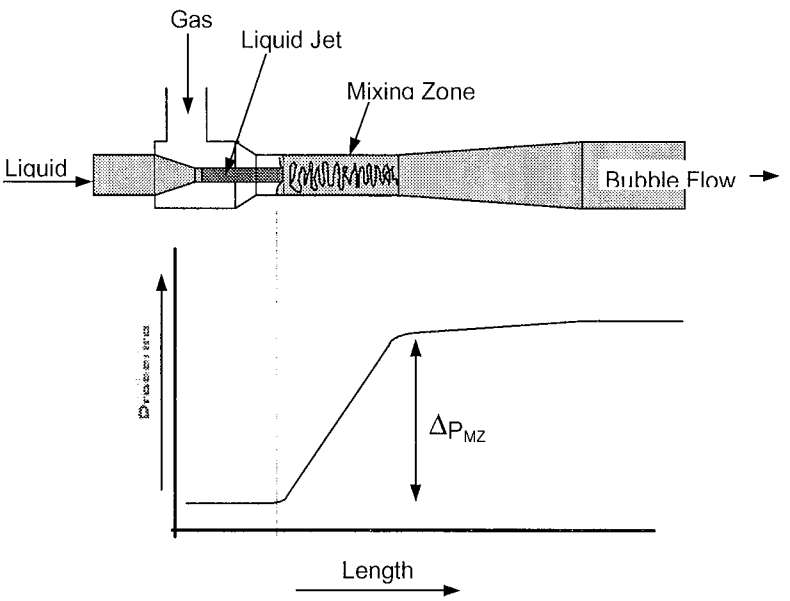

Fig. 1.1 Schematic representation of a gas-liquid ejector.

The operating principle of a gas-liquid ejector is shown in Fig. 1.1. The liquid, which is pumped continuously from the bottom of the autoclave through the external loop, enters

the nozzle of the ejector. Due to the reduced cross-sectional area at the outlet of the nozzle, the liquid stream is accelerated. Due to this acceleration, a high velocity jet discharges from the nozzle into the ejector. This high velocity jet causes entrainment (suction) of gas from the gaseous headspace of the autoclave. Inside the reaction mixer the gas phase is dispersed very finely in an intense turbulent field (the so-called mixing shock zone). Thereafter, both phases flow homogeneously through the diffuser and the remaining volume of the ejector.

1.2. STATE OF THE CURRENT KNOWLEDGE

Ejectors have received always a great deal of interest from researchers. They have advantages in many processes including gas suction and gas compression. Most investigations have been focused on the prediction of the gas compression ratio as function of the gas suction rate for a given set of design and operating parameters.

In the past twenty years, interest has focused increasingly on their mass transfer characteristics and on how changes in the ejector configuration influence the mass transfer characteristics of the entire reactor system. Whilst there is some common ground between many of the investigations, there remain also substantial inconsistencies. For example, almost no researcher worked with exactly the same ejector and vessel configuration. The operating parameters often are different (such as the gas phase pressure difference across the ejector and the gas-liquid flow ratio) whereas the experimental methods vary.

The precise modes of operation of ejectors investigated in the literature can be subdivided into three main categories:

i) Ejectors as gas entrainment/compression devices,
ii) Ejectors in Venturi reactors
iii) Ejectors as stand-alone device

Even within each category, many of the investigations are not comparable, making it difficult to present a unified picture of the state of the current knowledge of gas-liquid ejectors and hence of venturi reactors.

1.2.1 Ejectors as gas entrainment/compression devices,

Theoretical principles for a rational design of ejectors as evacuators have been given by Kastenek et al. (1950), Engel (1963) and Cunningham (1974). The relationships developed by them for the operating characteristics of jet pumps were derived from momentum and energy balance equations. This approach has been used by many authors to develop

expressions for relating gas suction rates of ejectors as function of the operating parameters. However, this type of analysis is only valid for the homogeneous bubble flow regime, which exists at high-pressure differentials across the ejector only, i.e. at very low gas to liquid flow ratios. An empirical method for correlating gas suction rates for all flow regimes, based on important ejector dimensions and operating parameters was first developed by Davies and Mitra (1966) and has been applied by several investigators since. However, this approach gives no insight in the physical phenomena occurring in ejectors and in how changes in physical properties and/or ejector configuration affects the gas suction rates.

So far, nearly all investigations have been carried out at atmospheric conditions, despite that most industrial reactors are operated at elevated pressures (up to 100 barg). Data on the influence of gas properties on the ejector performance are scarce. Three studies were devoted to the influence of the gas physical properties on the gas suction rates of ejectors.
Jekat (1975) studied the performance of jet-loop reactors at elevated pressures (system water/nitrogen up to 100 barg). In his thesis he mentions that the gas suction rate of the ejector is influenced by the reactor pressure, i.e. up to pressures of 60 barg the gas suction rate of the ejector increases whilst at higher pressures the suction rate decreases again. However, data concerning the pressure difference across the ejector were not disclosed. His experimental results show that the reactor pressure has a significant effect on the gas suction rate. A physical explanation for the observed phenomenon was not given.
Also Henzler (1981) takes into account the influence of the gas physical properties on the suction rate of ejectors. The gases used were helium, air and helium-air mixtures at ambient conditions. From the results of Henzler it is concluded that the gas molecular weight has an influence on the gas suction rates of ejectors. i.e. with increasing gas molecular weight more gas is entrained. Henzler (1981) developed design relations, which relate the gas suction rates to some geometrical and operating parameters of the ejector.
Lastly, Cramers et al. (1992) studied the influence of the gas density on the venturi reactor performance in an atmospheric column using various gases with different gas molecular weights. From his results it can be concluded that the gas density has a twofold effect on the venturi reactor performance, i.e. the gas suction rate of the ejector and the gas fraction in the main holding vessel both increase with increasing gas density. According to Cramers et al. (1992), the gas density affects the jet stability and hence the gas entrainment mechanism of the high velocity jets discharging through the ejector.

From the above it has to be concluded that the physical properties of the gas phase have a remarkable effect on both the ejector and the venturi reactor performance. However, a systematic study concerning the influence of the gas physical properties on the operating

characteristics of ejectors (and venturi reactors) has not been published yet.

1.2.2 Ejectors in Loop Reactors

Investigations of the hydrodynamic features and the mass transfer characteristics (like the specific gas-liquid interfacial area, a, and the volumetric mass transfer coefficient, $k_L a$) of venturi reactors with liquid driven ejectors have been reported by various authors. Most of the available literature concerns up flow systems where the ejector is located at the bottom of the vessel (Radharkrishnan and Mitra, 1984; Rylek and Zahradnik, 1984; Ogawa et al. 1983; Otake et al. 1981 and Zahradnik et al., 1982). Down flow reactors have been described by Dutta and Raghavan (1987), Van Dierendonck at al. (1988), Dirix and van de Wiele (1990) and Cramers et al. (1992). Nearly all of above-mentioned studies (except the last two) considered the venturi systems as a single unit ("black-box"). The mass transfer characteristics of BLR's were correlated in terms of power-per unit reactor volume as shown in Table 1.1.

A comparison of these literature data is difficult, since the volume averaged mass transfer characteristics of the entire system are expected to vary with:

- The gas flow rate
- The position of the ejector in the reaction vessel
- Volume ratio of the ejector and the reaction vessel,
- The ejector and vessel configuration/size
- Scale, etc.

The most detailed investigations concerning the mass transfer characteristics of venturi-reactors have been reported by Cramers et al. (1992) and Dirix and van der Wiele (1990). In these studies the ejector and the reaction vessel were studied separately and marked differences in their behaviour were found. These studies indicated that the mass transfer characteristics of ejectors are nearly two orders of magnitude higher than those of the reaction vessel. The proposed mass transfer relations are also summarised in Table 1.1.
In discussing the mass transfer characteristics of ejectors it is absolutely necessary to differentiate between coalescence inhibiting and promoting media. In coalescence inhibiting media the highest possible rate of local energy dissipation should be applied to realize the highest degree of gas phase dispersion. This dispersion is preserved to a large extent even if the bubbles enter regions where low rates of local energy dissipation rates prevail. Cramers et al. (1992) measured specific interfacial areas as high as 40'000 - 70'000 m^2/m^3 locally in the ejector using a coalescence inhibited system with the cobalt catalysed sulphite oxidation as a model reaction. In the reaction vessel (which is the region with local lower rates of energy dissipation) the interfacial areas were still 2'500-3'500

m^2/m^3. On the other hand, the improvement of the gas phase dispersion due to the ejector performance is less important in coalescence promoting systems. Here, the equilibrium bubble size established (due to bubble coalescence and break-up processes) is always larger than the size of the primary bubbles dispersed in the ejector section.

Dirix and van der Wiele (1990) measured the volumetric mass transfer coefficients of the ejector and reaction vessel separately using the desorption of oxygen from water (coalescence promoting system) as the model system. The k_La-values in the ejector were of the order of 1-3 s^{-1}, whereas the measured k_La-values of the reaction vessel were comparable with those of conventional bubble columns, i.e. 0.01-0.07 s^{-1}.

The studies of Dirix and van der Wiele (1990) and Cramers et al. (1992) showed that it is necessary to consider the ejector and the reaction vessel as two separate units in series, rather than lumping the ejector characteristics with those of the whole system. The benefits of the ejector are not restricted to a larger rate of mass transfer in the ejector section, but include also the generation of smaller bubbles, which are injected into the reaction vessel (particularly for coalescence inhibited systems).

1.2.3 Ejectors as stand-alone device

Only a few researchers treated ejectors as stand alone devices in studying their mass transfer performance. Most investigators have used ejectors in combination with a reaction vessel. To our knowledge there are only three investigations in the open literature that studied the hydrodynamics and mass transfer characteristics of two-phase ejectors separately (Dirix and Van der Wiele, 1990; Changfeng et al. 1991 and Cramers et al., 1992).

Typical rates of energy dissipation within an ejector fall in the range between 100-1000 W/kg. The power supplied is partly used for bubble break-up, whilst the remaining part is lost due to friction losses and gas compression. The power dissipation rate in ejectors is nearly two or three orders of magnitude higher in comparison to the energy dissipation rate in mechanically agitated vessels and bubble columns. Applying the above mentioned values of the energy dissipation rate to the correlation's in Table 1.1, yields k_La values between 2 and 16 s^{-1}, locally within ejectors.

The flow patterns (hydrodynamics) in an ejector mixing tube were studied in detail by Otake et al. (1981), which used an up-flow straight tube ejector to disperse gas into a liquid. Four flow regimes were observed, i.e. slug flow, annular flow, bubble flow and jet flow. Other researcher's (Dutta and Raghavan, 1987; Dirix and Van der Wiele, 1990 and Cramers et al, 1992) observed the bubble-jet flow transition also in down-flow ejectors,

though there was disagreement over the gas-liquid flow ratio at which the transition to jet flow occurred.

Table 1: Mass transfer relations for ejectors and LVR's

Authors	Mass transfer correlation	Ejector system
Changfeng et al. (1991)	$k_La=0.72\cdot \in^{0.492}\cdot \varepsilon_G^{0.88}$ $a=918\cdot \in^{0.372}\cdot \varepsilon_G^{0.74}$ $d_S=0.00652\cdot \in^{-0.372}\cdot \varepsilon_G^{0.261}$	Down-flow Ejector
Dirix and van de Wiele (1990)	$k_La=0.54\cdot \in^{0.66}\cdot \varepsilon_G^{0.66}\cdot \left(\frac{d_N}{d_D}\right)^{0.66}$ $k_La=0.085\cdot \in^{0.66}\cdot \left(\frac{d_N}{d_M}\right)^{0.66}$	Down-flow ejector (bubble flow) Down flow ejector (Jet flow)
Cramers et al. (1992)	$a=19500\cdot \in^{0.4}\cdot \varepsilon_G\cdot (1-\varepsilon_G)^{0.4}$	Down-flow ejector (Bubble flow)
Dierendonck et al. (1982)	$k_La=0.3\cdot \in^{0.9}$	Down-flow ejector + Separation vessel
Ogawa et al. (1983)	$k_La=0.084\cdot (Fr)^{1.0}\cdot (U_G)^{0.6}$	Down-flow ejector + Separation vessel
Dutta & Raghavan (1987)	$k_La=0.044\cdot \in^{0.76}$	Down-flow ejector + Separation vessel
Wong et al. (1985)	$k_La=3.13\cdot 10^{-6}\cdot (U_L)^{1.6}\cdot (U_G)^{1.05}$	Down-flow ejector + mini-separator

Probably, the ejector configuration influences the flow transition point and hence the mass transfer characteristics of ejectors. Dirix and Van der Wiele (1990) found that the flow regime has a significant effect on k_La indeed. In the so-called bubble flow regime k_La is proportional to the gas flow rate, whilst in the jet flow regime k_La turned out to be independent of the amount of gas sucked in by the ejector. Changfeng et al. (1991) observed no change in flow regime at all.

Another point of discussion is the modelling of ejectors. In all studies it has been assumed that the ejector can be modelled as one single unit. In reality, the ejector consists of two different hydrodynamic zones with distinct properties, as shown in Fig. 1.1. This figure shows the change in pressure across the ejector. There exists a zone were the high velocity jet discharges into the mixing zone, which is accompanied by a sudden pressure

build up ("mixing shock"). After this mixing zone both phases flow homogeneously through the remaining part of the ejector. It is expected that this difference in hydrodynamics of the two zones will cause different local mass transfer characteristics in both regions. However, there are no literature data that confirm the above-mentioned statements. Given the variety of ejector configurations used, it is not surprising that the proposed mass transfer correlations do not agree and predict considerably different values.

1.3 OBJECTIVES OF THE THESIS

For the design and scale-up of gas-liquid ejectors, reliable data are required which describe the gas suction rates and mass transfer characteristics as a function of the gas- and liquid physical properties; geometrical design and process related parameters. However, until now a systematic study concerning the influence of the above-mentioned parameters has not been published yet.

Therefore, the main objective of this thesis is to get more physical insight in the mechanisms of gas entrainment and gas dispersion within ejectors. Further, in order to obtain reliable design and scale rules/criteria, relations have to be formulated describing the gas entrainment rate and mass transfer rates of gas-liquid ejectors as a function of the gas- and liquid physical properties, the geometrical design parameters and the operating parameters.

NOTATION

a	specific gas/liquid interfacial area	m^2/m^3
d_D	draft tube diameter	m
d_M	mixing tube diameter	m
d_N	nozzle diameter	m
d_S	Sauter bubble diameter	m
Fr	Froude-number	-
k_La	volumetric mass transfer coefficient	1/s
U_G	superficial gas velocity	m/s
U_L	superficial liquid velocity	m/s
ε_G	gas fraction	-
ρ_G	gas density	kg/m^3
ρ_L	liquid density	kg/m^3
ϵ	energy dissipation rate	W/kg

Chapter 2
Gas entrainment by high velocity plunging liquid jets

SUMMARY

The influence of the physical gas properties (and operating parameters) on the gas entrainment rate and mechanism of plunging liquid jets discharging through a straigth tube are reported. Both, from literature data and present results it is demonstrated that the rate of gas entrainment of plunging jets consists of two components, i.e. gas trapped within the jet envelope at the plunging point and gas dragged below the liquid surface by the thin gas film between the liquid jet and the receiving liquid. The experimental results show that the gas entrainment rate and mechanism of plunging jets is influenced by the physical properties of the gas phase. The overall rate of gas entrainment increases when higher density gases are used. The influence of the gas density on the entrainment mechanism can be very well explained from a Kelvin-Helmholtz instability analysis, i.e. from the influence of the aerodynamic forces on the jet stability.

2.1 INTRODUCTION

It is well known, that a liquid jet discharging through a gaseous atmosphere entrains a considerable amount of gas into the receiving liquid. A review concerning the gas entrainment rate and mechanism of plunging liquid jets has been published by Bin (1988). The results of Bin clearly demonstrate that the gas entrainment rate of plunging liquid jets is influenced by the jet velocity, the jet length, the liquid physical properties and especially the nozzle design from which the jet discharges. Bin (1988) stated that the physical gas properties have no influence on the entrainment rate of high velocity jets.

However, Cramers et al. (1992) demonstrated that the gas suction rates of liquid driven ejectors are strongly influenced by the gas physical properties. The observed phenomenon could be explained by the influence of the gas density on the gas entrainment mechanism of high velocity jets. However, an explenation for the observed phenomenon was not given. In this chapter, the influence of the gas physical properties (and jet operating parameters) on the gas entrainment rate and mechanism is studied in more detail, both experimentally and theoretically.

2.2 LITERATURE REVIEW

2.2.1 Mechanism of gas entrainment

The studies and observations of many authors (see Bin, 1988) show that the gas entrainment mechanism is a very complex process. However, one can conclude that the gas entrainment rate is largely determined by the characteristics of the discharging jet. In addition to the jet diameter and velocity, the entrainment rate is largely controlled by the surface structure (read roughness) of the jet.

For jets having a smooth surface (laminar jets), entrainment occurs in the form of a thin gas film which is dragged below the receiving liquid (Lin and Donnely, 1966). For rough turbulent jets, Mc Carthy (1972) suggested that the volumetric gas entrainment rate Q_G is equivalent to the quantity of gas which is trapped within the jet indulations as it plunges into the receiving liquid. A scheme of this so-called "jet envelope" mechanism is shown in Fig. 2.1. The amount of gas entrained by this mechanism can quantitatively be written as

$$Q_{G,E} = \frac{\pi}{4} \cdot \left(d_J^2 - d_N^2\right) \cdot U_J = Q_L \cdot \left(\left(\frac{d_J}{d_N}\right)^2 - 1\right) \tag{2.1}$$

where Q_L is the volumetric liquid flow rate, d_J and d_N are respectively the jet diameter at distance z (as shown in Fig. 2.1) and the nozzle diameter and U_J is the jet velocity at the

nozzle exit. Eq. (2.1) shows that the actual jet width at the plunging point has a significant influence on the gas entrainment rate, i.e. the larger its change, the more gas is entrained.

In addition to the gas entrapped within the jet envelope, a quantity of gas is also entrained in the form of a thin film layer adjacent to the free surface of the plunging jet (McKeogh et al (1981); and Evans (1990)). A schematic representation of this mechanism is shown in Fig. 2.2.

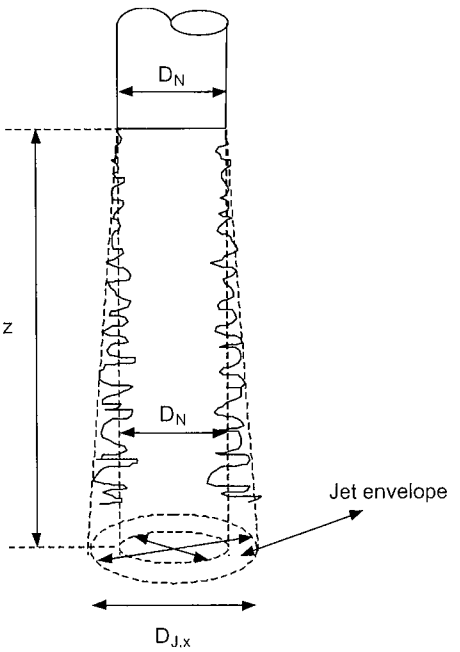

Fig. 2.1 Scheme of the jet envelope mechanism (McCarthy, 1972)

The plunging jet causes a depression in the receiving liquid and introduces a circulating flow there, whose streamlines are directed towards the jet. Fig. 2.2 shows the formation of the so-called "induction trumpet". It is through the induction trumpet that entrainment of gas also occurs. The curved opening at the top of the induction trumpet channels the incident developed gas boundary layer into the thin film of gas. It is important to mention at this stage that the quantity of gas inside the entrained gas film is not equal to the volumetric flux of gas inside the boundary layer being dragged along by the free jet surface (as assumed by van de Sande (1974)), as illustrated in Fig. 2.2 The remaining amount of gas travels radially out along the surface of the receiving liquid. Further downstream, the gas film is broken up into a succession of bubbles by instability waves on its surface. The film wise rate of entrainment is a function of the velocity profile of the gas inside the film and of the gas film thickness.

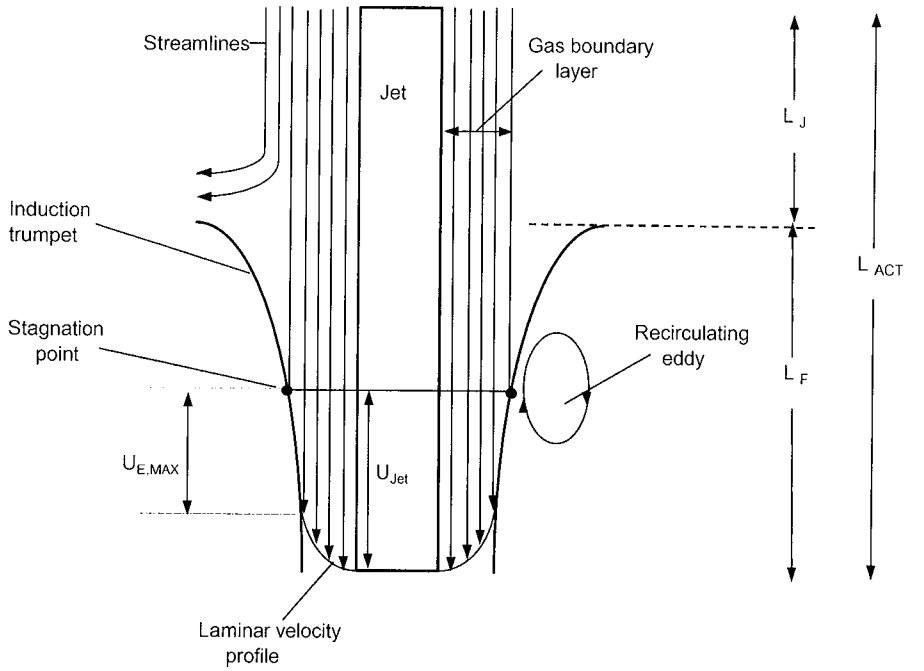

Fig. 2.2 Entrainment of gas film adjacent to the liquid jet (Evans, 1990).

Evans (1990) developed a theoretical model by which the film-wise rate of gas entrainment can be described. The basic assumption of this model is that the gas flow in the thin film resembles to Couette-flow, indicating that $\Delta\beta/\Delta x$ is much smaller than unity. Here $\Delta\beta$ and Δx equal the gas film thickness and length, respectively. A relation for the volumetric gas flow rate within this gas film was determined by applying a momentum balance over a volume of fluid flowing between two coaxial cylinders both of which are moving. In order to calculate the velocity of the free surface of the induction trumpet a direct link was made to the maximum circulating flows ($U_{E,MAX}$) observed for submerged confined jets (Barchilon and Curtet, 1964) in the absence of a secondary flow. The volumetric gas flow rate of the thin gas film is then determined by integrating the velocity profile across the gas film with thickness $\Delta\beta$.The final expression as obtained by Evans (1990) equals:

$$Q_{G,F} = \frac{2\Pi R_J^2}{\mu_G}\left\{\frac{\rho_L g R_J^2}{16}\left(\kappa^4 - 1\right) + \frac{C_1}{2}\left(\kappa^2 \ln(\kappa R_J) - \ln(R_J)\right) + \left(\frac{C_2}{2} - \frac{C_1}{4}\right)\left(\kappa^2 - 1\right)\right\} \tag{2.2}$$

where

$$C_1 = \frac{4\mu_G(U_J - U_{E,MAX}) + \rho_L g R_J^2(1 - \kappa^2)}{4\left(\kappa^2 \ln(\kappa R_J) - \ln(R_J)\right)}$$

$$C_2 = -\left(\mu_G U_J + \frac{\rho_L g R_J^2}{4} + C_1 \ln(R_J^2)\right)$$

$$\kappa = \frac{R_J + \Delta\beta}{R_J}$$

The derivation of this Equation is given in Appendix A1. Eq. (2.2) shows that the jet radius R_J, film thickness ($\Delta\beta$) and the gas properties have an effect on the film wise rate of gas entrainment ($Q_{G,F}$). For calculating $U_{E,MAX}$, see Appendix A1. Using Eq. (2.2) the film wise rate of gas entrainment can be calculated once the gas film thickness $\Delta\beta$ is known.

In order to obtain an expression for the gas film thickness, a similar but slightly different approach as given by Sene (1988) is used. Sene also considered that the motion of the gas with the thin gas film resembles to (laminar) Couette flow. Since $\Delta\beta$ is much smaller than the jet radius ($\Delta\beta << R_J$), a planar jet can be considered.

The laminar motion in a thin gas film is given by:

$$\frac{dP}{dx} = \mu_G \cdot \frac{d^2u}{d^2y} \tag{2.3}$$

and the boundary conditions are given by Eqs. (A1.12).

The solution of this velocity profile is straight forward and shows that as the pressure gradient in the gas flow in increased, the local velocity may go to zero or even become negative. A gas layer of reversed flow probably can not be supported in the receiving flow, so a quantitative estimate of the gas film thickness $\Delta\beta$ can be obtained by imposing the condition

$$\left|\frac{du}{dy}\right|_{y=\Delta\beta} = 0 \tag{2.4}$$

on the solution of Eq. (2.3). An approximate value of $\Delta\beta$ can than be determined using

$$\Delta\beta = \sqrt{\frac{2\mu_G(U_J - U_{E,MAX})}{\rho_L g}} \tag{2.5}$$

Using Eq. (2.2) and (2.5) the volumetric gas flow rate within the thin gas film can be determined theoretically.

Equations (2.1) and (2.2) clearly demonstrate that the jet diameter/radius at the plunging point are of extreme importance for the total rate of gas entrainment by plunging jets. In this section two separate mechanisms are discussed, i.e. the jet envelope and the film wise rate of gas entrainment. The total rate of gas entrainment is considered to be the sum of both entrainment mechanisms, i.e.:

(2.6) $$Q_{G,TOT} = Q_{G,E} + Q_{G,F}$$

Since the jet diameter plays such adominant role in the gas entrainment mechanism, parameters influencing the jet diameter will be discussed in more detail.

2.2.2 Parameters influencing jet stability

The phenomenon of jet stability (disintegration) has been subject to many investigations for more than 100 years. A comprehensive review of all break-up regimes is presented by Reitz and Bracco (1988). The various regimes observed appear to depend mainly on the jet velocity. Since the present study only high velocity jets are used (jet velocities higher than 15 m/s), the following discussion is restricted to these high velocity jets discharging to a gaseous atmosphere. According to Reitz and Bracco (1988) the high velocity jets used in the present study are classified as atomising jets.

The complexity of jet disintegration is related to the unusually large number of parameters which influence it, like:

- nozzle configuration
- initial turbulence level of jet leaving the nozzle
- jet velocity
- liquid physical properties
- gas physical properties
- swirling liquid
- swirling gas phase etc., etc..

While the seeds of the jet disintegration are already present in the flow inside the nozzle, the actual disintegration site is located at the gas-liquid interface of the discharging jet. For high velocity jets it is now generally accepted that the action of the surrounding gas is the primary cause of the atomisation process. The initial jet turbulence is a contributing factor, because it initially ruffles the jet surface, making it susceptible to the aerodynamic forces of the gas phase. This process, gas forces destabilizing the jet surface, is known as a Kelvin-Helmholtz instability. A very well known example of such an instability is the occurrence and growth of waves on water caused by wind (Taylor, 1958). Consider the system of forces acting on a slightly disturbed interface, as illustrated in Fig. 2.3.

The surface tension forces try to bring back the disturbed interface to its original position. On the other hand, the aerodynamic forces (proportional to $\rho_G(U_N)^2$) create a local decrease in pressure at the top of the disturbance and make it tend to expand further outward. This corresponds to the normal pattern of a wind induced instability. This indicates that wind induced instabilities are more pronounced if higher density gases are used, which promote the jet disintegration.

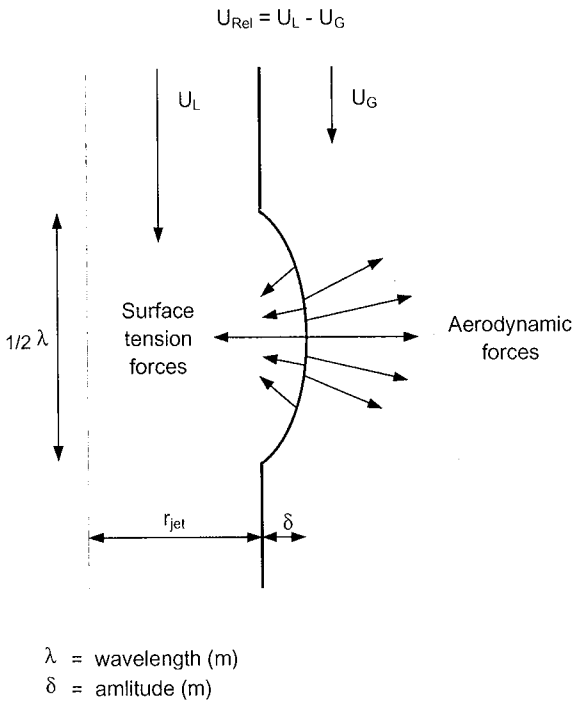

Fig. 2.3 System of forces acting on a slightly disturbed gas-liquid interface.

In order to show the influence of the gas density on the jet disintegration process, the simplified analyses of Taylor (1940) and Ranz (1958) can be used. Taylor analysed the unstable wave growth of a two-dimensional planar surface wave due to the relative motion between gas and liquid. He considered the limiting case $kR_J >> 1$ (the wavelength of the disturbance ($\lambda=2\pi/k$) is much smaller than the jet radius) and assumed that $\rho_G < \rho_L$. This analysis was applied by Ranz (1958) towards round jets and he argued that the jet spreading angle of an atomising jet can be estimated by combining the radial velocity of the fastest growing unstable wave with the axial jet velocity. This hypothesis resulted in the following relation for the divergence angle (Θ) of an atomising jet:

(2.7) $$\tan\left(\frac{\Theta}{2}\right) = \frac{4\Pi}{A} \cdot \sqrt{\frac{\rho_L}{\rho_G}} \cdot f\left(\frac{\rho_L}{\rho_G} \cdot \left(\frac{Re_L}{We_L}\right)\right)$$

where A is an empirical constant (depending on the nozzle configuration). The function f is shown in Fig. 2.4, which illustrates that for $\rho_L/\rho_G(Re_L/We_L)^2 >> 1$, the function f has an asymptotic value of approx. 0.288. This theoretical value has been verified experimentally by Wu et al. (1983) who studied atomising jets using liquids with a broad range of liquid physical properties. For $\rho_L/\rho_G(Re_L/We_L)^2 >> 1$ Eq. (2.7) indicates that the jet divergence angle is influenced by the gas density only. The effect of the gas density on the jet stability has been studied by Bracco et al. (1982) and Wu et al. (1983). From these results it follows that the jet divergence angle increases when using higher density gases.

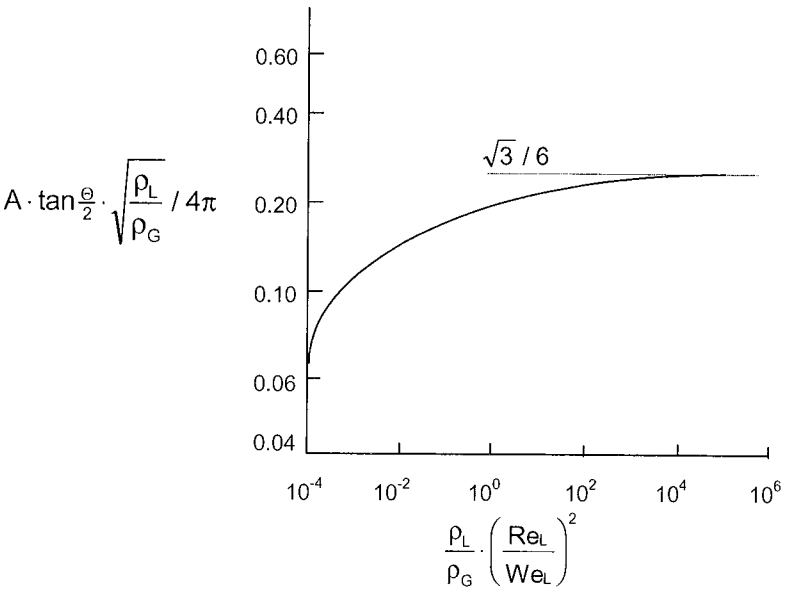

Fig. 2.4 Theoretical dependence of the jet divergence angle on the operating conditions (Ranz, 1958)

The results obtained in this section show that the gas density (read aerodynamic forces) at the gas-liquid interface result in the growth of unstable surface waves. As a result, the effective jet diameter at the plunging point increases (and hence the gas entrainment rate, see Eq. (2.1)) when higher density gases are used. To the best of our knowledge no experimental verification exists showing that the gas density influences the gas entrainment rate and entrainment mechanism of high velocity jets. It is the main objective of this chapter.

2.3 EXPERIMENTAL EQUIPMENT AND PROCEDURES

2.3.1 Experimental program

In order to investigate the gas entrainment mechanism of high velocity jets discharging through a straigth tube, the experimental program was divided into two sections. Firstly, the overall gas entrainment rate of a jet was measured as a function of the jet length and the jet velocity, using gases with different physical gas properties. In addition, the jet diameter was measured as a function of the parameters mentioned above.

In studying the influence of the gas physical properties on the gas entrainment rate and mechanism, the following gases were used in the present study: helium, nitrogen, carbon dioxide and sulphur hexafluoride. The physical properties of these gases are summarised in Table 2.1.

Table 2.1 Summary of gas physical properties.
(at 20 °C and 0.1 MPa)

Gas	Molecular weight (kg/kmol)	Density (kg/m^3)	Viscosity 10^5 (Pa.s)
He	4	0.17	1.86
N_2	28	1.19	1.66
CO_2	44	1.87	1.37
SF_6	146	6.18	1.46

2.3.2 Equipment

A general layout of the experimental equipment is given in Fig. 2.5. It consisted of a vertically positioned glass column (D = 48 mm and L = 1200 mm) with its base extending approx. 10 mm below the level of the degassing bath.

The top of the column was connected with the degassing bath, so that the gas can be re-entrained by the liquid jet discharging through the glass column. In the external gas loop a calibrated gas flow meter was installed. The nozzle was fixed at the top of the column in such a way that the liquid jet discharges centrally through the column. The liquid from the degassing column was re-circulated through the external liquid loop by means of a centrifugal pump, via a calibrated rotameter and a heat exchanger, back to the nozzle. The liquid temperature remained essentially constant for each experimental run at approx. 17 °C. The liquid used was de-ionised water.

2.3.3 Procedures

The general procedure involved selecting a gas flow rate into the top of the glass column by adjusting the valve in the external gas loop. Once the flows inside the column have reached equilibrium for those specific conditions, the free jet length was measured. This procedure was repeated for a number of gas flow rates.

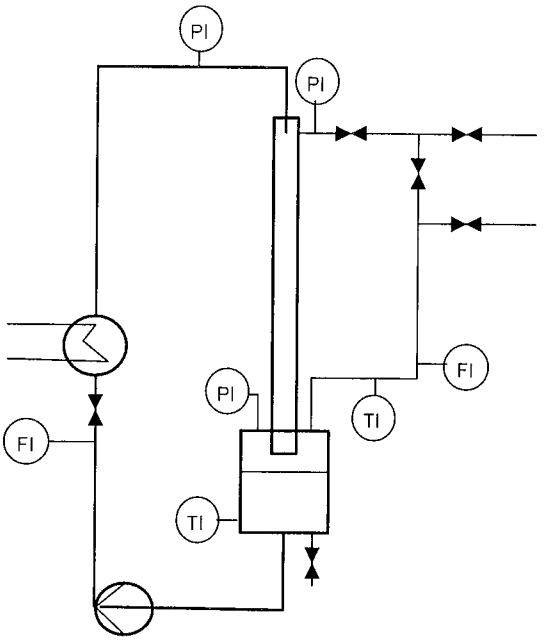

Fig. 2.5 Scheme of experimental equipment.

In addition, the jet diameter was photographed as a function of the free jet length. Photographs were taken of the discharging jet in order to determine the expansion in jet diameter. The high velocity jets were photographed using long exposure photography, which gave a time averaged outline of the jet envelope. From these photographs, jet diameter measurements were made as function of its length. The length of the free jet was measured from the tip of the nozzle to the point were the jet discharges into the bubbly mixture.

2.4 EXPERIMENTAL RESULTS

2.4.1 Gas entrainment rate

2.4.1.1 Jet length and velocity

The gas chamber, through which the plunging jet discharges into the straight tube, was connected to the head space of the gas-liquid separation vessel. The gas entrainment rate of the jet can be adjusted by throttling the valve in the gas loop.

Throttling results in a reduction in pressure in the gas chamber of the tube. A reduction in pressure inside the downcomer cause it to fill with a bubbly mixture as illustrated in Fig. 2.6. At very low rates of gas supply to the tube, the level of the bubbly mixture is sustained just below the level of the nozzle, see Fig. 2.6 A. As the gas rate is increased a point is reached where the jet can no longer entrain all of the gas. Since the entrainment abilty of a liquid jet is directly related to its diameter, the jet length must increase resulting in a drop of the bubbly mixture level inside the straight tube, as illustrated in Fig. 2.6 B. This new equilibrium level marks the position where the jet can effectively entrain the increased gas flow entering the top of the column. The level of the bubbly mixture inside the tube may stabilise at any level depending on the gas supply rate. However, at a maximum gas rate the bubbly mixture will eventually collapse at the base of the tube, as illustrated in Fig. 2.6 C. Indeed, this is the maximum rate of gas entrainment of the discharging jet.

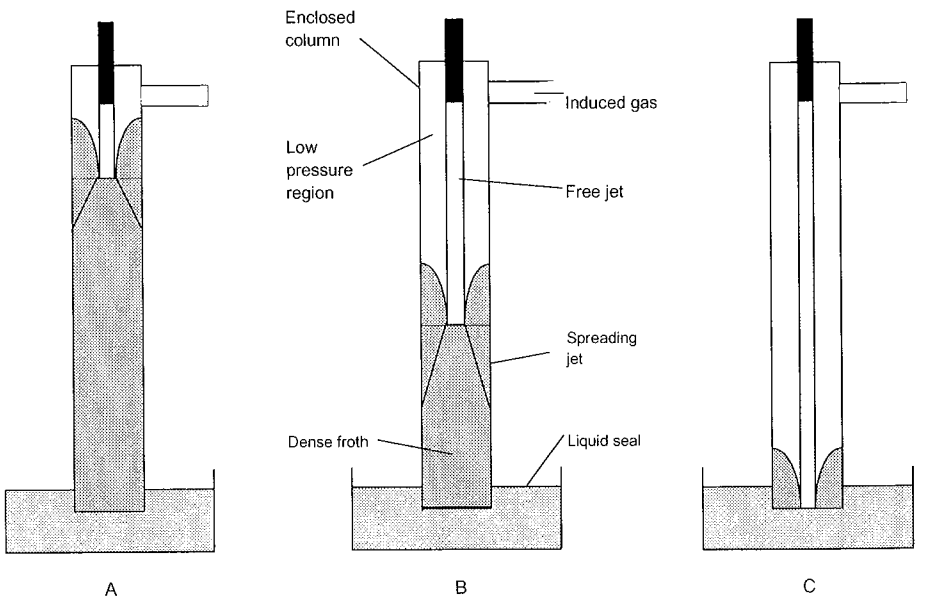

Fig. 2.6 Influence of gas entrainment rate of tube hydrodynamics

The influence of the jet length and velocity on the gas entrainment rate is discussed ibelow For a typical set of results, the normalised entrainment rate Q_G/Q_L is plotted against the jet length in Fig. 2.7 for various jet velocities. The shape of the curves are typical for all experimental runs and it shows that the entrainment ratio increases almost linearly with the jet length. Further it was observed that the entrainment ratio increases with increasing jet velocity. These results are in agreement with those of Bin (1988).

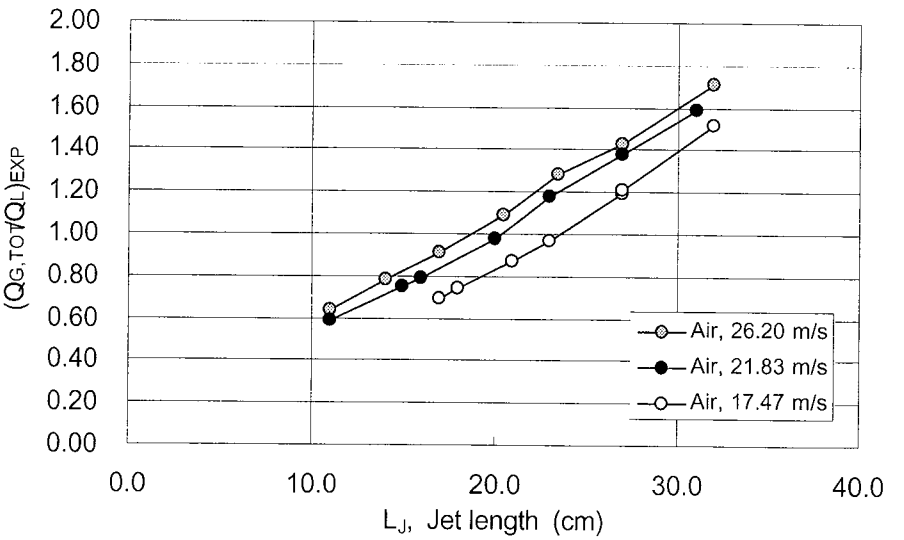

Fig. 2.7 Influence of the jet length (L_J) and jet velocity on the entrainment rate ($Q_{G,TOT}$). (System: water/air)

2.4.1.2 Effect of gas density

The effect of the gas density on the entrainment ratio is shown in Fig. 2.8. This figure clearly demonstrates that the entrainment ratio (when using longer jets) is strongly influenced by the physical gas properties, which is in contrast with the statements of Bin (1988). For short jets there is almost no effect of the gas density.

In order to explain the density effect, its influence on the jet stability must be verified.

2.4.2 Jet stability

For a typical set of results, the effect of the gas density and the jet velocity on the jet stability (jet diameter as function of the jet length) is shown in Figs. 2.9 and 2.10, respectively. The effective jet diameters ($d_{J,EXP}$)as a function of the jet length (L_J) have been obtained by using long time exposure photography.

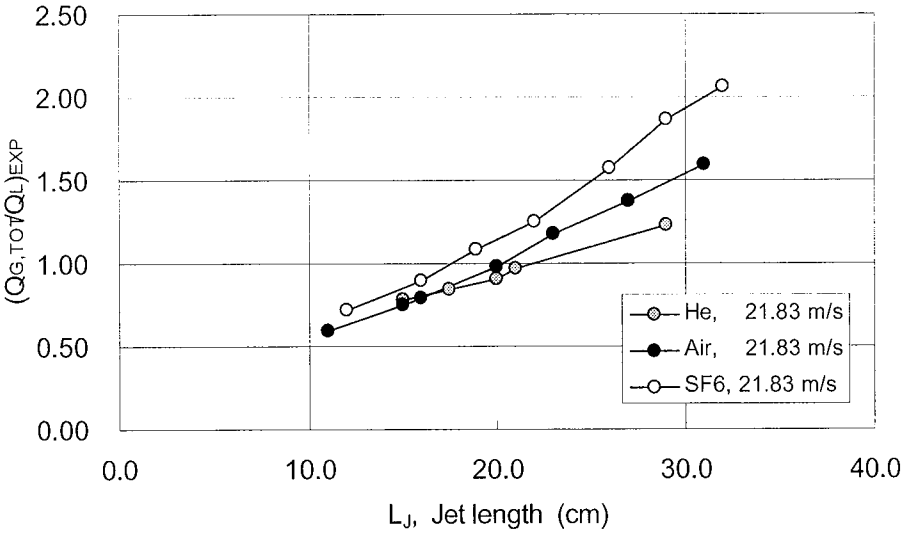

Fig. 2.8 Influence of the gas density on the gas entrainment ($Q_{G,TOT}$) ratio of plunging jets as function of the jet length (L_J).

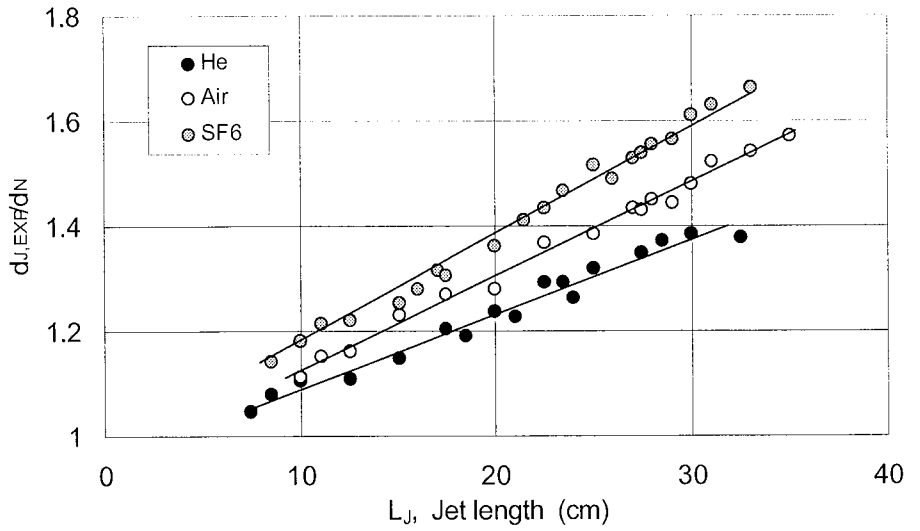

Fig. 2.9 Influence of the gas density on the jet stability.

Fig. 2.9 demonstrates that using a gas of higher density, results in a larger jet diameter as function of its length. This is in agreement with the theories of Ranz (1954) and Taylor (1940).

The effect of the jet velocity on the jet expansion is shown in Fig. 2.10. This figure indicates that the jet velocity has no influence on the jet stability, which is in agreement with the results reported in section 2.3, i.e. the asymptotic value of Fig. 2.4. All experimental data could be correlated by :

$$\frac{d_J}{d_N} = 1 + 0.022 \cdot \left(\frac{L_J}{d_N}\right)^{1.17} \cdot \left(\frac{\rho_G}{\rho_L}\right)^{0.15} \tag{2.8}$$

This empirical relation is valid for $0.18 < \rho_G < 6.18$ kg/m^3, $17.6 < U_N < 26.3$ m/s and $L_J/d_N < 35$ and predicts the jet diameter within 5 % accuracy. A parity plot of Eq. (2.8) is shown in Fig. 2.11. Eq. (2.8) shows that the gas density has a significant effect on the jet stability and the effect of the jet length is more than proportional.

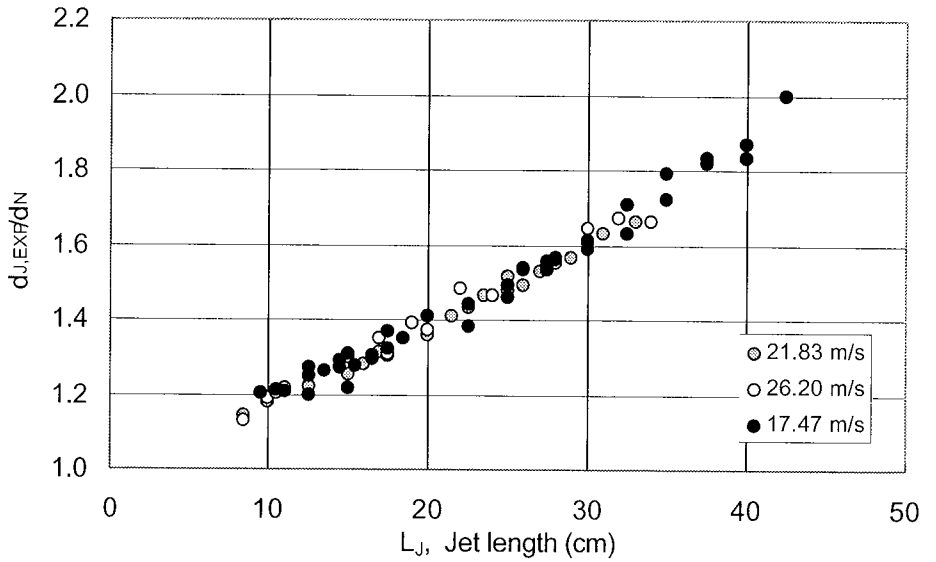

Fig. 2.10 Influence of the jet velocity on the jet stability.

2.5 DISCUSSION

Although the experimental results illustrate the influence of jet length, jet velocity and gas density on the gas entrainment rate, it does not give any physical insight into why the gas entrainment rate changes with the operating parameters and the gas density. According to section 2.2, the gas is entrained below the liquid surface by two mechanisms, i.e. the jet envelope and the film wise rate of entrainment. It was shown that the variable which directly controls the entrainment rate is the effective jet diameter at the plunging point, see Eqs. (2.1) and (2.2). Both equations show that liquid jets entrain more gas with increasing jet diameter.

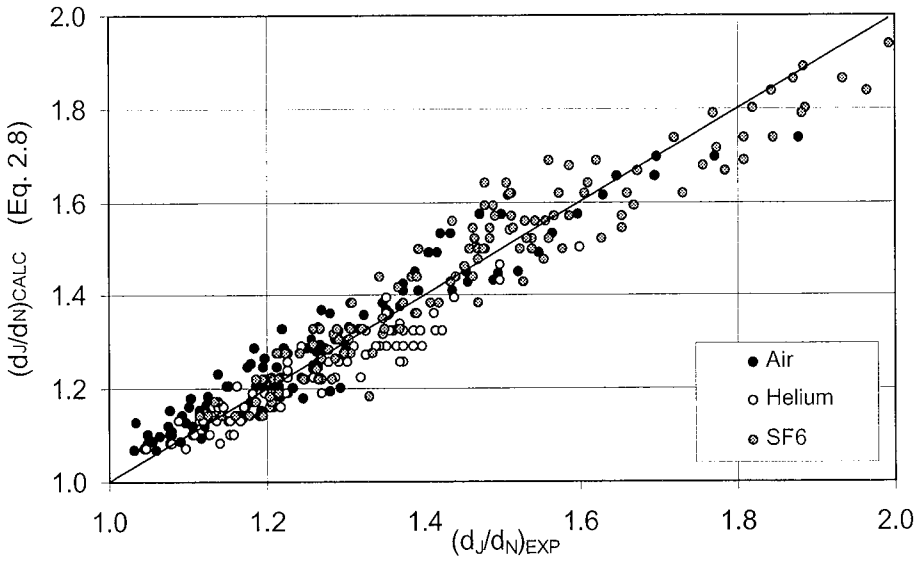

Fig. 2.11 Parity plot of predicted and experimental determined jet diameters.

The free jet length (L_J) is defined as the distance from the nozzle tip to the point were the jet discharges into the bubbly mixture. Fig. 2.2 (which is a schematic representation of the entrainment mechanism experimentally observed), shows that the actual entrainment occurs somewhere below the visually observed plunging point. Unfortunately, it was not possible to measure the gas film lengths (L_F) at this point in the experimental facility.

To discriminate between the two entrainment mechanisms, requires accurate knowledge of the gas film length, since the actual jet diameter at the plunging point is strongly affected by the actual jet length (and hence the amount of gas entrained by the envelope mechanism). To our knowledge, Kusabiraki et al. (1990) measured gas film length (L_F) of plunging jets. They studied the effect of the jet velocity and the physical liquid properties on the gas film length (L_F), using air as the gas phase. Their results show (see Fig. 2.12) that the gas film length is affected by by the jet velocity. A possible effect of the gas physical properties on L_F was not mentioned. Therefore, we analysed our data using the experimental data of L_F of Kusabiraki (1990). This way, a discrimination between the two entrainment mechanisms could be made since the actual jet length at the impact point (L_{ACT}) was taken from Kusabiraki et al. (1990), with $L_{ACT} = L_J + L_F$.

Influence of jet velocity

Fig. 2.7 shows that the entrainment ratio of the jet is influenced by the jet velocity. However, in this figure the actual free jet length (L_{ACT}) is not considered. If the data are based on the actual free jet length ($L_{ACT}=L_J+L_F$), the effect of the jet velocity is much less pronounced as is shown in Fig. 2.13. It proves that the jet velocity has only a very sligth influence on the gas entrainment ratio when the actual jet length (L_{ACT}) is considered.

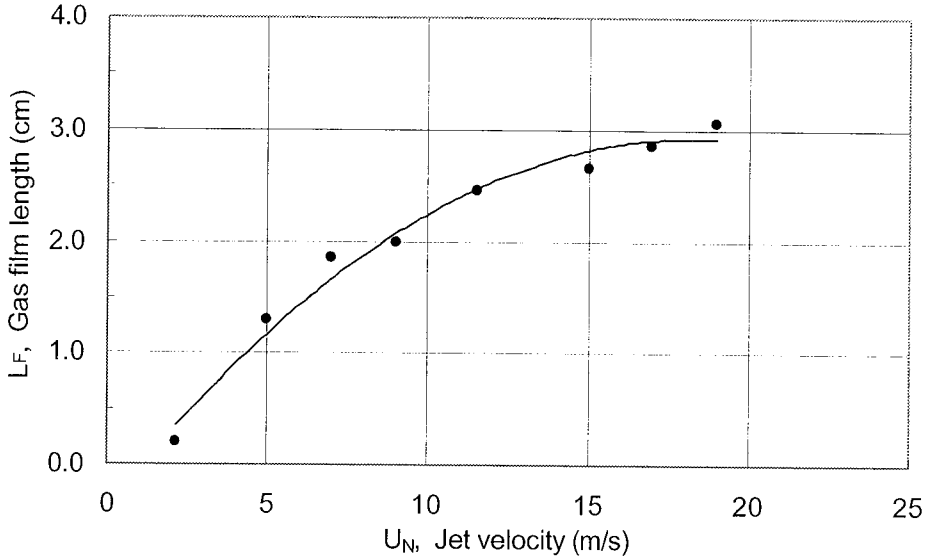

Fig. 2.12 Influence of the jet velocity (U_N) on the gas film length (L_F) (Kusabiraki (1990)). (System: Water/air)

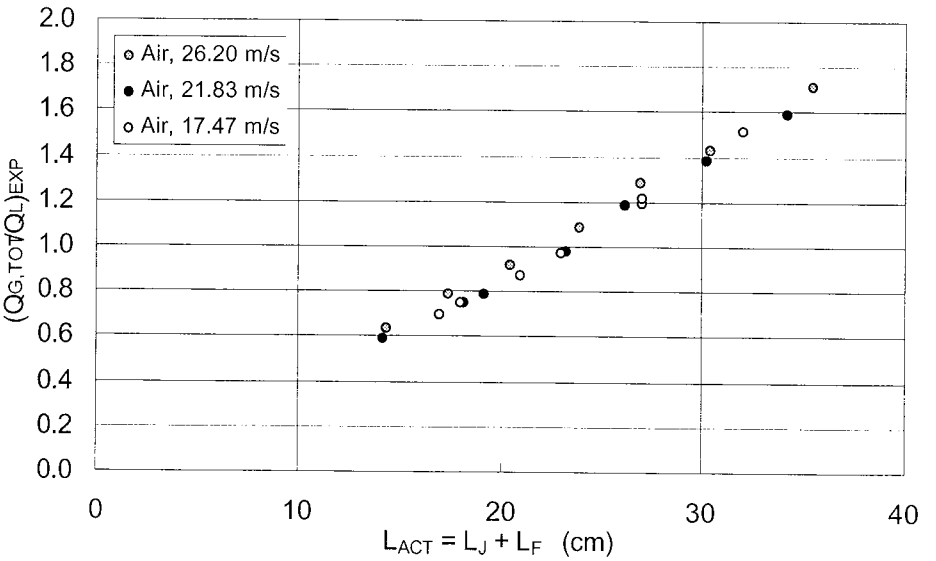

Fig. 2.13 Influence of the actual free jet length (L_{ACT}) and jet velocity on the actual entrainment ratio (system: water/air).

In order to discriminate between both entrainment mechanisms, the actual jet diameter at the plunging point is required. It follows from Eq. (2.8). Hence the amount of gas entrained by the jet envelope can be calculated using Eq. (2.1). Knowing this, the "experimental" film wise rate of gas entrainment can be obtained from $(Q_{G,F}/Q_L) = (Q_{G,EXP}/Q_L) - (Q_{G,E}/Q_L)$. The amount of gas entrained by the gas film $(Q_{G,F})$ can be calculated using Eqs. (2.2)-(2.6). The calculated and experimental extrapolated values are shown in Fig. 2.14. This figure shows that the "model" predicts the correct order of magnitude, despite the relative large scatter of the experimental data.

From this it can be concluded, that when a) the effective jet diameter as a function of its length and b) the gas film length (L_F) are known, the gas entrainment ratio of liquid plunging jets can be calculated using Eqs. (2.1) - (2.6).

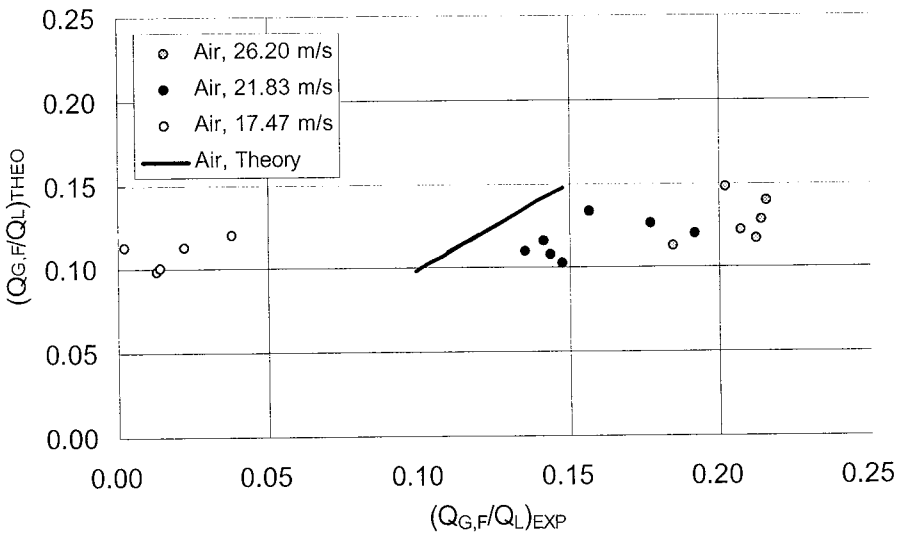

Fig. 2.14 Parity plot of the calculated and the experimental (extrapolated) gas entrainment ratios of the gas film (system: water/air).

Influence of the gas density

In section 2.4.1.2 it was shown that the entrainment ratio of plunging jets is affected by the gas density. Also, it was verified experimentally that the physical gas properties affect the jet stability. Using the procedure given above, the film wise rates of gas entrainment were also determined for jets entraining helium and sulphur hexafluoride. The result of this analysis is given in Fig. 2.15.

The analysis shows that the predicted and the extrapolated data deviate systematically. It is mentioned that the actual jet length was calculated using the gas film lengths obtained from the water/air experiments of Kusabiraki et al. (1990). Since there is a systematic deviation (helium vs. SF_6) this may be an indication that the length of the gas film adjacent to the liquid jet is also influenced by the gas physical properties. No experimental verification of this statement could be found in the literature.

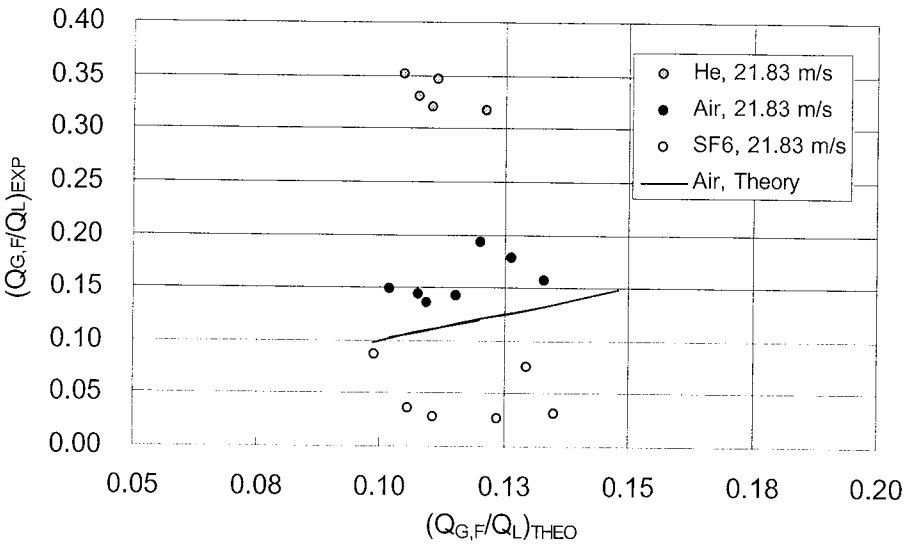

Fig. 2.15 Parity plot of the calculated and the experimental (extrapolated) gas entrainment ratios of the gas film (water/helium and water/SF_6).

In order to verify whether the gas film length (L_F) is affected by the physical gas properties additional experiments were carried out. The results are shown in Fig. 2.16 (For more details, see Appendix A2).

In this figure, the actually measured gas film lengths are shown as a function of the actual jet length and the gas physical properties. Contrary to the results of Kusabiraki et al. (1990), no systematic effect of the jet velocity was observed in our experiments, see Appendix A2. However, it shows that the gas physical properties effect gas film length, i.e. with increasing gas density L_F decreases.

Since L_F is influenced by the gas properties, the systematic deviation between the experimental and predicted values as shown in Fig. 2.15 can be explained qualitatively. For calculating the film wise rate of entrainment, the film lengths of Kusabiraki et al. (1990) were used. When using helium, the actual length of the helium gas film length L_F is underestimated and hence the rate of gas entrained by the jet envelope, resulting in a to high $Q_{G,F}$-value. The reverse reasoning holds for SF_6.

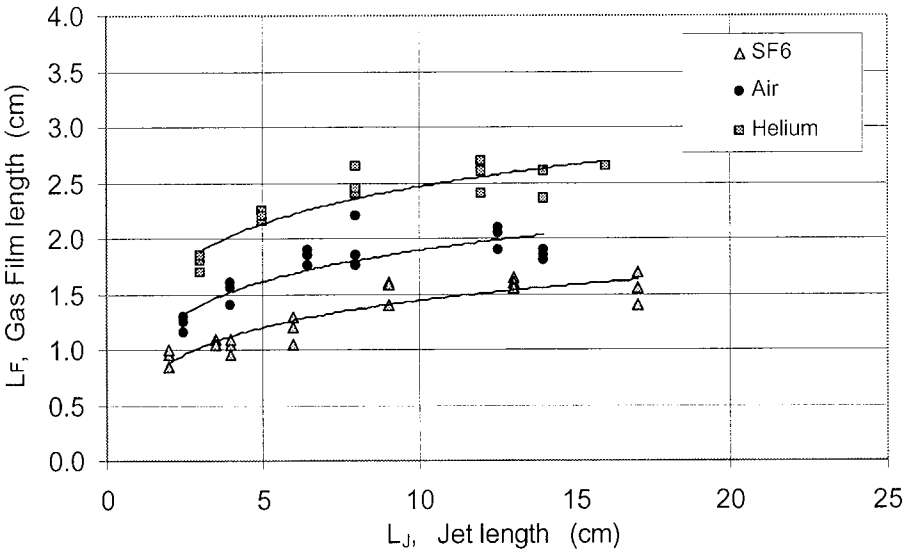

Fig. 2.16 Effect of the physical gas properties on the gas film length

A quantitative analysis is not possible because the results shown in Fig. 2.16 can not be translated to the jet discharging through a straight tube and due to the fact that other nozzle configurations were used.

The results obtained in this chapter show that the physical gas properties have a substantial effect on both the gas entrainment rate and the entrainment mechanism of liquid plunging jets. The model proposed by Evans (1990) is able to predict the film wise rate of gas entrainment, once the actual jet diameter (and hence the gas film length) at the plunging point is known.

2.6 CONCLUSIONS

1) The overall rate of gas entrainment of plunging jets consists of two entrainment mechanisms, i.e. the gas trapped between the jet envelope and the gas layer trapped between the liquid jet and the receiving liquid at the plunging point.
2) The model proposed by Evans (1990) is able to predict the film wise rate of gas entrain-ment, once the actual jet diameter (and hence the gas film length) at the plunging point is known.
3) The gas entrainment rate of plunging jets increases with increasing density of the gas phase. The physical explanation of this phenomenon can be attributed to the effect of the gas density on the jet envelope formation.

4) The gas film length adjacent to the liquid jet is affected by the gas physical properties.

5) The gas entrainment rate of liquid jets can be predicted theoretically once the jet diameter and the gas film length at the impact point are known as a function of jet length, jet velocity and physical gas properties.

NOTATION

A	emperical constant in Eq. 2.7	-
D	Column diameter	m
d_J	jet diameter at plunging point	m
d_N	nozzle diameter at outlet	m
g	acceleration due to gravity	m^2/s
L	column length	m
L_{ACT}	actual jet length ($L_J + L_F$)	m
L_F	gas film length	m
L_J	jet length	m
P	pressure	Pa
$Q_{G,TOT}$	total volumetric gas entrainment rate of liquid jet	m^3/h
$Q_{G,E}$	volumetric gas entrainment rate of jet envelope	m^3/h
$Q_{G,F}$	volumetric film wise rate of gas entrainment	m^3/h
Q_L	volumetric liquid flow rate	m^3/h
R_J	liquid jet radius	m
Re	Reynolds number	-
$U_{E,MAX}$	maximum circulation flow for submerged jets	m/s
U_J	liquid jet velocity	m/s
U_N	liquid jet velocity at nozzle exit	m/s
We	Weber number	-
u	gas velocity in gas film adjacent to liquid jet	m/s
β	gas film thickness	m
κ	dimensionless radius ratio, defined by Eq. 2.2	-
μ_G	dynamic gas viscosity	Pa.s
ρ_G	gas density	kg/m^3
ρ_L	liquid density	kg/m^3

Appendix A1:
Theoretical description of the film wise rate of gas entrainment (Evans, 1990)

Evans (1990) developed a theoretical model for the film wise rate of gas entrainment. Assuming that the gas flow pattern within the thin gas film resembles Couette-flow implies that $\Delta\beta/\Delta x << 1$, with $\Delta\beta$ the gas film thickness and Δx the gas film length. The volumetric gas flow rate inside the gas film, $Q_{G,F}$, can be found by applying a momentum balance over a volume of fluid flowing between two coaxial cylinders both of which are moving. The volumetric gas flow rate is then determined by integrating the velocity profile $u_G(r)$, across the gas film with thickness β, i.e.

$$Q_{G,F} = \int_0^{2\Pi} \int_{R_J}^{\kappa R_J} u_G(r) \cdot dr \cdot d\Theta \tag{A1.1}$$

where κ is defined as the ratio of the outside to the inside radius of the gas film, i.e.

$$\kappa = \frac{R_J + \beta}{R_J} \tag{A1.2}$$

Assuming laminar flow and no axial velocity component, the gas velocity profile is given by

$$\frac{d(r \cdot \tau)}{dr} = \frac{dP}{dz} \cdot r \tag{A1.3}$$

where dP/dz is the axial pressure gradient across the gas film, and τ is the radial shear stress

$$\tau = -\mu_G \cdot \frac{du_G}{dr} \tag{A1.4}$$

The pressure gradient can be replaced by the axial pressure difference across the induction trumpet and is approximately equal to $\Delta P/\Delta L = \rho_L.g$. Substitution of Eq. (A1.4) into Eq. (A1.3) gives

$$\rho_L \cdot g \cdot r = -\mu_G \cdot \frac{d}{dr}\left(r \cdot \frac{du_G}{dr}\right) \tag{A1.5}$$

The boundary conditions are

(A1.6 a) $u_G(r) = U_J$ at $r = R_J$

(A1.6 b) $u_G(r) = U_{E,MAX}$ at $r = \kappa R_J$

where $U_{E,MAX}$ is the velocity of the free surface of the induction trumpet, i.e. the velocity of the circulating eddy. The velocity profile inside the gas film can be found by integrating Eq. (A1.5). The volumetric gas flow rate is found by integrating Eq. (A1.1). The final expression for the volumetric gas flow rate entrained by the thin gas film equals

(A1.7 a) $$Q_{G,F} = \frac{2\pi R_J^2}{\mu_G} \cdot \left\{ \frac{\rho_L g R_J^2}{16}\left(\kappa^4 - 1\right) + \frac{C_1}{2}\left(\kappa^2 \ln(\kappa R_J) - \ln(R_J)\right) + \left(\frac{C_2}{2} - \frac{C_1}{4}\right)\left(\kappa^2 - 1\right) \right\}$$

where

(A1.7 b) $$C_1 = \frac{4\mu_G(U_J - U_{E,MAX}) + \rho_L g R_J^2 (1 - \kappa^2)}{4\left(\ln(\kappa R_J) - \ln(R_J)\right)}$$

and

(A1.7 c) $$C_2 = -\left(\mu_G U_J + \frac{\rho_L g R_J^2}{4} + C_1 \ln(R_J)\right)$$

Eqs. (1.7) represents an expression by which the entrainment rate of the thin gas layer adjacent to the free surface of the jet can be estimated.

In order to quantify this entrainment rate, an estimate is required of the velocity of the circulating eddy ($U_{E,MAX}$). In order to estimate the flow rate within this circulating eddy, Evans (1990) made a direct link to the circulating eddy observed in confined jets. For these confined jets Liu and Barkelew (1986) developed an experimental expression by which the maximum mass flow rate in the circulating eddy can be calculated, for systems where the secondary flow is zero, i.e.

(A1.8) $$\frac{m_{E,MAX}}{m_L} = \frac{0.37}{C_T} - 0.64$$

C_T is the Crayer-Curtet number. For confined jets where the secondary flow rate is zero, C_T follows from:

$$C_T = \frac{R_J}{\left(R_M^2 - 0.5 \cdot R_J^2\right)^{0.5}} \qquad \text{(A1.9)}$$

An estimate for $U_{E,MAX}$ can be obtained by assuming a solid body rotational velocity profile within the circulating eddy (Evans, 1990) as shown in Fig. 2.2

By considering the fluid in the downward section of the circulating eddy the volumetric recirculating eddy flow rate (Q_E) is then approximately equal to

$$Q_E = 2\Pi \frac{R_M}{2} \int_0^{R_M/2} u_E(r)dr \qquad \text{(A1.10)}$$

where R_M is the radius of the mixing tube, and πR_M is equivalent to the linear length of the eddy if it was sliced vertically in the radial direction and straightened out. The integral term represents the two-dimensional flow within the radial cross-section of the eddy. The integral term in (A1.10) represents the two-dimensional flow rotating within the radial cross-section of the eddy. The angular velocity u_E, in the radial cross-section of the eddy is obtained from

$$0 = \cdot \frac{d}{dr}\left(\frac{1}{r} \cdot \frac{d}{dr}(ru_E)\right) \qquad \text{(A1.12)}$$

where it has been assumed that the liquid recirculation in the radial plane of the eddy has the same velocity profile as that for a free vortex. The boundary conditions for Eq. (4.21) are:

(A1.12 a) $u_E = 0$ at $r = 0$

and

(A1.12 b) $u_E = u_{E,MAX}$ at $r = R_M$

where $U_{E,MAX}$ is the maximum value of the velocity component tangential to the outer boundary of the recirculating eddy. Applying these boundary conditions to Eq. (A1.12) gives

$$u_E(r) = \left(\frac{2u_{E,MAX}}{R_M}\right) \cdot r \qquad \text{(A1.13)}$$

Substitution of Eq. (A1.13) into (A1.10), the maximum recirculating flow inside the recirculating eddy is given by

$$Q_{E,MAX} = 2\Pi \int_0^{R_M/2} u_{E,MAX} \cdot r \cdot dr \qquad \text{(A1.14)}$$

which upon integrating gives an expression for $U_{E,MAX}$

$$U_{E,MAX} = \frac{4}{\Pi \cdot R_M^2} \cdot Q_{E,MAX} \qquad \text{(A1.15)}$$

where $Q_{E,MAX}$ is obtained from Eq. (A1.8). The maximum volumetric flow rates in the recirculating eddy ($Q_{E,MAX}$) equal

$$\frac{Q_{E,MAX}}{Q_L} = \left(\frac{0.37}{C_T} - 0.64\right) \cdot \left(\frac{\rho_E}{\rho_L}\right) \qquad \text{(A1.16)}$$

From Eqs. (A1.7), (A1.15 and (A1.16) the film wise rate of gas entrainment can be predicted once the gas film thickness β is known.

In order to obtain an expression for the gas film thickness, a similar but slightly different approach as given by Sene (1988) can be used. Sene also considered that the motion of the gas within the thin gas film resembles to (laminar) Couette flow. Since β is much smaller than the jet radius ($\beta << R_J$), a planar jet can be considered.

The laminar motion in a thin gas film is given by:

$$\frac{dP}{dx} = \mu_G \cdot \frac{d^2u}{d^2y} \qquad \text{(A1.17)}$$

and the boundary conditions are given by Eqs. (A1.12).

The solution of this velocity profile is straight forward and shows that for increasing pressure gradients in the gas flow, the local velocity may go to zero or even become negative. A gas layer of reversed flow probably can not transport the receiving flow, so a quantitative estimate of the gas film thickness β can be obtained by imposing the condition

$$\left|\frac{du}{dy}\right|_{y=\beta} = 0 \qquad \text{(A1.18)}$$

on the solution of Eq. (A1.17). An approximate value of β can then be determined using

$$\beta = \sqrt{\frac{2\mu_G(U_J - U_{E,MAX})}{\rho_L g}} \qquad \text{(A1.19)}$$

NOTATION

C_T	Crayer-Curtet number defined by Eq. A1.9	-
g	acceleration due to gravity	m^2/s
P	pressure	Pa
$Q_{G,F}$	volumetric film wise rate of gas entrainment	m^3/h
Q_L	volumetric liquid flow rate	m^3/h
R_J	liquid jet radius	m
R_M	column radius	m
$U_{E,MAX}$	maximum circulation flow for submerged jets	m/s
U_J	liquid jet velocity	m/s
u_E	eddy circulation velocity	m/s
u_G	gas velocity in gas film adjacent to liquid jet	m/s
β	gas film thickness	m
κ	dimensionless radius ration, defined by Eq. 2.2 d	-
μ_G	dynamic gas viscosity	Pa.s
ρ_G	gas density	kg/m^3
ρ_L	liquid density	kg/m^3
τ	shear stress	Pa

Appendix A2:
Influence of the gas physical properties on the gas film length, i.e. the induction trumpet

A2.1 Introduction

In Chapter 2 of this thesis the gas entrainment rate and the entrainment mechanism of a liquid plunging jet were studied. It was verified that the gas physical properties influence the gas entrainment rate and mechanism of high velocity jets. A possible effect of the gas properties on the gas induction trumpet formation (read gas film length) could not be verified experimentally. The main objective of this study described in this appendix is to verify whether the gas physical properties affect the gas film length adjacent to the plunging jet.

A2.2 Experimental set-up and procedures

A scheme of the experimental is shown in Fig. A2.1. The experimental set-up consisted of a transparant acrylic resin bath (1400 x 500 x 400 mm) and an external liquid loop with a liquid recirculation pump. A nozzle with an inside diameter of 3.5 mm was used. The inclination angle of the nozzle to the liquid surface of the bath was 45 degrees. The jet velocity was varied between 9.23 and 16.73 m/s. The nozzle length to diameter ratio was approx. 50 and the free jet length, defined as the distance between the nozzle exit to the liquid bath surface was varied between 20 and 150 mm.

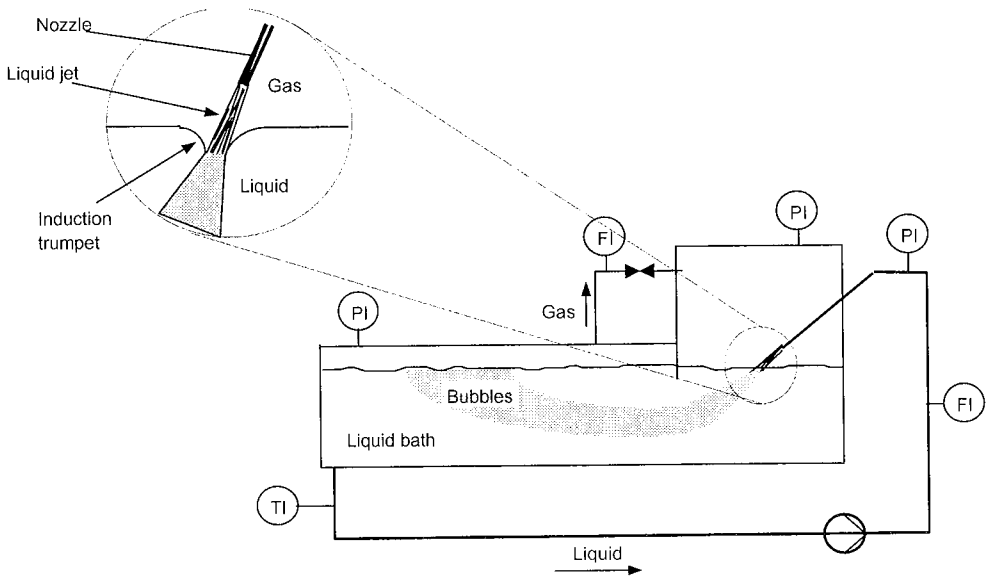

Fig. A2.1 Scheme of experimental facility.

De-ionised water was used at room temperature. The effect of the gas properties on the gas film length was studied using helium, air and sulphur hexafluoride as the gas phase. The physical properties of these gases were given in Chapter 2.

The experimental procedures involved were the adjustment of the free liquid jet length and the jet velocity. The gas film lengths were recorded on video (for a given set of operating parameters and gas type) and from detailed stand still pictures a photograph was taken and analysed. From these photographs the gas film lengths were measured.

A2.3 Experimental results & discussion

The maximum gas film length (L_F) was defined as the distance from the liquid bath surface to the point were the gas film breaks up. The influence of the jet velocity on the gas film length was investigated. However, in contrast to the results of Kusabiraki et al. (1990) no systematic effect was experimentally verified.

However, that the gas physical properties influence the gas film length could be demonstrated successfully, as shown in Fig. 2.16. This figure shows that the gas film lengths decrease with increasing molecular weight of the gas. Whether it is the gas density or the gas viscosity which causes the observed effects can not be elucidated from the present results.

Robertson et al. (1973) discussed the mechanism of gas film formation of liquid plunging jets. Their experiments showed that the gas film formation should be affected by the gas viscosity. Under conditions of very low pressures (< 0.5 mm Hg column), where the gas does not behave as a continuum and viscous flow does not occur, no gas film formation was observed. The experimental results may indicate that the dynamic viscosity of the gas affect the gas film stability/formation. On the other hand' the gas density influences the stability of the gas film also (Kelvin Helmholtz stability). The disturbances on the free surface of the gas film can be amplified by the gas aerodynamic forces, indicating that the break-up rate of the gas film increases with increasing gas density. Both considerations may be correct. It may suggest that the kinematic viscosity plays a role. Indeed, a proportionality between μ_G/ρ_G and L_F also agrees with our observations.

However, a clearer understanding of the gas film break-up rates and lengths (in terms of changes of L_F as function of the jet operating parameters and the physical gas and liquid properties) ask for additional research.

A2.5 Conclusions

The results as presented in this appendix demonstrate that the physical gas properties affect the gas film length adjacent to the free surface of the plunging jet. However, whether it is the gas density or the dynamic viscosity which causes the observed effects, can not be elucidated from the present experiments.

Chapter 3
Gas suction rates of ejectors at elevated pressures

SUMMARY

For the design of gas-liquid ejectors, reliable data are required which describe the gas entrainment characteristics as function of the gas- and liquid physical properties, ejector geometry and the operating conditions.

The effect of the physical gas properties was studied by varying the reactor pressure between 0.1 and 1.6 MPa and by using gases with various molecular weights. The effect of the physical liquid properties and the presence of fine solid particles on the gas suction rates were also studied. The results have shown that the gas density has a significant effect on the gas suction rates, whereas the effect of the liquid physical properties can be neglected as long as the Taylor parameter, $((\rho_L/\rho_G)(\sigma/(\mu_L U_N))^2$, is larger than unity. Design correlations are presented for a Henzler type of ejector as function of the jet velocity, gas phase pressure differential across the ejector and the gas- and liquid physical properties.

3.1. INTRODUCTION

Recently, specific attention has been paid to the effect of the reactor pressure on the hydrodynamics and mass transfer characteristics in various gas-liquid contactors like: bubble columns (Deckwer and Schumpe, 1993; Wilkinson, 1991; Wilkinson and van Dierendonck, 1990; and Ozturk et al., 1987), mechanically agitated vessel (Sridhar and Potter, 1980), trickle bed reactors (Wammes, 1990) venturi reactors (Jekat, 1975).
All these studies showed such significant pressure effects (read gas density) that the data as obtained at atmospheric pressures are inadequate for the design and scale-up of the various high pressure gas-liquid reactors in general.

Industrial Venturi reactors are mostly operated at elevated pressures (up to 10 MPa) and various gas-liquid reactions have been carried out in these reactors (hydrogenations, oxidations, alkoxylations, aminations, etc.). This indicates that in these industrial Venturi reactors the gas physical properties vary within a very broad range. Despite this fact, research as presented in the literature has been focused on venturi reactors operating at atmospheric conditions.
In Loop reactors the gas is dispersed into the liquid by the liquid driven gas ejector. Since the ejector performance has a significant effect on the mass transfer characteristics of the Venturi reactor as a whole (Cramers et al., 1992 and Dirix and van de Wiele, 1990), it is essential to know the parameters, which affect the ejector performance. In order to design these gas-liquid ejectors effectively, the effect of geometrical parameters, operating parameters and gas- and liquid physical properties on the amount of gas sucked in by ejectors have to be known.

The main objective of this chapter is to determine the effect of the gas- and liquid physical properties and operating conditions on the hydrodynamics and the gas suction rates of a Henzler-type of ejector without swirl device in the upstream section of the nozzle. Therefore, experiments have been performed in a high-pressure venturi reactor (up to 1.6 MPa) and with gases with various molecular weights. Data from the open literature are used to see whether the liquid physical properties affect the ejector performance.

3.2. LITERATURE

3.2.1 Effect of the gas physical properties on the gas suction rates

Data concerning the effect of the gas physical properties on the gas suction rates of ejectors are scarce and to our knowledge there are only three papers that studied this effect. Firstly, Jekat (1975) studied the reactor performance of jet-loop reactors at elevated pressures (up to 10 MPa using water-nitrogen). In his thesis Jekat only mentioned that the

reactor pressure affected the gas suction rates of the ejector. Jekat's results show that up to reactor pressures of 6 MPa the gas suction rates increased with the pressure, whilst at higher pressures the gas suction rates decreased with the pressure. A physical explanation for the phenomenon observed was not given. The second paper, which takes into account the effect of the gas density on the gas suction rates of ejectors, was reported by Henzler (1981). Henzler performed experiments at atmospheric conditions using gases with different molecular weights (helium, air and air-helium mixtures). From his results it has to be concluded that the gas suction rates of the ejector increases when higher density gases are used. However, the density range studied varied only between 0.18 and 1.8 kg/m^3. The last paper has been reported by Cramers et al. (1992). In an atmospheric Loop Venturi reactor it was experimentally verified that the gas physical properties have a twofold effect on the Venturi-reactor performance, i.e. the gas suction rates of the ejector and the gas fraction in the main holding vessel both increased when higher density gases were used. The density range studied varied between 0.17 and 6.18 kg/m^3.

From these three papers, it has to be concluded that the gas physical properties have an effect on the gas suction rates of ejectors. However, a systematic experimental investigation concerning gas density effects has not been reported yet. In addition, it could not be elucidated which of the physical gas a property causes the observed phenomenon.

3.2.2 Hydrodynamics

Generally, two types of flow appear in ejectors without swirl device in the upstream section of the nozzle, i.e. bubble and jet flow. In the bubble flow regime gas dispersion occurs in the mixing tube and is characterised by the formation of very small bubbles. Bubble flow occurs at relatively low gas-liquid flow ratios and high gas phase pressure differentials across the ejector ($\Delta P_{G,EJ}$). At higher gas-liquid flow ratios, i.e. lower gas phase pressure differentials, the so-called jet flow regime is observed. Both flow regimes are illustrated in Fig. 3.1.

3.3. EXPERIMENTAL FACILITY

In order to investigate in the effect of the gas physical properties on the gas suction rates of ejectors, experiments have been carried in a high-pressure reactor. A schematic representation of the reactor is shown in Fig. 3.2.

The autoclave consisted of a metal vessel with three pairs of high-pressure sight glasses. Inside this metal vessel a glass column was placed, which functioned as the actual main holding vessel. The internal diameter and height of this glass vessel were 0.23 m and 1.2 m, respectively. The Henzler-type of ejector was mounted at the top of the vessel in a

downward direction. The dimensions of the ejector used in this study fall within the optimum dimensional range as described by Henzler (1981).

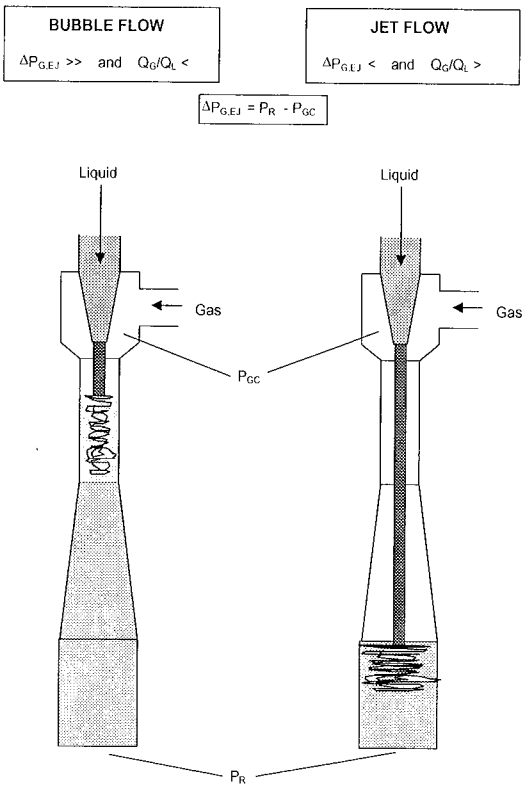

Fig. 3.1 Effect of the gas phase pressure differential on the gas suction rates and the hydrodynamics of the ejector.

At the start of each experiment, the autoclave was filled with water (20 °C). Since it is known that the gas phase pressure differential across the ejector has a significant effect on the gas suction rates of ejectors, it was assured that the ejector outlet was just dipped into the liquid phase (approximately 10 mm). Due to this arrangement, the ejector outlet pressure equals to the reactor pressure (P_R). The liquid and the gas flow rates were measured with a calibrated EMF (Fisher and Porter) and a swirl meter (Fisher and Porter), respectively.

Most of the experiments were performed with nitrogen as the gas. However, for a number of experiments other gases with a large variation of molecular weight have been used (helium, argon and sulphurhexafluoride). The physical properties of the gases used in the present study are summarised in Table 3.1.

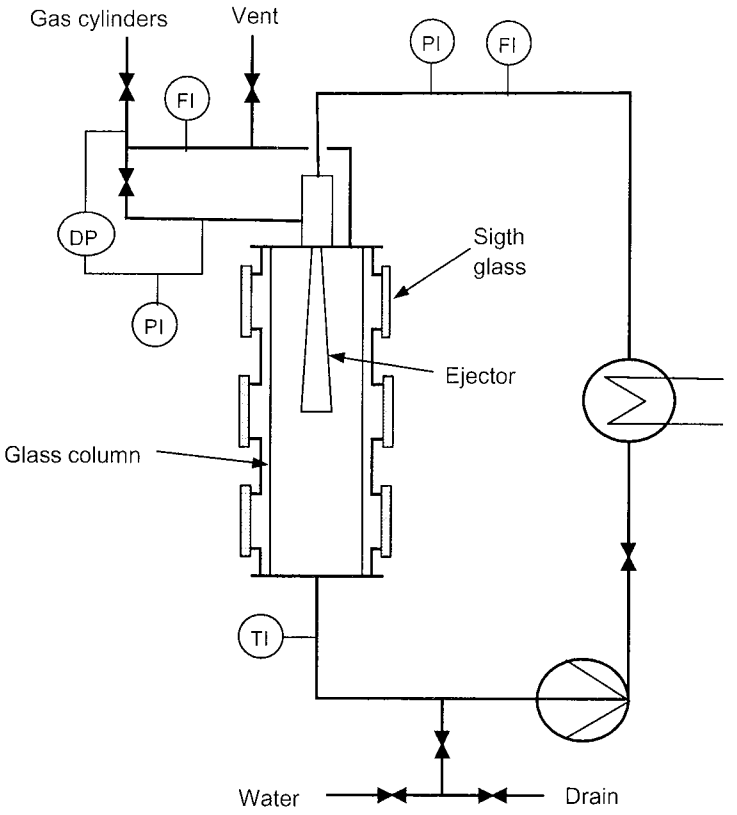

Fig. 3.2 Scheme of the experimental facility.

Table 3.1 Physical properties of the gases used in the experiments (at 0.1 MPa and 20 °C)

Gas	Molecular weight (kg/kmol)	Density (kg/m^3)	Viscosity 10^5 (Pa.s)
Helium	4	0.17	1.86
Nitrogen	28	1.19	1.66
Argon	40	1.67	2.11
SF_6	146	6.18	1.46

3.4. EXPERIMENTAL RESULTS

3.4.1 Effect of the jet velocity

Typical results showing the effect of the velocity (U_N) and the gas phase pressure differential across the ejector ($\Delta P_{G,EJ}$) on the gas entrainment ratio ($Q_{G,GC}/Q_L$) are shown in Fig. 3.3. $Q_{G,GC}$ is defined as the actual volumetric gas flow rate through the gas suction chamber of the ejector, Q_L is the volumetric liquid flow rate through the ejector and $\Delta P_{G,EJ}=P_R - P_{GC}$, where P_R and P_{GC} are the reactor pressure and absolute pressure in the head space of the ejector, respectively.

Fig. 3.3 shows that both the jet velocity and the gas phase pressure differential have a huge effect on the gas entrainment ratio. The curves show that the rate of increase in $Q_{G,GC}/Q_L$ with decreasing $\Delta P_{G,EJ}$ is initially not large, while in the later stage (lower $\Delta P_{G,EJ}$-values) it is steep. Further it is seen that for a constant $\Delta P_{G,EJ}$ the entrainment ratio increases when applying higher jet velocities. The question why the gas entrainment ratio is influenced by $\Delta P_{G,EJ}$ and the initial jet velocity will be discussed in paragraph 3.6.

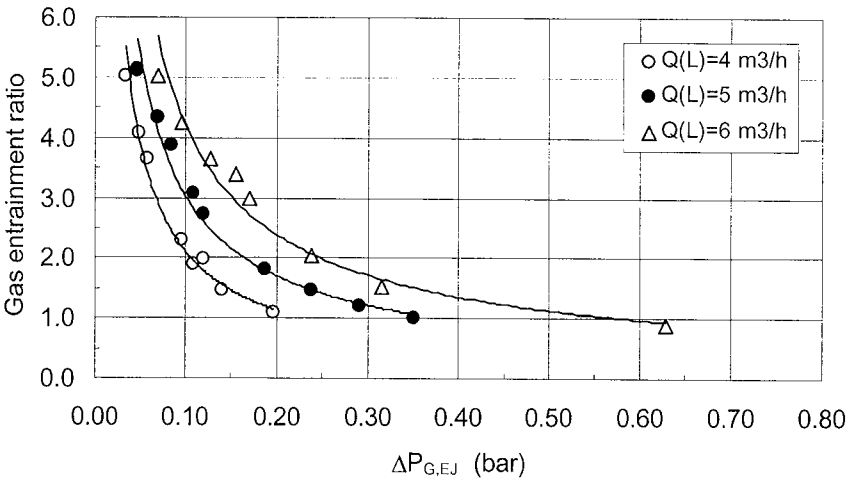

Fig. 3.3 Effect of the jet velocity and the gas phase pressure differential on the actual volumetric gas-liquid flow ratio (reactor pressure is 0.5 MPa and the system used was water-nitrogen).

3.4.2 Effect of the gas density

The effect of the reactor pressure on the gas entrainment ratio of the ejector is shown in Fig. 3.4 a, b, c and d. These figures show that the shape of all the curves is similar, however, all the figures clearly demonstrate that the ratio of $Q_{G,GC}/Q_L$ increases when higher reactor pressures are applied, independently of the gas used.

The effect of the gas molecular weight on the gas entrainment ratio, for a constant reactor pressure, is illustrated in Fig. 3.5. This figure shows that although the reactor pressure is constant, there is still a huge effect of the gas used. Figs. 3.4 and 3.5 may indicate that it is the gas density, which causes the observed phenomenon, since $Q_{G,GC}/Q_L$ increases systematically with the gas density, independently of the other physical properties.

In order to elucidate whether it is the gas density causing the observed phenomenon, some experiments were carried out with various gases at different reactor pressures. In these experiments, the reactor pressure was adjusted in such a way that the gas density in the reactor was constant. A typical illustrative example is shown in Fig. 3.6. From this figure it can be concluded that the gas density affects the gas suction rates of ejectors, since for a constant gas density all the data fall on one single curve independently of the gas and the reactor pressure used. These experiments show that the effect of the reactor pressure and the molecular weight of the gas can be attributed to there effect on the gas density.

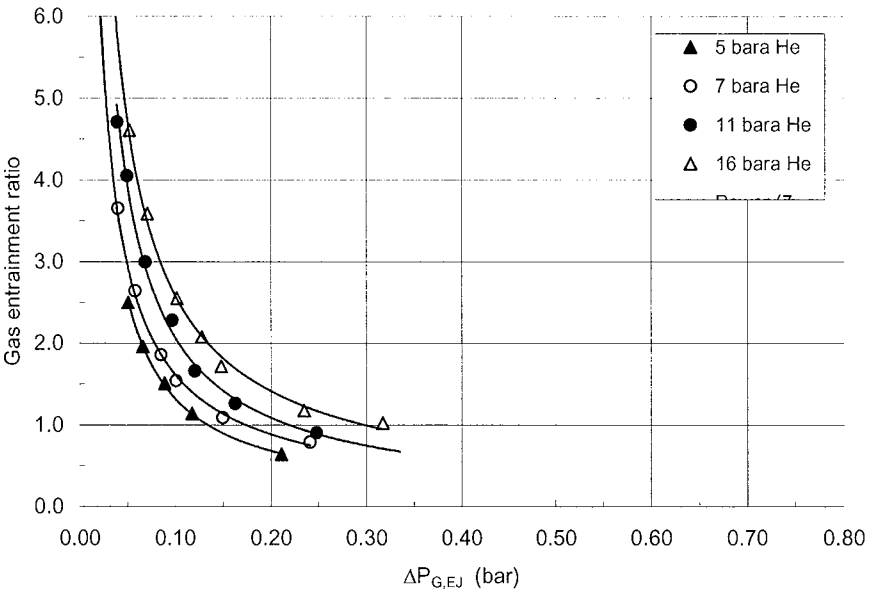

Fig. 3.4 (a) Effect of the reactor pressure on the gas suction rates of ejectors.
System: Water-helium (Q_L = 5 m^3/h)

3.4.3 Effect of suspended solids

Industrial venturi reactors are mostly used for reactions that require suspended catalyst in order to enhance the reaction or to improve the selectivity. Therefore, the effect of the presence of solids in the liquid on the gas entrainment ratio has to be verified.

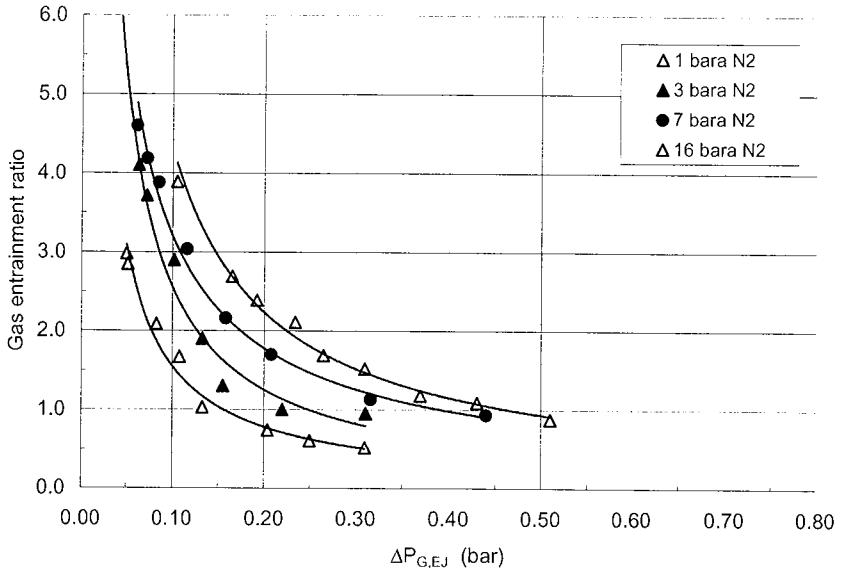

Fig. 3.4 (b) Effect of the reactor pressure on the gas suction rates of ejectors.
System: Water-nitrogen (Q_L = 5 m^3/h)

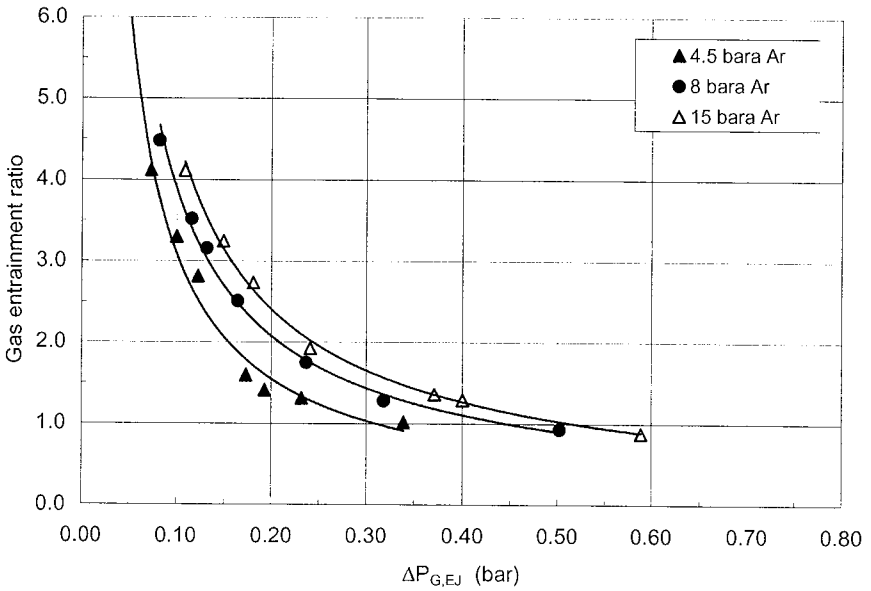

Fig. 3.4 (c) Effect of the reactor pressure on the gas suction rates of ejectors.
System: Water-argon (Q_L = 5 m^3/h)

Some experiments were performed with activated carbon slurry. The weight fraction of the carbon slurries used was 0, 0.3, 1.6 and 4.96 wt %, respectively. The size of 99 % of the carbon particles was below 115 μm. The effect of the fraction of solids on the gas entrainment ratio is shown in Fig. 3.7.

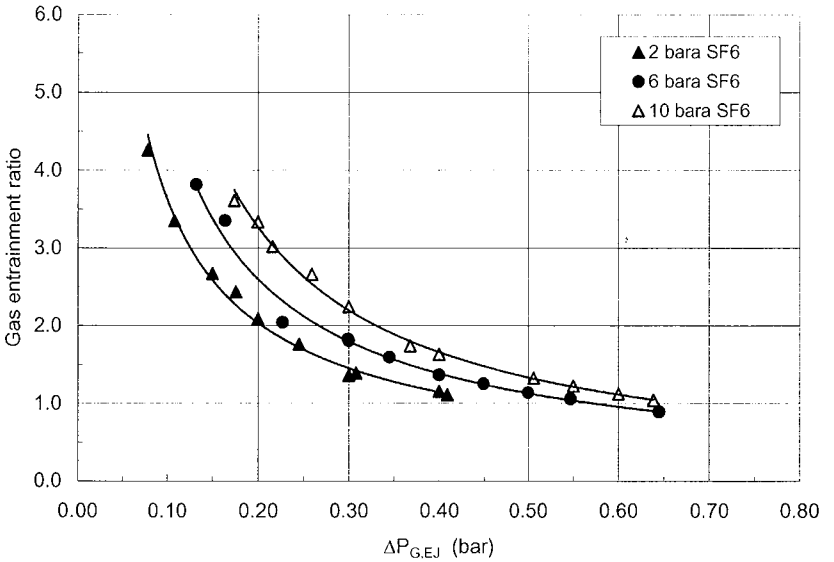

Fig. 3.4 (d) Effect of the reactor pressure on the gas suction rates of ejectors. System: Water-SF_6 (Q_L = 5 m^3/h)

Fig. 3.7 indicates that the weight fraction of solids has no effect on the gas suction rates of ejectors. This conclusion is in agreement with the experimental results of Bhutada and Pangarkar (1989) who used spherical glass beds with various diameters (150, 250 and 450 μm) and weight fractions up to 5 wt %.

3.5. EFFECT OF THE LIQUID PHYSICAL PROPERTIES

The effect of the liquid physical properties on the gas suction rates of ejectors have been studied by Bhutada and Pangarkar (1989), Henzler (1981), Brahim et al (1984) and Bhat et al (1972).

Bhutada and Pangarkar (1989) used non-Newtonian viscous liquids (CMC-solutions) and water as the liquid phase. From there experimental results, it is evident that irrespective of the liquid viscosity used, there was no change in the gas suction rates of the ejector for a set of constant operating parameters. They concluded from their investigations that the entrainment ratio depends mainly on the primary jet velocity and the mixing tube to nozzle configuration used. Exactly the same conclusion applies for the results of Henzler (1981).

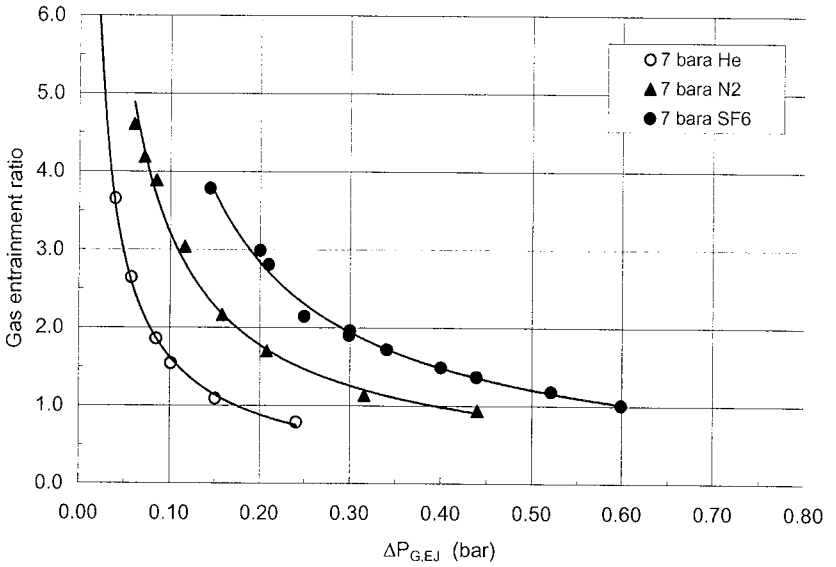

Fig. 3.5 Effect of the gas molecular weight on the gas suction rate of the ejector (P_R=0.5 MPa and Q_L=5 m^3/h).

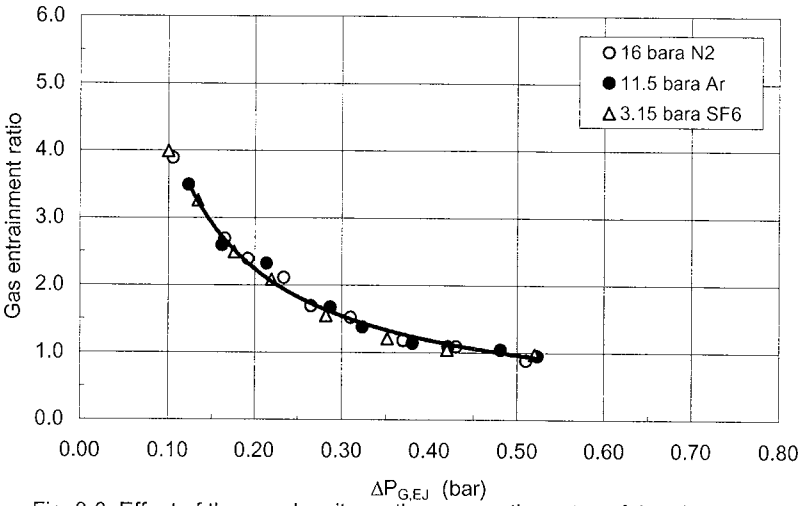

Fig. 3.6 Effect of the gas density on the gas suction rates of the ejector (Q_L=5 m^3/h)

Henzler stated that the gas suction rates are not affected by the liquid physical properties provided that the Reynolds-number, based on the jet velocity and the nozzle diameter, is higher than 10^5. Unfortunately, the viscosity range considered was not reported by Henzler.

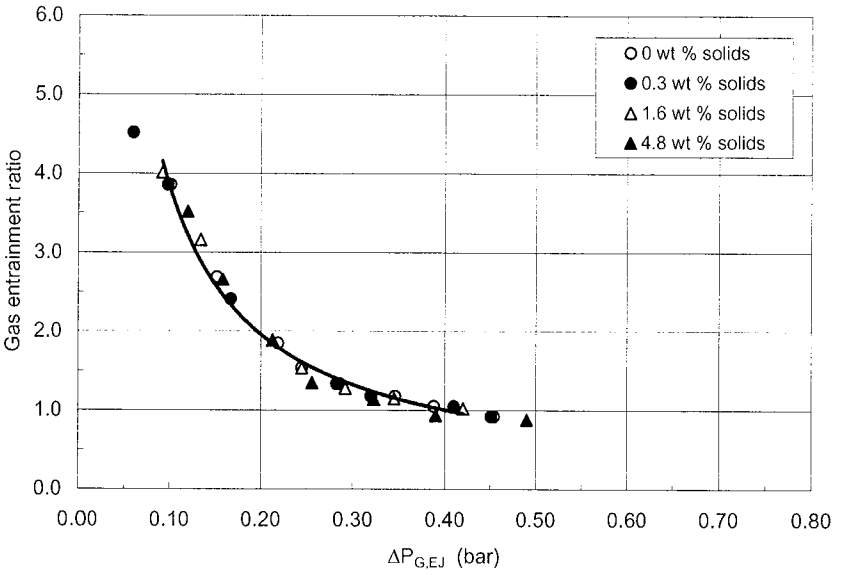

Fig. 3.7 Effect of the solids concentration on the gas suction rates of ejectors. System: water-air and activated carbon particles

The most comprehensive study concerning the effect of the liquid physical properties on the gas suction rate of ejectors has been reported by Brahim et al. (1984). Brahim varied the liquid physical properties in a very broad range. The liquids used were water, mono ethylene glycol (MEG) and tellus oil (TO). The physical properties of these liquids are summarised in Table 3.2. The experimental results of Brahim et al. (1984) are represented in Fig. 3.8 for all the jet velocities and liquids used in the experiments.

In this figure $Q_{G,GC}/Q_L$ is shown against the Euler-number ($Eu = 2\Delta P_{G,EJ}/(\rho_L (U_N)^2)$). It is seen that the data of water and mono ethylene glycol fall on one single curve, despite the fact that the liquid viscosity differs a factor of 20. Increasing the liquid viscosity up to 0.084 Pa.s results in a dramatic decrease in the amount of gas sucked in by the ejector. These experiments indicate that for a certain range of liquid properties the gas suction rates of ejectors are independent of the physical properties, as will be discussed in the next section.

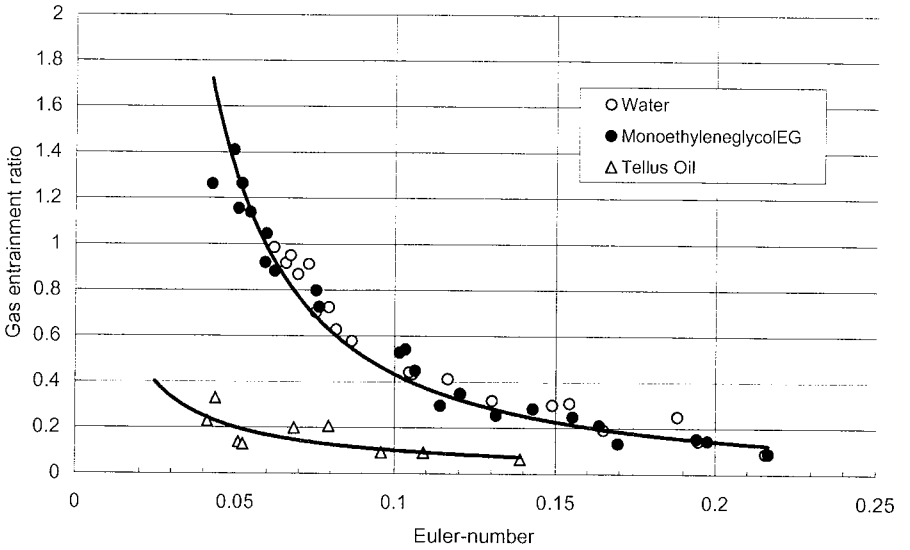

Fig. 3.8 Effect of the liquid physical properties on the gas suction rate of ejectors (Brahim et al, 1984)

Table 3.2 Physical properties of the liquids used by Brahim et al. (1984)

Liquid	Molecular weight (g/mol)	Density (kg/m^3)	Viscosity 10^2 (Pa.s)	Surface tension (N/m)	Taylor parameter (Γ)
Water	18	1000	1.002	0.072	>7000
MEG	62	1102	20.53	0.094	> 25
TO	280	848	83.96	0.034	0.2-0.5

3.6. DISCUSSION

The effect of the gas and liquid physical properties, the gas phase pressure differential across the ejector and jet velocity on the gas suction rates of ejectors can be explained when the gas entrainment mechanism of high velocity jets are considered. In Chapter 2 it has been demonstrated that nearly all of the gas is entrained by the so-called jet envelope mechanism. The amount of gas entrained by the jet envelope formation equals

$$\frac{Q_G}{Q_L} = \left(\frac{d_J}{d_N}\right)^2 - 1 \qquad (3.1)$$

where d_J and d_N are the actual jet diameter at the plunging point and the nozzle diameter, respectively. Relation (3.1) shows that the amount of gas entrained by the jet envelope formation increases with the diameter of the high velocity jet. For high velocity jets

operating in the atomisation regime the jet divergence angle equals to

$$\tan\left(\frac{\Theta}{2}\right) = \frac{4\Pi}{A}\cdot\left(\frac{\rho_G}{\rho_L}\right)^{0.5}\cdot f(\Gamma) \qquad (3.2)$$

where Γ equals $(\rho_L/\rho_G)(\sigma/(\mu_L U_N))^2$ and A is an empirical constant depending on the nozzle configuration (see Chapter 2.2.2). Substitution of Eq. (3.2) into (3.1) and rearranging gives

$$\left(\frac{d_J}{d_N}\right) = 1 + \frac{8\Pi}{A}\cdot\left(\frac{\rho_G}{\rho_L}\right)^{0.5}\cdot f(\Gamma)\cdot\left(\frac{L_J}{d_N}\right) \qquad (3.3)$$

Relation (3.3) shows that the jet diameter is effected by the jet length, the gas density and the liquid physical properties (Γ). In Chapter 2 (Fig. 4), the function $f(\Gamma)$ was shown against Γ. This figure showed that in case $\Gamma > 1$, the function $f(\Gamma)$ has an asymptotical value of 0.288. In other words when $\Gamma > 1$, the liquid physical properties should have no effect on the jet divergence angle and hence on the amount of gas entrained by the jet envelope formation.

In order to explain the experimental results of Brahim et al. (1984), the Taylor-parameter for the liquids used in the experiments are also given in Table 3.2. Table 3.2 shows that for water and mono ethyleneglycol Γ is always larger than 1, indicating that the jet divergence angle is not affected by the liquid physical properties. Since nearly all of the gas is entrained by the jet envelope formation, it is now obvious that under these conditions $Q_{G,GC}/Q_L$ is not affected by σ or μ_L. When using Tellus oil, Γ is smaller than 1. If $\Gamma < 1$, $f(\Gamma)$ decreases rapidly. From this consideration, it is concluded that the jet divergence angle decreases and hence the amount of gas entrained by the jet. From the reasoning as given above, it can be concluded that when Γ is larger than unity, the liquid physical properties have no effect on the jet envelope formation (i.e. the gas entrainment rate of the high velocity jet) and thus cannot affect the amount of gas sucked in by the ejector.

The effect of the gas density on the gas entrainment mechanism has been discussed in Chapter 2, but will be briefly repeated. Relation (3.3) shows that for a constant jet length the jet diameter increases when higher density gases are used and hence the gas entrained by the jet envelope formation increases as well.

The effect of the gas phase pressure differential across the ejector can also be explained when considering the jet envelope formation. In Fig. 3.1 it was shown that $\Delta P_{G,EJ}$ and the liquid jet length (L_J) are interrelated. When applying high gas phase pressure differentials, the mixing zone is located in the mixing tube of the ejector resulting in a short jet. At low

$\Delta P_{G,EJ}$ –values, gas dispersion occurs in the draft tube resulting in an increase in the free jet length and thus the jet diameter at the plunging point. When using longer jets, the jet envelope entrains more gas and hence the ejector sucks in more gas.

3.7. DESIGN CORRELATONS FOR THE GAS SUCTION RATES INCORPORATING REGIME TRANSITION

3.7.1 Theoretical development

Theoretical principles for the rational design of gas-liquid ejectors as evacuators or as gas compression devices laid down over the years have been discussed by Kastenar et al. (1950), Engel (1963) and Cunningham (1974). The relationships developed by these authors for predicting compression ratios as a function of the operating characteristics of the jet pump and its entrainment ratio were derived from momentum and energy balances. Many authors to arrive at expressions for the correlation of the gas suction rates as function of the operating parameters have used this approach. However, this type of analysis is only valid for the homogeneous bubble flow regime and for very high gas phase pressure differentials across the ejector (Cunningham, 1974). Moreover, a possible change in flow regime (as shown in section 3.2.2) was never considered.

The most general model for predicting gas suction rates of gas-liquid ejectors has been developed by Henzler (1981). Based on momentum conservation balances, Henzler derived a semi-empirical expression for the minimum liquid flow rate at which gas entrainment commences ($Q_{L,0}$), i.e.

$$Q_{L,0} = \frac{d_M}{d_N} \cdot A_N \cdot \left(\frac{P_R - P_{GC}}{\rho_L} \right)^{0.5} \tag{3.4}$$

where d_M, d_N, A_N, P_R and P_{GC} are the mixing tube diameter, nozzle diameter, cross sectional area of the nozzle, the pressure at the ejector outlet and the pressure in the gas suction chamber, respectively.

According to Henzler's results, it has to be concluded that $Q_{L,0}$ is effected by the density ratio of the liquid and the gas phase (ρ_L/ρ_G). Based on extensive experimental effort Henzler obtained the following expression for $Q_{L,0}$.

$$Q_{L,0} = C_1 \cdot \left(\frac{\rho_G}{\rho_L} \right)^{C_2} \cdot \frac{d_M}{d_N} \cdot A_N \cdot \left(\frac{P_R - P_{GC}}{\rho_L} \right)^{0.5} \tag{3.5}$$

The constants C_1 and C_2 have to be determined experimentally.

When considering the gas entrainment mechanism (jet envelope formation) of jets, it is obvious that these empirical constants are strongly dependent on the nozzle configuration, since the spreading angle is affected by the nozzle configuration, see Eq. 3.2. This indicates that the experimentally determined C_1- and C_2-values are characteristic for the nozzle configuration applied.

For liquid flow rates above the minimum liquid flow rate at which gas suction starts, the volumetric gas flow rate was found to be proportional to the liquid flow rate (Jekat, 1975 and Henzler, 1981). According to these authors, the gas suction rates of the ejector can be expressed as

(3.6) $$Q_{G,GC} = B \cdot (Q_L - Q_{L,0})$$

where $Q_{G,GC}$ and Q_L are the actual volumetric gas and liquid flow rates discharging through the gas suction chamber of the ejector. Dividing Eq. (3.6) by Q_L and substitution of Eq. (3.5) gives after rearranging

(3.7) $$\frac{Q_{G,GC}}{Q_L} = B \cdot \left\{ 1 - C_1 \cdot \left(\frac{\rho_G}{\rho_L}\right)^{C_2} \cdot \frac{d_M}{d_N} \cdot \left(\frac{P_R - P_{GC}}{0.5 \cdot \rho_L \cdot U_N^2}\right)^{0.5} \right\}$$

The empirical constant B is strongly affected by the ejector configuration and in particular by the mixing tube to nozzle diameter ratio (d_M/d_N), i.e.

(3.8) $$B = B_1 \cdot f\left(\frac{d_M}{d_N}\right)$$

The empirical values of B were graphically presented and the following polynomial function for $f(d_M/d_N)$ was proposed

(3.9) $$f\left(\frac{d_M}{d_N}\right) = \left(\frac{d_M}{d_N}\right)^{2.4} - 0.15 \cdot \left(\frac{d_M}{d_N}\right)^{3.48}$$

for (d_M/d_N) ratios between 1.29 and 4.2 and nozzle and ejector configuration as used by Henzler. The main objection of the use of relation (3.9) is that it predicts negative values for $f(d_M/d_N)$ when larger (d_M/d_N) ratios are used, which has no physical meaning. Therefore, in the following, a theoretical relation for $f(d_M/d_N)$ will be derived.

In order to obtain a theoretical relation for $f(d_M/d_N)$, the phenomena occurring at the mixing zone location have to be considered in detail. In other words, which forces determine the

mixing zone location in the ejector as a function of the ejector configuration, the jet velocity and the gas phase pressure differential across the ejector. Therefore, a schematic representation of the mixing zone is shown in Fig. 3.9.

The high velocity jet tries to push the mixing zone further downward, whereas the forces as exposed by the gas phase pressure differential (suction forces) maintain the mixing zone at the fixed location. When the mixing zone is fixed at a given location, the powers supplied by the jet to the mixing zone surface and the power of the gas phase pressure differential are in equilibrium. The power per unit surface area of the jet (W_N/A_N), supplied to the mixing zone can be written as

$$\left(\frac{W_N}{A_N}\right) = 0.5 \cdot \rho_L \cdot U_N^2 \cdot \left(\frac{Q_L}{A_N}\right) \tag{3.10}$$

whereas the power required to maintain the mixing zone at a fixed position inside the tube equal

$$\left(\frac{W_{\Delta P}}{A_{AN}}\right) = \Delta P_{G,EJ} \cdot \left(\frac{Q_{G,GC}}{A_{AN}}\right) \tag{3.11}$$

where A_N and A_{AN} are the cross-sectional areas of the nozzle and the gas annulus between the jet and the tube, respectively.

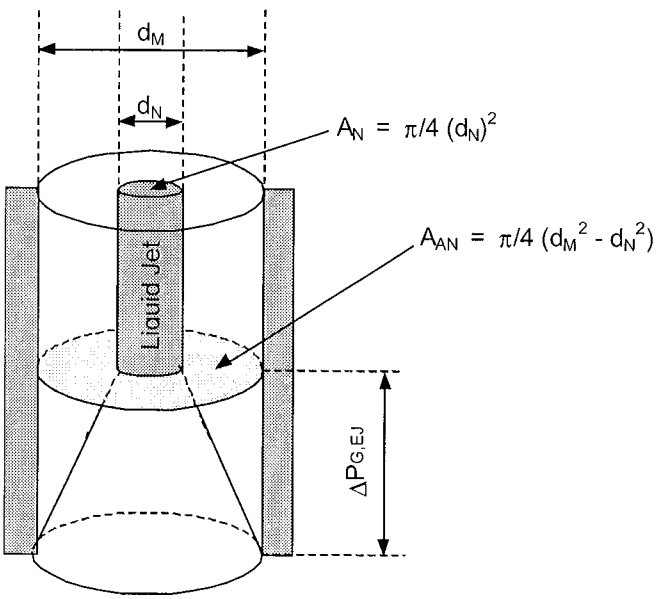

Fig. 3.9 Schematic representation of the mixing zone and of the forces which determine its location in the ejector.

From the considerations as mentioned above, it can be concluded that for a constant mixing zone location both powers per unit surface area are in equilibrium. When considering the jet envelope formation this indicates that then $Q_{G,GC}/Q_L$ is constant, i.e

$$\frac{Q_{G,GC}}{Q_L} = \left(\frac{0.5\rho_L U_N^2}{\Delta P_{G,EJ}}\right)^{0.5} \cdot \left(\frac{d_M^2}{d_N^2} - 1\right)^{0.5} \tag{3.12}$$

The applicability of Eq. (3.12) can be validated by its ability to describe the experimental data of Biswas et al. (1982). They investigated the effect of the jet velocity, the gas phase pressure difference and the mixing tube to nozzle diameter ratio on the gas suction rates of ejectors. The experimental results of Biswas et al. (1982) are shown in Fig. 3.10.

In this figure $(Q_{G,GC}/Q_L)/\{(d_M/d_N)^2-1\}^{0.5}$ has been plotted against $Eu^{-0.5}$. Fig. 3.10 shows that all the data fall on one single curve, independently of d_M/d_N, U_N and $\Delta P_{G,EJ}$. This indicates that our physical reasoning is correct. In other words, $\{(d_M/d_N)^2-1\}^{0.5}$ determines the slope of the $Q_{G,GC}/Q_L$ versus the $\Delta P_{G,EJ}$ plots.

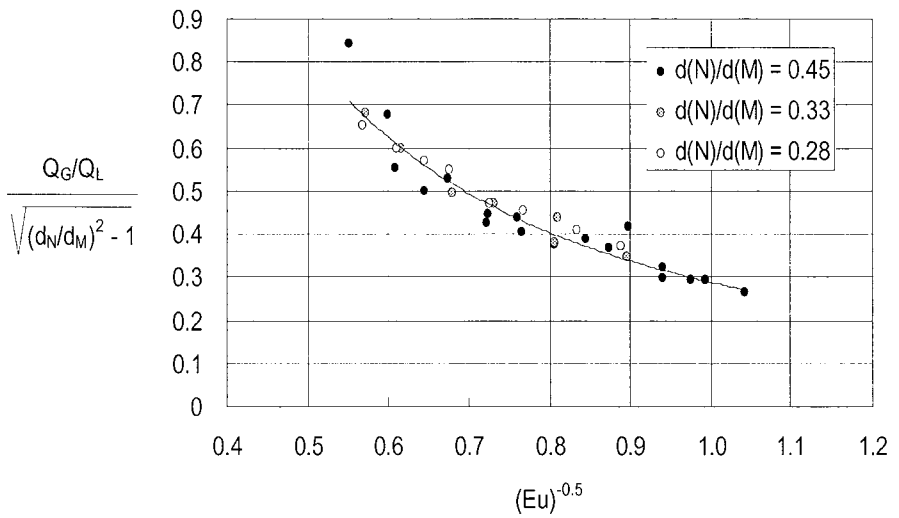

Fig. 3.10 Effect of the mixing tube to nozzle diameter ratio on the entrainment ratio of ejectors (Biswas et al., 1982).

Based on these mechanistic arguments it can be concluded that the function $f(d_M/d_N)$ in relation (3.8) can be written as

$$f\left(\frac{d_M}{d_N}\right) = \left(\frac{d_M^2}{d_N^2} - 1\right)^{0.5} \tag{3.13}$$

Substitution of Eq. (3.13) and (3.8) into (3.7) and rearranging finally gives

$$\frac{Q_{G,GC}}{Q_L} = B_1 \cdot \left(\frac{d_M^2}{d_N^2} - 1\right)^{0.5} \cdot \left\{1 - C_1 \cdot \left(\frac{\rho_L}{\rho_G}\right)^{C_2} \cdot \frac{d_M}{d_N} \cdot \left(\frac{P_R - P_{GC}}{0.5 \cdot \rho_L \cdot U_N^2}\right)^{0.5}\right\} \tag{3.14}$$

With the aid of Eq. (3.14) the experimental data are correlated.

3.7.2 Regime transition

Here it is essential to consider that two different flow regimes are encountered in the ejector, depending on the gas phase differential. As mentioned, at high $\Delta P_{G,EJ}$-values bubble flow occurs, whilst at lower gas phase pressure differentials jet flow occurs. Although these flow regimes cannot be determined visually, as in the atmospheric column, it is possible to determine the transition point graphically, with the aid of Eq. (3.12). The relation shows that the flow transition point can be determined if the gas entrainment ratio is plotted against $Eu^{-0.5}$. The slopes of the curves are determined by the mixing tube to nozzle diameter ratio, where d_M equals the mixing tube diameter in the bubble flow regime and d_D the draft tube diameter in the jet flow regime. Some illustrative examples are given in Fig. 3.11. This figure shows clearly the existence of the two regimes with different slopes. Further it is seen that the gas density has a systematic effect on the flow transition point and that at higher pressures the transition point shifts to higher Eu_C-values.

$$Eu_C = \left(\frac{\Delta P_{G,GC}}{0.5 \cdot \rho_L \cdot U_N^2}\right) \tag{3.15}$$

In case $Eu > Eu_C$, the ejector operates in the bubble flow regime, whereas jet flow occurs if $Eu < Eu_C$.

The critical Euler-number for the ejector configuration used in the present investigation could be empirically correlated as

$$Eu_C = 0.49 \cdot \left(\frac{\rho_G}{\rho_L}\right)^{0.29} \tag{3.16}$$

The experimental data and Eq. (3.16) are shown in Fig. 3.12. Using Eq. (3.16) it is possible to determine whether the experiments were performed in the bubble or in the jet flow regime. Further it is essential to mention that Eq. (3.15) is valid for the nozzle and ejector configuration used in the present study only.

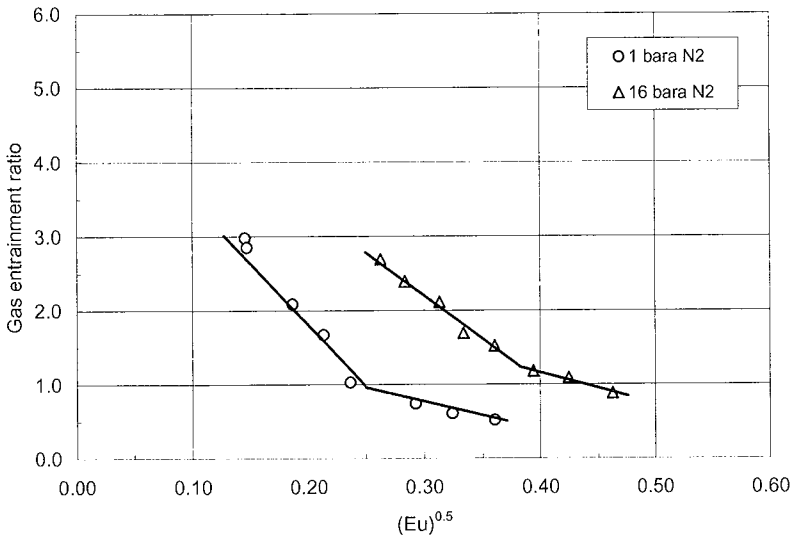

Fig. 3.11 Graphical determination of the flow transition point

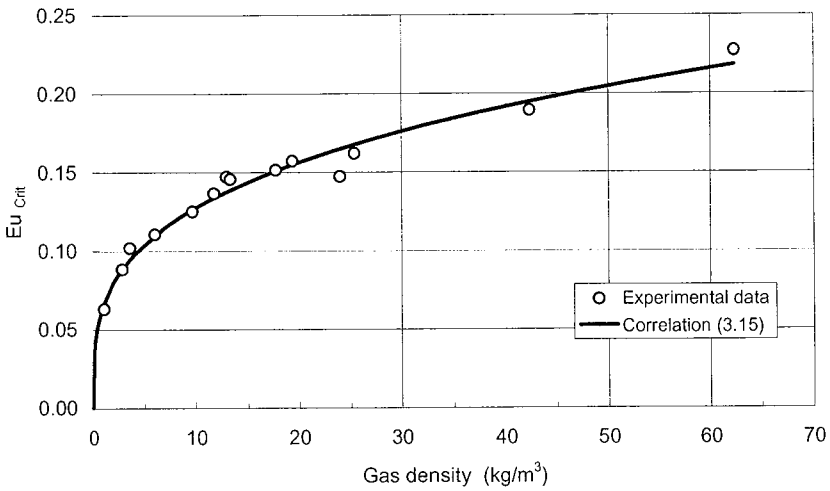

Fig. 3.12 Effect of the gas density on the critical Euler-number

3.7.3 Design Correlations

Optimal values for the empirical constants B_1, C_1 and C_2 of Eq. (3.14) were determined with the aid of a non-linear regression analysis.

For the bubble flow regime ($Eu > Eu_C$) the best result with the smallest average error was obtained with

$$\frac{Q_{G,GC}}{Q_L} = 1.50 \cdot \left(\frac{d_M^2}{d_N^2} - 1\right)^{0.5} \cdot \left\{1 - 0.38 \cdot \left(\frac{\rho_G}{\rho_L}\right)^{0.15} \cdot \frac{d_M}{d_N} \cdot \left(\frac{\Delta P_{G,EJ}}{0.5 \rho_L U_N^2}\right)^{0.5}\right\} \tag{3.17}$$

whereas the data of the jet flow regime ($Eu < Eu_C$) were correlated as Eq. (6.18)

$$\frac{Q_{G,GC}}{Q_L} = 1.50 \cdot \left(\frac{d_D^2}{d_N^2} - 1\right)^{0.5} \cdot \left\{1 - 0.38 \cdot \left(\frac{\rho_G}{\rho_L}\right)^{0.15} \cdot \frac{d_D}{d_N} \cdot \left(\frac{\Delta P_{G,EJ}}{0.5 \rho_L U_N^2}\right)^{0.5}\right\} + 1.55 \tag{3.18}$$

The ranges in which the operating and geometrical parameters and the liquid physical properties have been varied are

$$0.2 < d_N/d_M < 0.5$$
$$L_M/d_M = 8$$
$$16.7 < U_N < 26.3 \text{ m/s}$$
$$0.005 < \Delta P_{G,EJ} < 0.08 \text{ MPa}$$
$$0.18 < \rho_G < 73 \text{ kg/m3}$$

Although relations Eq. (3.17) and (3.18) have been obtained with water as the liquid phase, the developed relations can also be applied for other liquids with different physical properties, as long as the Taylor parameter $\Gamma = (\rho_L/\rho_G)(\sigma/(\mu_L U_N))^2$ is larger than unity, as explained in section 3.6.

A parity plot of the predicted and the experimental entrainment ratios is shown in Fig. 3.13. This figure demonstrates that the average error of these equations is around 10 %, while the largest error is approximately 20 %.

Comparison of Eqs. (3.17) and (3.18) shows that the empirical constants are not affected by the change in flow regime. The change in flow regime only effects the diameter ratio, d_M/d_N for the bubble flow regime and d_D/d_N for the jet flow regime. Also, it is seen that an empirical constant (1.55) had to be added, in order to correlate the data of the jet flow regime.

The physical explanation for this constant is really simple when considering the change in flow regime. The amount of gas which is already present in the jet envelope where jet discharges into the diffuser cq. draft tube has to be added to the amount of gas which will be entrained by the jet envelope when the liquid jet discharges through the draft tube.

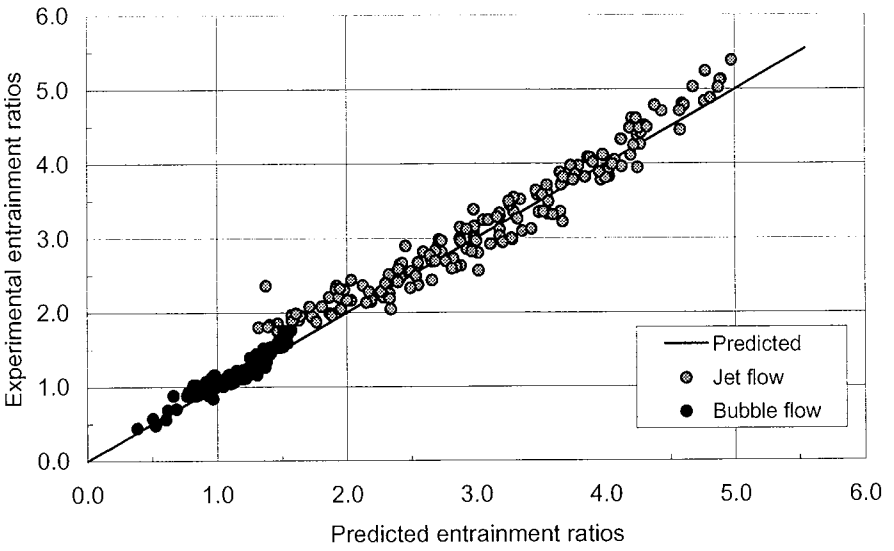

Fig. 3.13 Parity plot of the experimental and predicted (Eqs. (3.17) and (3.18)) gas entrainment ratios.

3.8 CONCLUSIONS

The following conclusions can be drawn from the present investigation:

1) The effect of the reactor pressure and the gas molecular weight on the suction rates of gas-liquid ejectors can be attributed to their effect on the gas density.
2) The gas suction rate of gas-liquid ejectors increases when higher gas densities are applied.
3) The liquid physical properties have no effect on the gas suction rates as long as the Taylor parameter Γ is larger than unity. The same arguments apply for the presence of small-suspended solid particles.
4) The gas density affects the flow regime (hydrodynamics) of the ejector. Using higher gas densities, higher gas phase pressure differences across the ejector are required to maintain bubble flow.
5) The correlations developed for predicting the flow transition point and the gas suction rates of ejectors are specific for the nozzle and the ejector configuration used in the present study. Transition to other ejector geometries is not recommended.

NOTATION

A_N	cross-sectional area of the nozzle	m
A_{AN}	cross-sectional area of the gas annulus	m
B	constant in Eq. (3.7)	-
B_1	constant in Eq. (3.8)	-
C_1	constant in Eq. (3.5)	-
C_2	constant in Eq. (3.14) -	-
d_D	draft tube diameter	m
d_J	jet diameter	m
d_M	mixing tube diameter	m
d_N	nozzle diameter	m
Eu	Euler-number	-
P_{GC}	pressure in the gas suction chamber	Pa
P_R	pressure at the ejector outlet	Pa
$\Delta P_{G,EJ}$	gas phase pressure differential (P_R-P_{GC})	Pa
$Q_{G,GC}$	actual volumetric gas flow rate in the gas suction chamber	m^3/h
Q_L	volumetric liquid flow rate	m^3/h
$Q_{L,0}$	liquid flow rate at which gas suction commences	m^3/h
U_N	liquid jet velocity	m/s
W_N	power supplied by the jet	W
W?P	power gained by the gas phase	W
Γ	Taylor parameter, $(\rho_L/\rho_G)(\sigma/(\mu_L U_N))^2$	-
μ_G	gas viscosity	Pa.s
μ_L	liquid viscosity	Pa.s
ρ_G	gas density	kg/m^3
ρ_L	liquid density	kg/m^3
σ	surface tension	N/m

Chapter 4
Influence of the gas density and gas fraction on bubble break-up

SUMMARY

A semi-theoretical relation is presented for predicting the maximum stable bubble size present in an isotropic turbulent flow field with a dispersed phase hold-up up to 40 %. As a starting point, the theory of Levich (1962) is used. This theory includes the influence of the dispersed phase density on the maximum stable bubble size, which is not included in the theories as presented by Kolmogoroff (1949) and Hinze (1951). Using the experimental data of Wilkinson (1993), it is shown that the Levich theory predicts the influence of the gas density on the bubble stability. Via mechanistic arguments the theory of Levich could be extended to incorporate the effect of the dispersed phase hold-up on the maximum stable bubble size. Using the experimental data of Evans (1990) it is shown that the proposed relation predicts the maximum stable bubble size in dispersed phase fractions up to approximately 40 %, within 8% accuracy.

4.1 INTRODUCTION

Efficient gas dispersion with a view to obtain large interfacial areas is of great importance for mass transfer processes in gas-liquid and liquid-liquid systems. The interfacial area of a dispersion can easily be calculated when the dispersed phase fraction and the bubble or droplet sizes are known. For diluted dispersions (up to 2 or 3 %) the maximum stable bubble or droplet size present in an isotropic turbulent flow field can be derived from the well-known Kolmogoroff/Hinze and from the less known Levich theories. The main difference between these theories is that the Levich theory (1961) includes the effect of the dispersed phase density on the bubble/droplet size, whilst this effect is not included in the theories of Kolmogoroff (1949) and Hinze (1951).

Hesketh et al. (1987) compared both theories, using experimental data from the literature. It was shown that the Levich theory was able to predict bubble as well as droplet sizes with a single constant, i.e. critical Weber-number. However, how the Levich theory predicts the influence of the gas density on the maximum stable bubble size has not been verified experimentally yet. Recently, it has been recognised that the gas density has a significant effect on both the bubble break-up rate and the bubble size (Wilkinson et al. 1993). Wilkinson showed that the bubble break-up rate increases when using higher density gases. However, a relation predicting the bubble size as a function of gas density was not given.

The main objective of this chapter is to verify whether the Levich theory is able to predict the influence of the gas density on the bubble break-up rate and hence whether it can predict the maximum stable bubble size. Additionally, a general relation for predicting the maximum bubble size is proposed (based on the Levich theory) including the influence of the dispersed phase fraction on the maximum bubble size present in an turbulent flow field.

4.2 DISPERSION THEORIES

4.2.1 Bubble/Drop sizes in dilute systems

Fundamental work in dispersion theory was conducted independently by both Kolmogoroff (1949) and Hinze (1955). They postulated that the maximum stable bubble (or drop) size, d_M, is determined by the balance between the turbulent (eddy) pressure fluctuations (τd^2) tending to deform and break the bubble, and the surface tension forces (σd) resisting the bubble deformation. When the local shear stress, τ, is greater than the surface tension force, bubble break-up will occur:

$$\tau \geq \frac{\sigma}{d_B} \tag{4.1}$$

or, in dimensionless form, break-up occurs when:

$$We = \frac{\tau \cdot d_B}{\sigma} \geq 1 \tag{4.2}$$

The dynamic pressure force τ of the continuous phase was expressed by Hinze as:

$$\tau = \rho_L \cdot \overline{U}_{e,o}^2 \tag{4.3}$$

The (average) value of the fluctuating (eddy) velocity, $\overline{U}_{e,o}$, is based on an expression for the inertial sub range of isotropic turbulence:

$$\overline{U}_{e,o}^2 = 2 \cdot \left(l_e \cdot \in\right)^{2/3} \tag{4.4}$$

Finally, Hinze postulated that bubble or droplet break-up is mainly caused by eddies of the same scale as the bubble size ($l_e = d_B$). The latter assumption is based on the idea that eddies larger than the bubble will only transport the bubble whereas smaller eddies will not have enough momentum to disturb the bubble surface. Combining Eqs. (4.2)-(4.4) gives the relation for predicting the maximum stable bubble size present in an isotropic turbulent flow field:

$$d_M = \left(\frac{We_C}{2}\right)^{0.6} \cdot \left(\frac{\sigma}{\rho_L}\right)^{0.6} \cdot \left(\in\right)^{-0.4} \tag{4.5}$$

Levich (1961) postulated a similar force balance as Kolmogoroff, but considered the balance of the internal pressure fluctuations within the bubble with the capillary pressure of the deformed bubble. Levich postulated the following hypothesis for the mechanism of bubble break-up. The dynamic pressure fluctuations of the turbulent eddy in the liquid set the gas inside the bubble into motion. This motion, being rotational or turbulent in nature, creates a dynamic pressure fluctuation ($\rho_G(U_{e,G})^2$) within the bubble. This dynamic pressure is directed outward from inside the bubble. If the gas phase dynamic pressure fluctuations exceed the capillary forces holding the bubble together, the bubble must inevitably break-up. Since the density of the gas is very low compared to the surrounding medium, Levich assumed that there is complete entrainment of gas at the surface, so that the velocity of the gas is equal to that of the turbulent eddy fluctuation of the liquid phase. Using this concept, Levich introduced the dispersed phase density. Following Levich's concept, the following expression for the maximum stable diameter is obtained:

$$d_M = \left(\frac{We_C}{2}\right)^{0.6} \cdot \left(\frac{\sigma^3}{\rho_C^2 \cdot \rho_D}\right)^{0.2} \cdot (\epsilon)^{-0.4} \quad (4.6)$$

For most liquid-liquid dispersions, the densities of the dispersed and continuous phase are nearly equal and it is seen that under these condition Eq. (4.6) reduces to (4.5). Hence it can be concluded that in the case of liquid-liquid dispersions the critical Weber-numbers of the Kolmogoroff/Hinze and the Levich theory should be equal.

Hesketh et al. (1987) compared both theories using experimental data from the open literature. Both, liquid-liquid and gas-liquid dispersions were compared. For liquid-liquid dispersions, Hesketh proved that Eqs. (4.5) and (4.6) were able to predict the experimental data when using a critical Weber-number of approximately 1.1. However, for gas-liquid dispersions the critical Weber numbers were 10.6 and 1.1 for the Kolmogoroff/Hinze theory (Eq. 4.5) and the Levich theory (Eq. 4.6), respectively. The difference between these two values shows that the fluid properties are not properly accounted for in at least one theory.
For liquid-liquid dispersions, We_C calculated from the Kolmogoroff/Hinze theory is approximately 10 times smaller than the values obtained for the gas-liquid dispersion. This discrepancy would imply that the break-up mechanism of drops and bubbles is different. Yet, photographs from Holmes (1971) and Wilkinson et al. (1991) have shown that bubbles break by forming a dumbbell shape, similar to that observed by Collins and Knudson (1970) for droplet break-up. This implies that the values of We_C for droplet and bubble break-up should in principle be equal. The theory of Levich gives this result, since the values of We_C for both droplet- and bubble break-up are close to unity.
Therefore, the Levich theory is able to describe both, the break-up of bubbles and droplets in a turbulent liquid. This is demonstrated by a regression analysis of the experimental results with Eq. (4.6) as shown in Fig. 4.1.

We_C obtained from the regression is approximately 1.1. The data shown in Fig. 4.1 cover a large range of physical properties: Surface tension from 0.072 to 0.05 N/m, continuous phase viscosity between 0.001 to 0.016 Pa.s and dispersed phase density between 1 to 1000 kg/m^3.

The main objection against relation (4.6) is, that its validity is restricted to isotropic turbulent flow fields with low dispersed phase fractions (below approx. 3 %). In order to predict bubble sizes in commercial installations, the influence of the dispersed phase fraction on the bubble size has to be taken into account. It is the topic of next section.

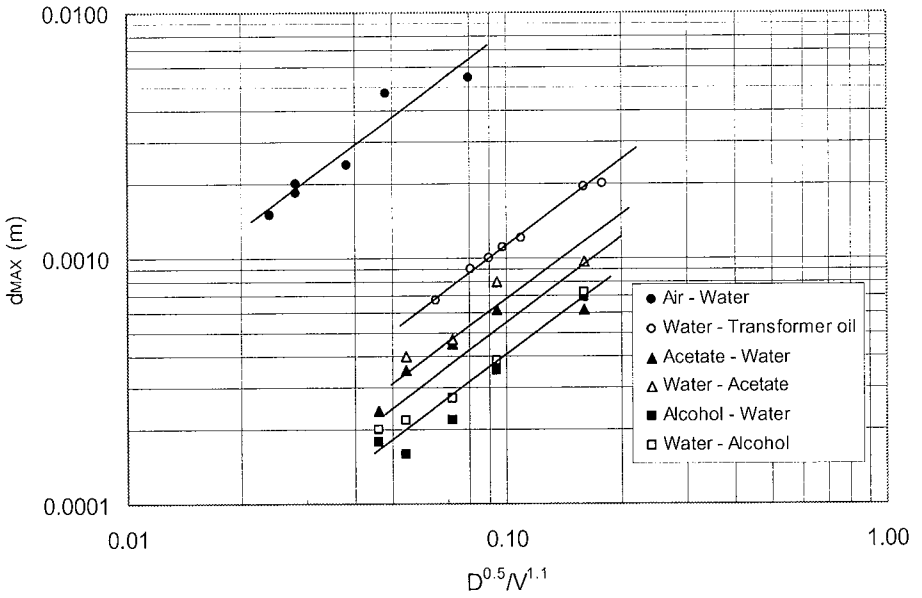

Fig. 4.1 Comparison of the experimental and calculated bubble sizes, using the Levich theory (Hesketh et al., 1987)

4.2.2 Bubble/Drop sizes in non-dilute systems

It is still not possible to give an exact description of the influence of a dispersed phase on the local turbulence intensity. However bubble break-up is determined by the local turbulent flow conditions in the neighbourhood of the bubble, so that for turbulent flows it should be sufficient to know the flow regime around the bubble. In this way bubble break-up can still be modelled using the theory of isotropic turbulence. When the micro scale of turbulence, η, is much smaller than the primary eddy size, L, the assumption of isotropic flow is fulfilled. Moo-Young and Blanch (1981) suggested that isotropy is guaranteed when the maximum stable bubble size is much larger than the micro scale of turbulence, i.e.:

(4.7) $$d_M >> \eta$$

with η defined as:

(4.8) $$\eta = \left(\frac{\nu_L^3}{\epsilon}\right)^{0.25}$$

where ϵ is the energy dissipation rate per unit mass. If Eq. (4.7) is fulfilled, eddies causing bubble break-up are in the inertial sub range and hence the characteristic eddy fluctuating velocity can be approximated using Eq. (4.4). However, relation (4.4) is only valid for diluted dispersions.

For higher dispersed phase fractions, the dispersed phase causes "damping" effects on the local turbulence intensity. Laats and Frishman (1971) postulated that the eddy fluctuation velocity for systems with higher dispersed phase fractions can be expressed as:

$$\overline{U}_{e,d} = \delta(\varepsilon_d) \cdot \overline{U}_{e,0} \tag{4.9}$$

where $\overline{U}_{e,d}$ is the mean turbulent fluctuation velocity in the presence of the dispersed phase and $\overline{U}_{e,0}$ the fluctuation velocity at zero volume fraction of the dispersed phase. The function $\delta(\varepsilon_d)$ accounts for the "damping" effect of the dispersed phase on the local turbulence intensities. $\delta(\varepsilon_d)$ must satisfy the following two conditions:

i) $\delta(\varepsilon_d=0) = 1$ and

ii) $\delta(\varepsilon_d)$ is a monotonic decreasing function of the dispersed phase fraction.

Laats and Frishman (1971) performed experiments in turbulent two phase jet flows, where rigid solid particles were used as the dispersed phase fraction. The particle diameters used ranged from 15 µm to 170 µm and the solids loading was increased up to 65 %. Their experiments showed that the function $\delta(\varepsilon_d)$ could be correlated as:

$$\delta(\varepsilon_D) = \left(\frac{1 + 0.2 \cdot \varepsilon_D}{1 + \varepsilon_D} \right) \tag{4.10}$$

It is expected that Eq. (4.10) also holds for small rigid gas bubbles. According to Beek and Muttzall (1975), gas bubbles have rigid surfaces as long as

$$d_B \leq \sqrt{\frac{\sigma}{g \cdot (\rho_L - \rho_G)}} \tag{4.11}$$

For the system water/air, bubbles will have rigid surfaces as long as the bubble diameter is less then approximately 3 mm. Combining Eqs. (4.6), (4.3), (4.9) and (4.10) and rewriting, finally gives the following relation for d_M

$$d_M = \left(\frac{We_C}{2} \right)^{0.6} \cdot \left(\frac{\sigma^3}{\rho_C^2 \cdot \rho_D} \right)^{0.2} \cdot (\epsilon)^{-0.4} \cdot \left(\frac{1 + \varepsilon_D}{1 + 0.2 \cdot \varepsilon_D} \right)^{1.2} \tag{4.12}$$

which includes both the effect of the dispersed phase hold-up and density on the maximum stable bubble size.

4.3 EXPERIMENTAL VALIDATION

4.3.1 Influence of the gas physical properties

In most papers on bubble break-up it is assumed (without experimental evidence) that the physical properties of the gas have no influence on bubble break-up. In recent papers however, bubble break-up experiments have been carried out with various gases of different molecular weight (Wilkinson (1993) and Walter and Blanch (1986)). The conclusions of these two papers regarding the influence of the gas properties are significantly different, however.

The influence of the physical gas properties on the bubble stability was studied in detail by Wilkinson (1993). Instead of maximum stable bubble sizes, Wilkinson measured bubble break-up fractions in turbulent pipe flows. The bubble break-up fraction was defined as $P_B = (N_0-N_i)/N_0$, where N_0 and N_i are the number of injected bubbles and the number of single (unbroken) bubbles. In order to evaluate this fraction, the number of injected bubbles (N_0) was at least 150.

Wilkinson (1993) performed experiments with different bubble sizes and used various gases (at ambient conditions) with a broad range in physical gas properties (density and viscosity). The results of his experiments are shown in Fig. 4.2, where the bubble break-up fraction (P_B) is plotted against the gas density for four (4) bubble sizes.

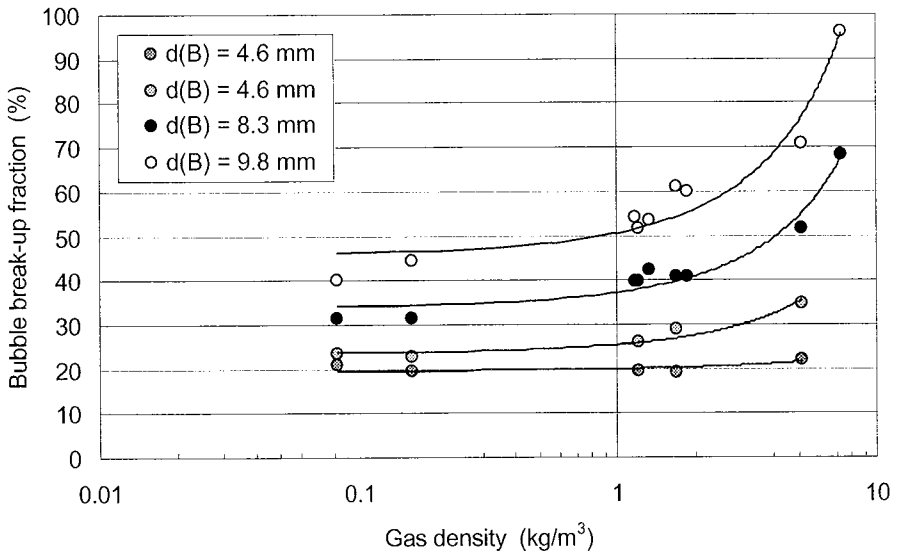

Fig. 4.2 Bubble break-up fraction vs. gas density for four bubble diameters
d(B) = diameter of injected bubble, (Wilkinson, 1993)

The fact that the results in this figure for all the different gases lie on a single line for each of the four bubble sizes clearly demonstrates that bubble break-up depends on bubble size. More surprisingly, however bubble break-up appear to depend on the gas density and not on the gas viscosity. The latter can be seen from Table 4.1, which shows that the results are well correlated with the gas density, whereas the results show no correlation with the gas viscosity. According to Walter and Blanch (1986), the difference in bubble stability between helium, nitrogen, air and argon could be attributed to the difference in gas viscosity.

Table 4.1 Summary of bubble break-up experiments of Wilkinson (1993).

Gas	$10^5 \mu_G$ (Pa.s)	ρ_G (kg/m^3)	$d_{B,EXP}$ (mm)	P_B(1) (%)	We(2) (-)
Hydrogen	0.87	0.083	4.6	21.00	0.38
Helium	1.94	0.16	4.6	19.50	0.48
Air	1.84	1.21	4.6	19.5	0.94
Argon	2.1	1.69	4.6	19.02	1.05
Freon 12	1.28	5.16	4.6	22.20	1.52
Hydrogen	0.87	0.083	5.8	23.40	0.56
Helium	1.94	0.16	5.8	22.80	0.7
Air	1.84	1.21	5.8	26.10	1.38
Argon	2.1	1.69	5.8	28.80	1.54
Freon 12	1.28	5.16	5.8	34.70	2.24
Hydrogen	0.87	0.083	8.3	31.5	1.03
Helium	1.94	0.16	8.3	31.5	1.28
Nitrogen	1.75	1.18	8.3	39.6	2.49
Air	1.84	1.21	8.3	39.67	2.51
Oxygen	2.02	1.33	8.3	42.4	2.59
Argon	2.10	1.69	8.3	40.7	2.8
Propane	0.81	1.87	8.3	40.8	2.9
Freon 12	1.28	5.16	8.3	51.6	4.07
Freon 114	1.08	7.36	8.3	68.3	4.58
Hydrogen	0.87	0.083	9.8	40.2	1.35
Helium	1.94	0.16	9.8	44.5	1.69
Nitrogen	1.75	1.18	9.8	54.2	3.28
Air	1.84	1.21	9.8	51.6	3.31
Oxygen	2.02	1.33	9.8	53.3	3.41
Argon	2.10	1.69	9.8	60.9	3.70
Propane	0.81	1.87	9.8	59.9	3.82
Freon 12	1.28	5.16	9.8	70.6	5.36
Freon 114	1.08	7.36	9.8	96.2	6.04

(1) P_B: bubble break-up frequency
(2) Calculated using Eq. (4.6), where $d_M = d_{B,EXP}$

A reinterpretation (by Wilkinson, 1993) of these results of Walter and Blanch however showed that their results can equally well be correlated with gas density which is again in accordance with the experimental observations of Wilkinson.

An alternative way for proving Levich's theory is to calculate the Weber number of the bubbles of Wilkinson's break-up experiments. Using Eq. (4.6) the Weber-number of the injected bubbles, i.e. $d_M = d_{B,EXP}$, was calculated. These results are shown in Table 4.1 in the last column. It is seen that as long as the Weber-numbers are less than 1, the bubble break-up fraction P_B remains at a nearly constant minimum value. These results are an additional support for the conclusion that the gas density influences bubble break-up and that We_C at which bubble break-up commences is of the order of one (1).

4.3.2 Influence of the dispersed phase fraction

In order to verify, the validity of Eq. (4.12) with respect to the effect of the dispersed phase hold-up, the correlation is tested with experimental data from the open literature (Evans, 1990). Evans measured bubble size distributions in the mixing zone at the top of a plunging liquid jet column. From these experiments the maximum stable bubble size present in the mixing zone was determined as a function of a) the energy dissipation rate and b) the gas hold-up within this section. Most experiments were carried out with gas fractions of approximately 10-12 % but in some experiments gas fractions went up to 40 %. A summary of these experiments is given in Table 4.2. A parity plot, Fig. 4.3, shows that Eq. (4.12) is able to predict the experimental data very well, over the whole range.

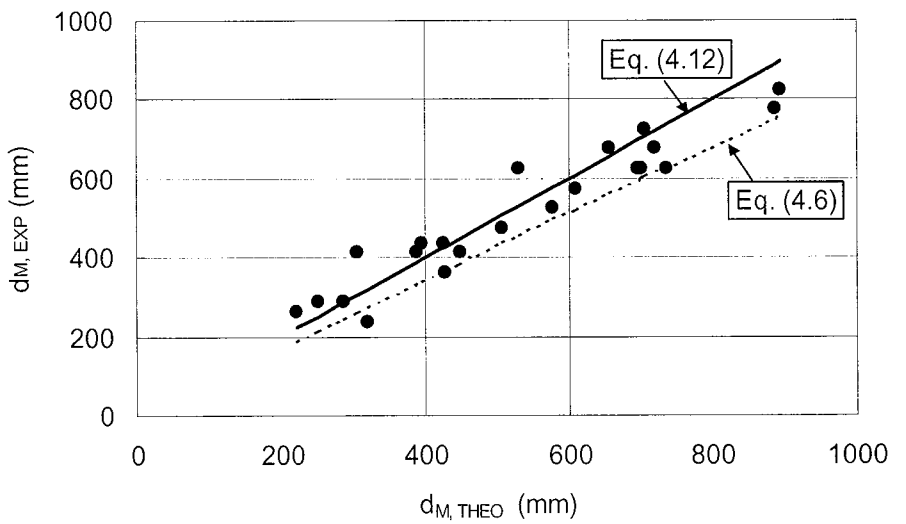

Fig. 4.3 Parity plot between the predicted and experimental maximum stable bubble sizes, reported by Evans (1990) and predicted values from Eqs. (4.6) and (4.12).

For calculating the maximum stable bubble size, the critical Weber-number was taken as 1.1, as proposed by Hesketh and validated by Wilkinson's experiments. Fig. 4.3 shows that the predicted values generally are accurate within 8 %, relative to the measured values. Neglecting the damping effect of the dispersed phase fraction on the liquid turbulence results in a systematic underestimation of d_B by approximately 10 to 12 %. From this it is concluded, that application of Eq. (4.12) is validated for turbulent flow fields with higher dispersed phase fractions.

Table 4.2 Summary of experimental conditions and results of Evans (1990).

Exp. No	σ (N/m)	ρ_L (kg/m^3)	ε_G	$\in$ (W/kg)	$d_{B,MAX}$ (μm)
2	0.048	997	0.106	2691	237.5
5	0.054	998	0.104	5881	287.5
8	0.062	998	0.105	4429	412.5
11	0.047	997	0.114	3466	287.5
14	0.053	997	0.114	7885	262.5
17	0.063	997	0.113	2549	412.5
23	0.054	998	0. 113	1604	437.5
32	0.064	1061	0.113	1934	362.5
41	0.065	1114	0.116	1690	412.5
64	0.065	999	0.111	2544	437.5
72	0.063	998	0.102	1275	475
74	0.065	999	0.112	1224	625
75.1	0.063	999	0.112	824	575
75.2	0.063	999	0.228	647	625
75.3	0.063	999	0.392	538	775
76.1	0.064	999	0.111	584	725
78	0.064	998	0.116	609	625
81	0.061	998	0.102	879	525
84	0.069	990	0.113	793	675
87	0.062	998	0.115	310	825
95.1	0.063	999	0.111	542	675
101	0.062	998	0.110	564	625

4.5 CONCLUSIONS

A relation has been derived, based on fundamental considerations, predicting the maximum stable bubble size present in an isotropic turbulent liquid flow field up to 40 ç gas hold-up. As a basis, the theory of Levich (1962) was used. This theory was extended to systems where the effect of the dispersed hold-up on the local turbulence intensity can no longer be neglected. The novel relation proved to predict the experimental data of Evans (1990), who used dispersed phase fractions up to 40 %. It is also demonstrated that the experimental results of Wilkinson (1993), dealing with the effect of the gas density on the

bubble stability, can be understood from Levich's theory of the effect of turbulence on bubble size.

NOTATION

d_B	bubble diameter	m
d(B)	bubble diameter	m
d_M	maximum stable bubble diameter	m
d_S	Sauter mean bubble diameter	m
d_T	tube diameter	m
l_e	turbulence size in the inertial sub-range	m
L	scale of the main flow	m
P_B	bubble break-up frequency	m
$\overline{U}_{e,o}$	eddy fluctuation velocity	m/s
We	Weber-number	
We_C	critical Weber number at which bubble break-up commences	
ε_G	dispersed gas phase fraction	
$\in$	energy dissipation rate	W/kg
η	micro scale of turbulence	m
μ_G	dynamic gas viscosity	Pa.s
μ_L	dynamic liquid viscosity	Pa.s
ν_L	kinematic liquid viscosity	m^2/s
ρ_C	continuous phase density	kg/m^3
ρ_D	dispersed phase density	kg/m^3
ρ_G	gas density	kg/m^3
ρ_L	liquid phase density	kg/m^3
ρ_M	mixture density = $\rho_L(1-\varepsilon_G)$	kg/m^3
σ	surface tension	N/m
τ	turbulent stresses	N/m^2

Chapter 5
Influence of the ejector configuration and the gas density on the mass transfer characteristics of gas-liquid ejectors

SUMMARY

For the design and scale-up of gas-liquid ejectors, reliable data are required which describe the mass transfer characteristics as a function of the physical fluid properties, the geometrical design and the process related parameters. Therefore, the mass transfer characteristics of various ejector geometries and scales were investigated using desorption of the oxygen from water, by means of an inert gas, as a model system. In order to investigate scale-up, the ejector was geometrically scaled-up by a factor of 2 (and hence a volumetric scale-up by a factor of 8). Since industrial venturi reactors are operated at elevated pressures, the influence of the gas density on the mass transfer characteristics was also studied. The experimental results show that geometrical design parameters, like the presence of a swirl device in the upstream section of the nozzle, the mixing tube length and the nozzle to mixing tube diameter ratio, all influence the mass transfer characteristics significantly. Further, it was experimentally verified that the gas density influences the mass transfer characteristics also. It was observed that the volumetric mass transfer coefficient (k_La) increased when higher density gases are used. The main objective of this chapter is investigating the influence of the ejector geometry on the mass transfer characteristics of gas-liquid ejectors and to formulate design and scale-up rules/criteria.

5.1 INTRODUCTION

Gas-liquid interfacial mass transfer often controls the overall production rate of gas-liquid reactors. High intensity "gas-liquid (in line) mixers", like static mixers, rotor stators and ejectors, are increasingly used as a primary gas dispersion device in gas-liquid reactors (Zhu et al., 1992 and Schugerl, 1982). These high intensity mixers can improve the mass transfer rates by generating small bubbles, which are then injected into a reaction vessel/column, thereby improving the mass transfer characteristics of the entire system.

A typical example of such a gas-liquid reactor is the "Loop Reactor" (BLR). In this reactor type, the gas phase is initially dispersed in the venturi (ejector) section. Recently, these venturi reactors have frequently been recommended for processes where gas-liquid interfacial mass transfer was the rate-controlling step of the process.
Systematic investigations concerning venturi-reactors have been reported by Cramers et al. (1992) and Dirix and van de Wiele (1990). According to these authors, it is very important to investigate the mass transfer characteristics of the ejector and reaction vessel separately. Their studies showed that the ejector and the reaction vessel have to be considered as two reactor units in series. The ejector can be modelled as a plug flow reactor, whereas the reaction vessel has to be considered as ideally mixed. Experimental verifications showed that the k_La-values of the ejector and the reaction vessel differ nearly two orders of magnitude.

Although there have been a number of papers on liquid jet ejectors, none of them provides all the information that is required for a reliable design and scale-up as a function of geometrical and process related parameters. To our knowledge there are only three papers in the open literature were the mass transfer characteristics of ejectors have been studied in more detail. The proposed correlations, which describe the liquid side volumetric mass transfer coefficient of the ejectors used, are given in Table 5.1. This table shows that the mass transfer characteristics of ejectors improve when:

a) more energy is dissipated per unit mass (ϵ) and
b) the gas fraction (higher Q_G/Q_L ratios) is increased.

Further, Dirix and van de Wiele (1990) showed that higher k_La-values are obtained when the nozzle to mixing tube diameter ratio is increased. How the other design parameters affect the mass transfer rates has not been reported. Given the variety of ejector configurations studied, it is not surprising that the constants and exponents of the correlations in Table 5.1 vary considerably.

It should be mentioned that the data of Dirix and van de Wiele (1990) were obtained with a spinner (swirl device) in the upstream section of the nozzle, whereas in both other studies no spinner was present. Whether the presence of this swirl device affects the mass transfer characteristics of the ejector section is still an open question. It is known that the swirl device improves the maximum amount of gas sucked in by ejectors (Henzler, 1981). However, whether the swirl device influences the mass transfer characteristics was not reported.

Table 5.1 Correlations for ejector systems from literature

Authors	Correlations	Flow regime
Cramers et al. (1992)	$a = 19500 \cdot (\in)^{0.40} \cdot (1-\varepsilon_G)^{-0.4}$	Down flow ejector Non coalescing system
Changfeng et al. (1991)	$k_La = 0.7206 \cdot (\in)^{0.492} \cdot (\varepsilon_G)^{0.88}$ $a = 918 \cdot (\in)^{0.372} \cdot (\varepsilon_G)^{0.74}$ $d_S = 6.52 \cdot 10^{-3} \cdot (\in)^{-0.372} \cdot (\varepsilon_G)^{0.261}$	Down flow ejector Coalescing system
Dirix et al. (1990)	$k_La = 5.4 \cdot 10^{-3} \cdot (\in)^{0.66} \cdot \varepsilon_G \cdot \left(\frac{d_N}{d_D}\right)^{0.66}$ (1) $k_La = 8.5 \cdot 10^{-4} \cdot (\in)^{0.66} \cdot \left(\frac{d_N}{d_M}\right)^{0.66}$ (2)	Down flow ejector Coalescing system (1) Bubble flow regime (2) Jet flow regime

The main objective of this chapter is investigating the influence of the ejector geometry on the mass transfer characteristics of gas-liquid ejectors and to formulate design and scale-up rules/criteria.

5.2 DEVELOPMENT OF DESIGN RELATIONS

In order to develop design relations for the mass transfer characteristics of ejectors, the following theoretical approach is followed. The volumetric mass transfer coefficient (k_La) consists of the physical mass transfer coefficient (k_L) and the specific interfacial area (a).

In case homogeneous gas dispersion is considered, the specific interfacial area follows from:

$$a = \frac{6 \cdot \varepsilon_G}{d_S} \tag{5.1}$$

The specific interfacial area (a) can be calculated once the gas fraction (ε_G) and Sauter mean bubble diameter (d_S) is known.

Bubbly flow is assumed in which small discrete bubbles move downward with nearly the same velocity as the liquid phase, i.e. no slip conditions. Due to the high-energy dissipation rates within ejectors the bubble sizes dispersed within the ejector section are relatively

small. Cramers et al. (1992) reported averaged bubble sizes in the range between 30-60 μm when using coalescence-inhibited medium. When using a coalescence promoting fluid, the averaged bubble sizes were in the range between 0.1 and 1 mm. Therefore is it justified to assume that the relative velocity difference between the gas and the liquid phase can be neglected. Under these conditions the gas fraction is approximated by:

$$\varepsilon_G = \frac{Q_G}{Q_G + Q_L} \tag{5.2}$$

where Q_L and Q_G are the volumetric liquid and gas flow rates, respectively.

In order to predict d_S, it is assumed that the Sauter bubble diameter can be related to the maximum stable bubble size present in a turbulent flow field (d_M). The size distribution of bubbles formed by breaking up in a turbulent flow field has been studied extensively by many workers (Lewis and Davidson, 1982; Unno and Inoue, 1980; Hesketh et al, 1987 and Evans, 1990; Brown and Pitt, 1972; Zang et al., 1985; Calabrese et all., 1986). These studies show that for coalescing media the ratio of the Sauter mean bubble and the maximum stable bubble diameter in turbulent pipe flows is constant, i.e.

$$\frac{d_S}{d_M} = \text{constant} = C_1 \tag{5.3}$$

From the experimental results of the above-mentioned studies, it follows that the value of C_1 is nearly constant and varies between 0.6 and 0.7.

In Chapter 4 it was shown that the maximum stable bubble diameter present in a turbulent flow field is approximated by:

$$d_M = \left(\frac{We_C}{2}\right)^{0.6} \cdot \left(\frac{\sigma^3}{\rho_L^2 \cdot \rho_G}\right)^{0.2} \cdot (\epsilon)^{-0.4} \cdot \left(\frac{1+\varepsilon_G}{1+0.2\cdot\varepsilon_G}\right)^{1.2} \tag{5.4}$$

Substitution of Eqs (5.3) and (5.4) into (5.1) gives a relation for the specific gas-liquid interfacial area as a function of the physical gas and liquid properties of the liquid phase, the power input per unit mass input and the gas fraction, i.e.:

$$a = C_2 \cdot (\epsilon)^{0.4} \cdot \varepsilon_G \cdot \left(\frac{1+0.2\cdot\varepsilon_G}{1+\varepsilon_G}\right)^{1.2} \tag{5.5}$$

where

$$C_2 = C_1 \cdot \left(\frac{\rho_L^2 \cdot \rho_G}{\sigma^3}\right)^{0.2} \cdot \left(\frac{We_C}{2}\right)^{-0.6} \tag{5.6}$$

The physical mass transfer coefficient (k_L) is obtained from the equation of Kawase and Moo-Young (1991), i.e.

$$k_L = C_3 \cdot \sqrt{D_L} \cdot \left(\frac{\in}{\nu_L}\right)^{0.25} \tag{5.7}$$

where D_L and ν_L are the diffusion coefficient of the gas in the liquid and kinematic viscosity, respectively. This equation was obtained from both experimental and theoretical studies. Application of Eq. (5.7) is most successful for gas-liquid dispersions in which the energy dissipation rate is homogeneously distributed over the entire flow field.

Combination of Eqs. (5.5) and (5.7) gives than finally the semi-theoretical relation for k_La:

$$k_La = C_4 \cdot (\in)^{0.65} \cdot \varepsilon_G \cdot \left(\frac{1+0.2 \cdot \varepsilon_G}{1+\varepsilon_G}\right)^{1.2} \tag{5.8}$$

where

$$C_4 = C_3 \cdot \left(\frac{D_L^2}{\nu_L}\right)^{0.25} \cdot \left(\frac{\rho_L^2 \cdot \rho_G}{\sigma^3}\right)^{0.2} \cdot \left(\frac{We_C}{2}\right)^{-0.6}$$

Eq. (5.8) underlines the importance of the local energy dissipation rate. Therefore, it is essential to define a relation for the energy dissipation rate that is effectively used for gas dispersion.

The energy supplied by a high velocity jet (P_{Jet}) can be expressed as

$$P_{Jet} = 0.5 \cdot \rho_L \cdot U_N^2 \cdot Q_L \tag{5.9}$$

provided, the kinetic energy of the upstream velocity for the nozzle and the downstream velocity of the two phase mixture at the ejector outlet can be neglected. In Eq. (5.9) U_N equals to the jet velocity at the nozzle exit. The energy supplied by the high velocity jet is mainly used for dispersing the gas phase. However, also a considerable amount of this energy input is used for compressing the gas. In fact, the energy used for gas compression is not effectively used for "mixing" of both phases and should be taken in consideration when calculating the effective energy input by the liquid jet used for gas dispersion. The energy consumed for compressing the gas phase ($P_{Compres}$) can be estimated by

$$P_{Compres} = \Delta P_{G,Ej} \cdot Q_G \tag{5.10}$$

where $\Delta P_{G,EJ}$ equals the gas phase pressure differential across the ejector.

The importance of Eq. (5.10) is shown in the following example. In Chapter 3 it was shown that the amount of gas sucked in by the ejector is influenced by the gas phase pressure differential. As an example, a jet velocity of 20 m/s and gas- and liquid flow rates of 5 m^3/h will be assumed. For a Henzler type of ejector, the pressure differential required for obtaining Q_G/Q_L of 1 is approximately 40 kPa. Substitution of these data in Eqs. (5.9) and (5.10) shows that under these conditions approximately 20 % of the energy supplied by the liquid jet is used for gas compression instead of gas dispersion.

The energy dissipation rate effectively used for gas dispersion ($\in_{Dis}$) can than be calculated as:

$$\in_{Dis} = \frac{(P_{Jet} - P_{Compres})}{\rho_M \cdot V_{Ej}} \qquad (5.11)$$

where ρ_M is the density of the two-phase mixture in the ejector and V_{EJ} is the ejector volume. In order to develop design relations for the mass transfer characteristics of ejectors, Eqs. (5.8) and (5.11) will be used.

5.3 EXPERIMENTAL FACILITY AND PROCEDURES

5.3.1 Experimental set-up

A schematic diagram of the ejector and the experimental facility used is shown in Fig. 5.1. The volumetric gas-liquid mass transfer rates were calculated from the measured desorption rate of oxygen from the liquid phase (deionized water) into an inert gas phase (when not mentioned, the gas phase used is nitrogen) as a model system. The liquid was first aerated in a large supply vessel (V=500 litre) before entering the ejector. The temperature and oxygen concentration in the liquid phase were measured continuously at the ejector entrance, ejector outlet and outlet of the reaction vessel (as shown in Fig. 5.1). The flux of oxygen transferred in the ejector and the reaction vessel could, thus be evaluated separately.

A special measuring cell was developed in which a separation of the gas and the liquid phase was realised. This was necessary to prevent that the gas bubbles interfered with the measurement of the actual oxygen concentration in the liquid phase.

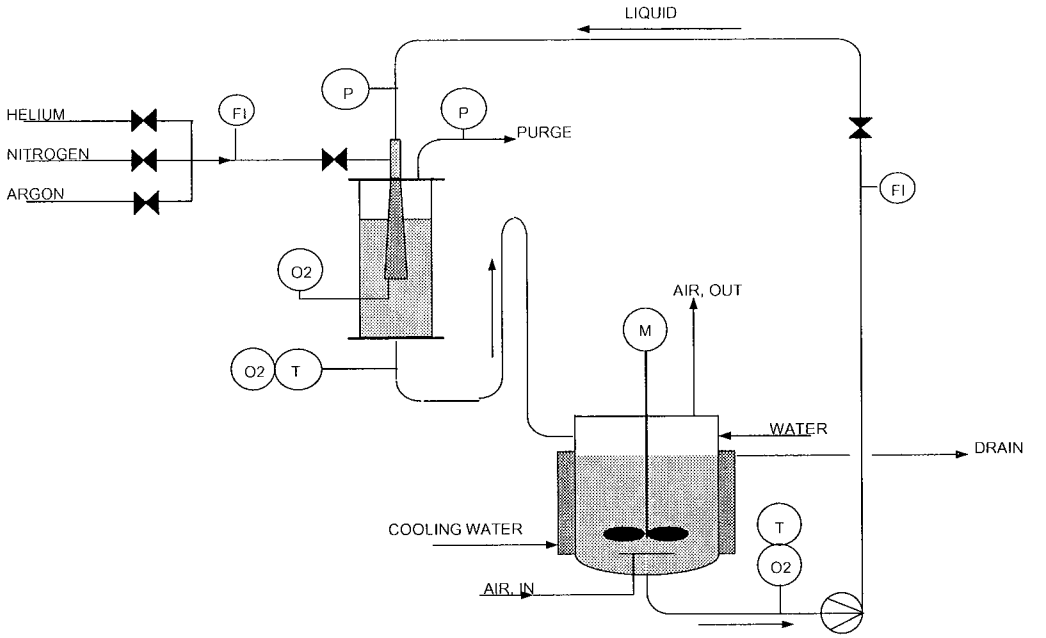

Fig. 5.1 Scheme of the experimental set-up

The ejector configuration used in the present study had a mixing tube diameter (d_M) of 12 mm, diffuser outlet diameter of 35 mm (i.e. diffuser angle of approx. 3) and a draft tube length (L_D) of 630 mm. The mixing tube lengths was varied between 24 and 120 mm, respectively. The nozzle diameters used were 4.0 mm, 4.7 mm and 5.3 mm. In order to investigate scale-up, the ejector was geometrically enlarged with a factor 2 (the ejector with the mixing tube length of 24 mm).

5.3.2 Procedures

To gain more insight in the behaviour of venturi reactors it is necessary to quantify to what extent the mass transfer takes place in the ejector. A first order differential equation and a mass balance for oxygen can describe the decrease of the oxygen concentration in the liquid phase of the ejector. The following assumptions are made:

- in the ejector, the gas and the liquid move in cocurrent plug flow
- the gas flow is considered to be constant
- a pure inert gas is supplied
- the gas side mass transfer resistance is negligible (He k_G >>k_L), where He is the Henry coefficient for oxygen in water

(5.12) $$Q_L \cdot dC_L = k_L a \cdot (C_{L,i} - C_L) \cdot dV$$

(5.13) $$Q_L \cdot (C_{L,in}-C_L) = Q_G \cdot C_G = Q_G \cdot He \cdot C_{L,i}$$

The concentration of the oxygen in the liquid phase at the ejector outlet can then be represented by:

(5.14) $$C_{L,out} = C_{L,in} \cdot \left(\frac{\frac{Q_L}{Q_G \cdot He} + EXP\left(-k_L a \cdot \frac{V_{Ej}}{Q_L} \cdot \left(1 + \frac{Q_L}{Q_G \cdot He} \right) \right)}{1 + \frac{Q_L}{Q_G \cdot He}} \right)$$

where V_{Ej} is the dispersion volume in the ejector and He is the Henry coefficient for oxygen in water. Based on molar concentrations and a temperature of 20 °C the Henry-number (He) equals to 29.

5.4 EXPERIMENTAL RESULTS HYDRODYNAMICS

5.4.1 Hydrodynamics

In this section the influence of a swirl device in the upstream section of the nozzle, the d_N/d_M-ratio, the mixing tube length and the scale on the ejector hydrodynamics will be discussed.

5.4.1.1 Influence of swirl device on flow regime

The experiments have proved that two different flow regimes can be distinguished in ejectors, depending on the gas-liquid flow ratio. At low Q_G/Q_L-ratios (and hence high gas phase pressure differentials) bubbly flow was observed, independent whether a swirl device was present or not. At higher Q_G/Q_L-ratios there was a change in flow regime as illustrated schematically in Fig. 5.2.

In the absence of a swirl device, a slowly widening liquid jet exists which abruptly transforms into a gas-liquid dispersion in the ejector. It was observed that the mixing zone location (the place where the liquid jet discharges into the bubbly mixture) was influenced by the gas-liquid flow ratio, i.e. with increasing gas flow rates (and hence decreasing $\Delta P_{G,Ej}$) the mixing zone location shifts from the mixing tube entrance towards the ejector outlet. If the gas dispersion takes place in the mixing tube, so-called "bubble flow" occurs. If gas dispersion takes place in the diffuser or draft tube, the system operates in the so-called "jet-flow" regime.

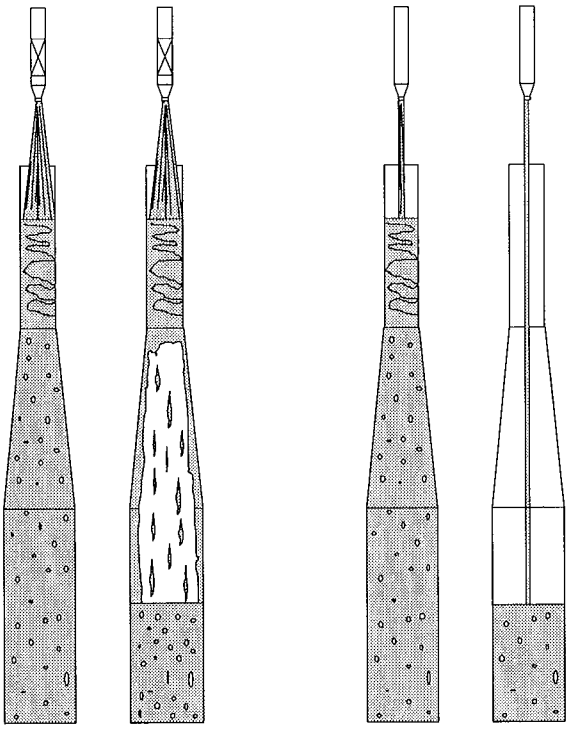

(a) ejector with swirl device (b) without swirl device

Fig. 5.2 Flow regimes in the ejector

When a swirl device was present in the up-stream section of the nozzle, the liquid jet "disintegrated" rather fast, compared to the situation in absence of the swirl device. This fast widening of the liquid jet is caused by the centrifugal forces caused by the tangential velocity component of the swirl. Visually it was observed that the mixing zone location in the ejector remains nearly fixed in the mixing tube, independent of the gas-liquid flow rate. Although there was no change in the mixing zone location, there was still a change in flow regime. At low gas-liquid flow ratios bubbly flow appeared, with similar characteristics as observed for bubble flow regime without a swirl device in the nozzle. When using a swirl device, at higher Q_G/Q_L-ratios the so-called "jet-annular" flow was observed as illustrated in Fig. 5.2. In this "jet-annular" flow regime, the gas is dispersed in the mixing tube and is then ejected through out of the mixing tube in the diffuser. At the diffuser wall a "stagnant" liquid layer is formed. The jet in the core of the ejector seemed to consist of a gas stream carrying rags (ligaments) of liquid.

The experimental observations, as described above, have shown that the presence of a swirl device in the nozzle has a significant effect on the ejector hydrodynamics. Below the

influence of the d_N/d_M-ratio, the mixing tube length and the scale, all on the flow transition point (the Q_G/Q_L flow ratio at which the change in flow regime occurs).

5.4.1.2 Influence of geometrical design and scale on flow regime

The influences of the geometrical parameters on the flow transition point are shown in Figs. 5.3a and b.

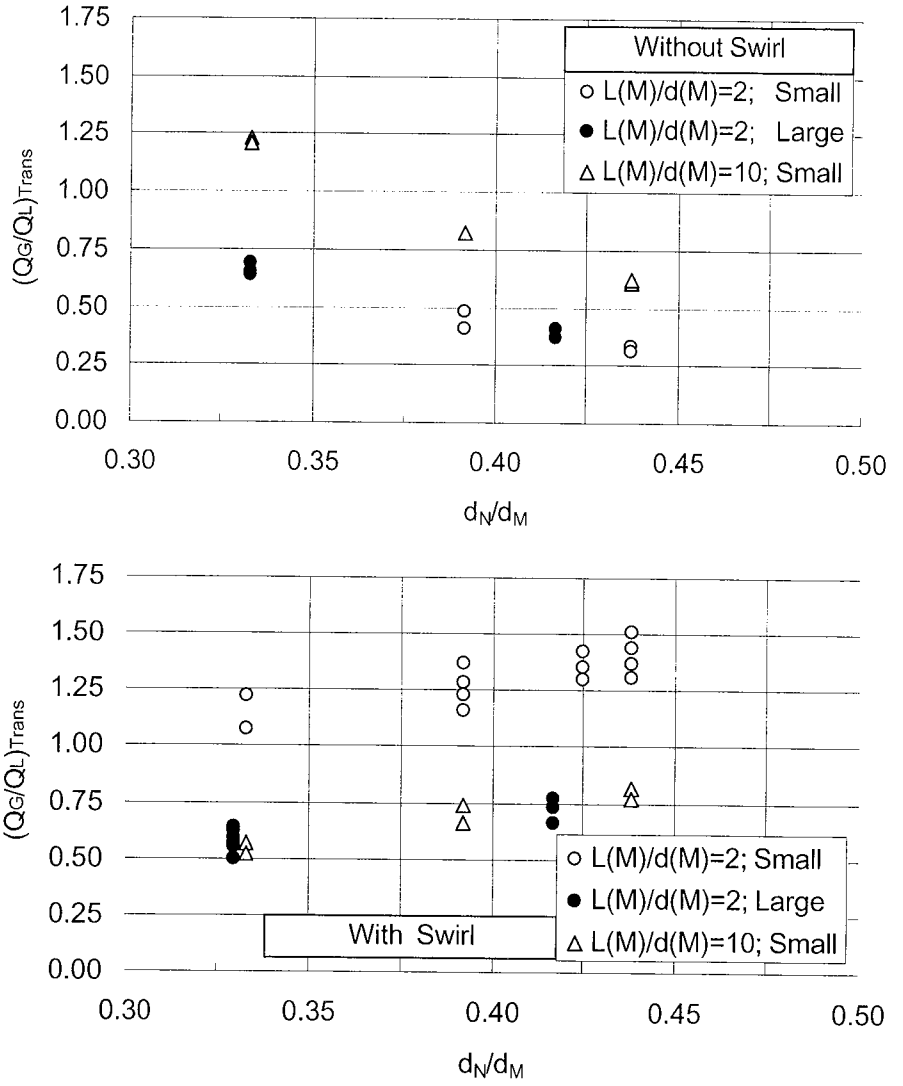

Fig. 5.3 Influence of the geometrical parameters on flow regimes in the ejector: (a) without swirl device and (b) ejector with swirl device

Fig. 5.3a shows that in the absence of a swirl device the flow transition point increases with increasing mixing tube L/D-ratio and decreasing d_N/d_M-ratio. Further it is seen that the transition point is independent of scale.

If a swirl device is present, Fig. 5.3b shows that the reverse is true. In order to explain this scale effect, the spinning action of the high velocity jet has to be considered. The swirl device in the upstream section of the nozzle gives a tangential velocity component to the liquid flow. The ratio of the tangential to the axial jet velocity can be characterised with a Swirl number (Sw) which is defined as (see Appendix A3 and/or Palmer and Musketh ,1984):

$$Sw = \left(\frac{U_{Tan}}{U_{Ax}}\right) = \left(\frac{\Theta \cdot r_N}{l_s}\right) \tag{5.15}$$

where r_N, Θ and l_s are the nozzle outlet radius and the angle and the length of the swirl device, respectively.

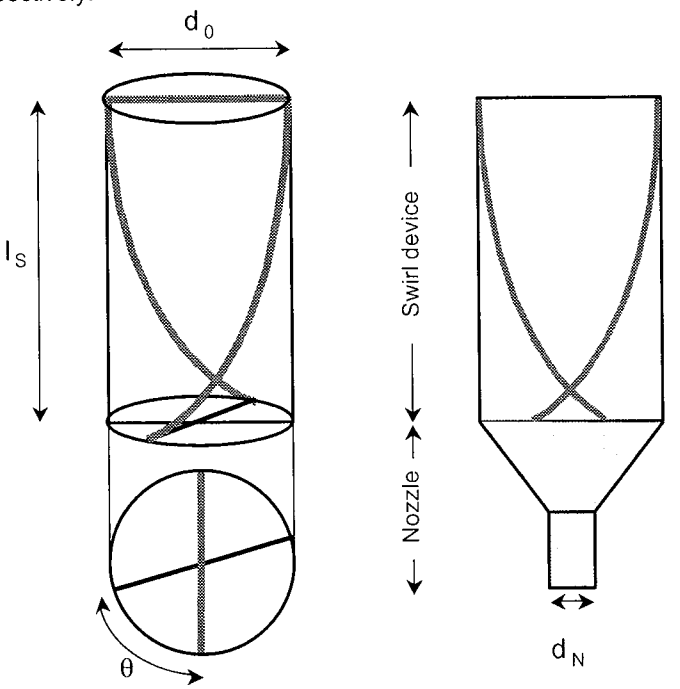

Fig. A 3.1 Geometrical parameters of Swirl device and connection to ejector nozzle.

Eq (5.15) shows that in a non-linear scale-up of the swirl device and nozzle, the tangential velocity of the liquid jet changes (since the Swirl number changes), resulting in scale effects.

During our scale-up experiments, the linear dimensions of the ejector and nozzle were enlarged in size linearly. However, the swirl device used in the experiments (for the small and enlarged ejector) remained the same and hence the swirl number (Sw) increased when using the enlarged ejector sizes.

Since the swirl device causes rotation of the liquid phase, the mixing tube of the ejector can be compared to a hydrocylone when high swirl numbers are present. With increasing centrifugal forces, separation of the gas and liquid phase is enhanced, resulting in a decrease of the flow transition point upon linear scale-up and longer mixing tube lengths. These centrifugal forces are also responsible for the characteristic "jet-annular" flow regime when applying a swirl device in the nozzle. Due to the rotational forces, both phases will be separated, resulting in a characteristic gas core in both the diffuser and the draft tube section when applying a swirl device.

From the above observations it is concluded that a direct linear scale-up is only possible when no swirl device is used. When using a swirl device, the geometry of the swirl has to depent on a constant Swirl-number, to allow a reliable scale-up of the ejector. Since, geometrical parameters affect the local ejector hydrodynamics, it is expected that the mass transfer characteristics of ejectors are also influenced by these parameters, as will be discussed below.

5.5 EXPERIMENTAL RESULTS MASS TRANSFER RATES

5.5.1 Influence of the ejector configuration

In the previous section it has been demonstrated that the ejector configuration has a significant effect on the flow regime in the ejector. Therefore, we investigated the influence of the swirl device, the mixing tube length, the d_N/d_M-ratio and the effect of scale, all on the mass transfer performance of ejectors.

5.5.1.1 Influence of the swirl device

A systematic investigation concerning the influence of a swirl device on the volumetric mass transfer coefficient (k_La) has not been reported in the literature yet. Therefore some preliminary experiments were carried out with an ejector with an L_M/d_M-ratio of 2 and a nozzle diameter of 4.7 mm. In Fig. 5.4 the experimentally determined $(k_La)_{Ej}$-value is plotted against the volumetric gas/liquid flow ratio. Fig. 5.4 shows that the ejector without a swirl device creates higher k_La-values compared to the ejector with a swirl device in the nozzle and it is seen that k_La increases with Q_G/Q_L. In case a swirl device is present, two different flow regimes can be clearly distinguished, i.e. the diagram shows a discontinuity at the flow transition point from bubble- to jet-annular flow, respectively. The experimental data as shown in Fig. 5.4 give a representative example of all the experiments performed.

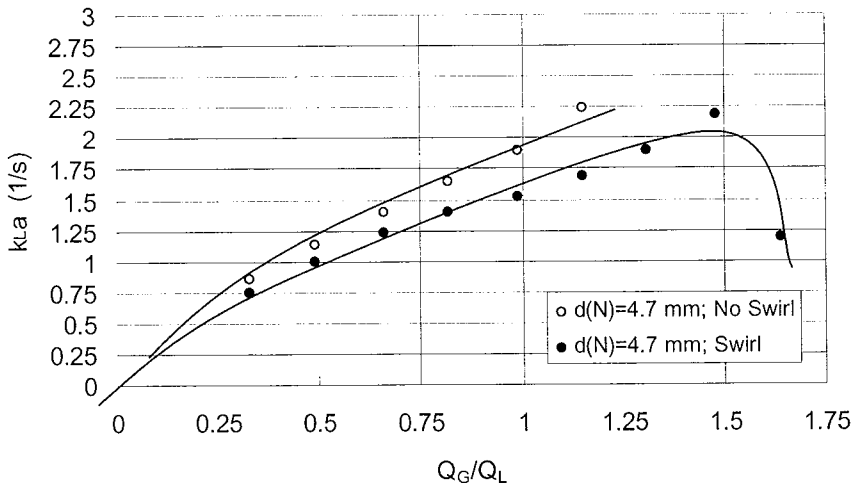

Fig. 5.4 Influence of a swirl device on the volumetric mass transfer coefficient (Q_L=0.5 l/s, d_N =4.7 mm, L_M/d_M =2, System: water/nitrogen).

Since the ejector without a swirl device creates higher k_La-values it is concluded that this ejector configuration utilises the supplied energy more effective. In order to verify this statement, the gas phase pressure differential across the ejector ($\Delta P_{G,Ej}$) is plotted versus Q_G/Q_L in Fig. 5.5. This figure shows that the ejector with swirl device requires higher gas

phase pressure differentials for the same Q_G/Q_L. In other words, when using a swirl device, more energy is used for gas compression instead of gas dispersion.

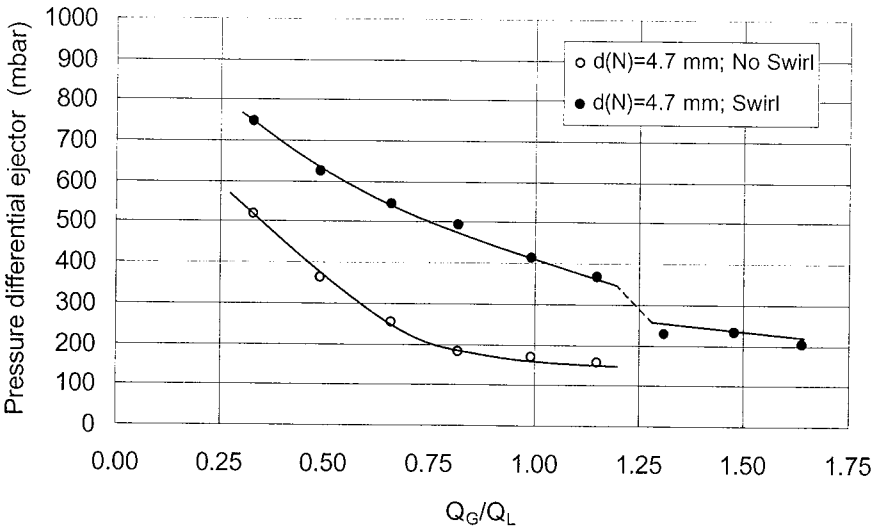

Fig. 5.5 Influence of a swirl device on the gas phase pressure differential (Q_L = 0.5 l/s, d_N =4.7 mm, L_M/d_M =2, System: water/nitrogen).

In order to exclude the effect of the energy consumed for compressing the gas phase, use will be made of Eqs. (5.8) and (5.11). Therefore in Fig. 5.6, $(k_La)^*_{Ej}$ is plotted versus $(\varepsilon_G)^*$ in the ejector. In these figures $(k_La)^*_{Ej}$ and $(\varepsilon_G)^*$ are defined as

$$(k_La)^*_{Ej} = \left(\frac{k_La}{(\in_{Dis})^{0.65}}\right) \tag{5.16}$$

and

$$(\varepsilon_G)^* = \varepsilon_G \cdot \left(\frac{1+0.2\cdot\varepsilon_G}{1+\varepsilon_G}\right)^{1.2} \tag{5.17}$$

Fig. 5.6 shows that at a constant energy dissipation rate based on ejector volume, $\in_{Dis}$, the ejector without swirl device still creates slightly higher k_La-values.

From this it can be concluded that a swirl device decreases the efficiency of the ejector with respect to mass transfer. A physical explanation for this observation will be given in Chapter 6.

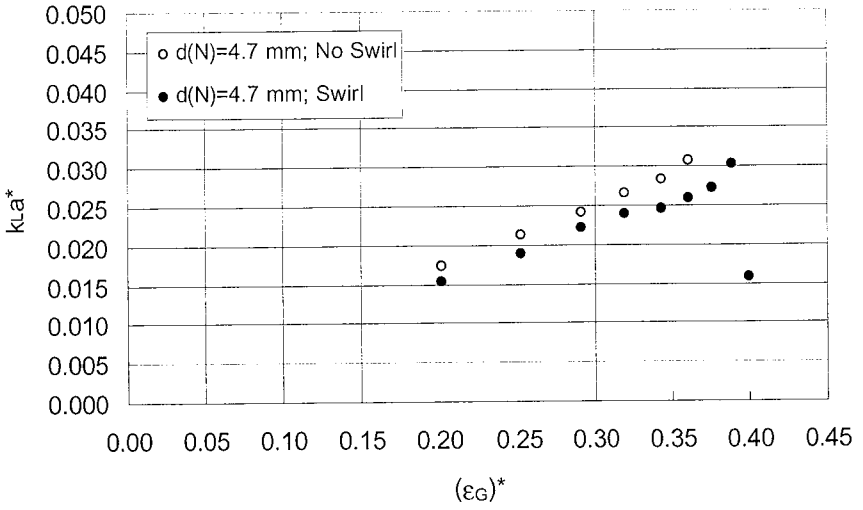

Fig. 5.6 $(k_La)^*_{Ej}$ versus $(\varepsilon_G)^*$; Q_L = 0.5 l/s; d_N =4.7 mm, L_M/d_M =2 (System: water/nitrogen).

5.5.1.2 Influence of the nozzle to mixing tube diameter ratio

Dirix and Van de Wiele (1990) have already shown that the ratio between the nozzle to mixing tube diameter (d_N/d_M) affects the volumetric mass transfer coefficient of ejectors. According to these authors $(k_La)_{Ej} \approx (d_N/d_M)^{0.65}$. The ejector configuration used in their experimental investigation included a swirl device in the upstream section of the nozzle.

Our experimental results of the influence of the nozzle to mixing tube diameter ratio on $(k_La)_{Ej}$ are shown in Figs. 5.7.

The observations clearly demonstrate that the nozzle diameter, i.e. the d_N/d_M ratio, influences the volumetric mass transfer coefficient of the ejector. However, it is seen that contradicting effects are observed. When using a swirl device it is seen that $(k_La)^*_{Ej}$ decreases when the nozzle diameter is increased. In other words, for a constant power supply to the ejector, the k_La-value is influenced by the geometrical parameters (read the d_N/d_M ratio). When no swirl device is included, it is seen that there exists an optimum at a d_N/d_M-ratio of approximately 0.38. A physical explanation for this optimum will be given in Chapter 6.

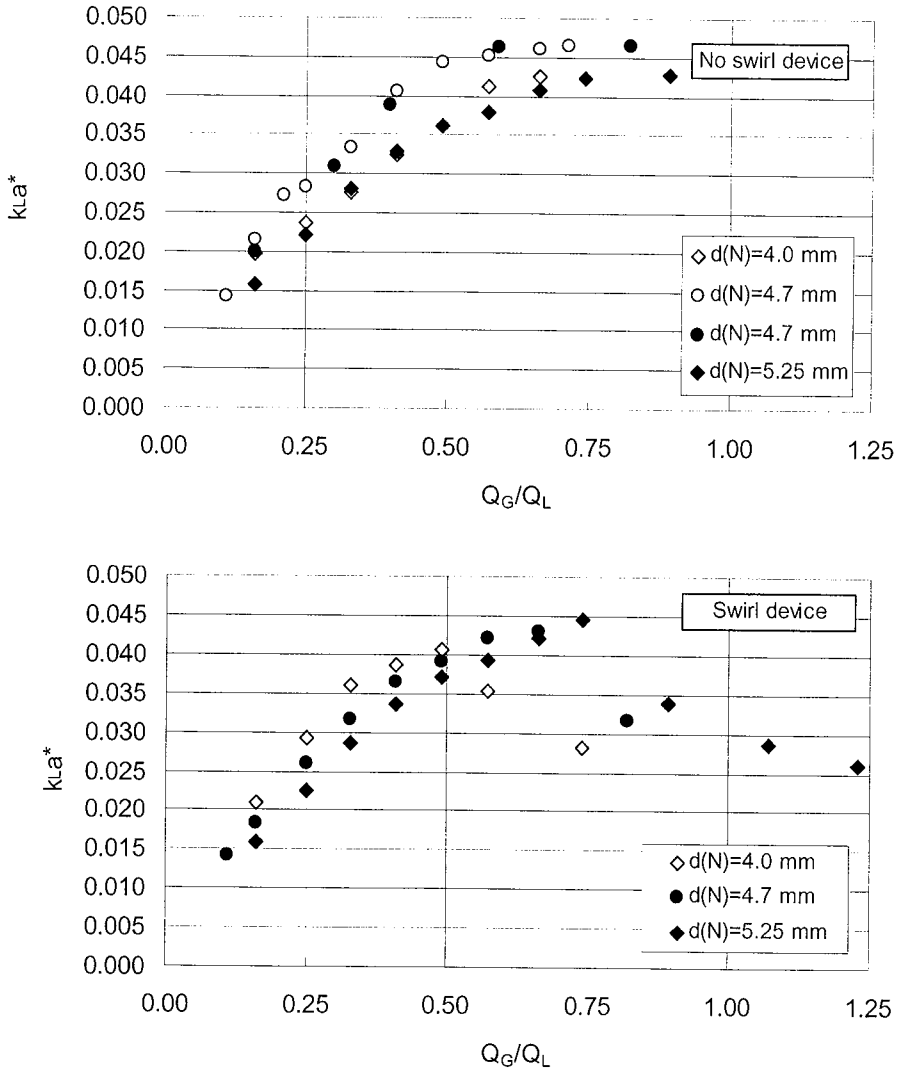

Fig. 5.7 Influence of the nozzle to mixing tube diameter ratio on $(k_La)^*_{Ej}$; (a) Ejector without swirl device and (b) ejector with swirl device. (L_M/d_M =10 and d_M = 12 mm, System: water/nitrogen)

The data could be correlated by:

(5.18) $(k_La)^*_{Ej} \approx (d_N/d_M)^{0.65}$ with swirl device and

(5.19) $(k_La)^*_{Ej} \approx (1\text{-}0.55(0.38 - d_N/d_M)^2)$. without swirl device

as shown in Figs. 5.8 (a) and (b).

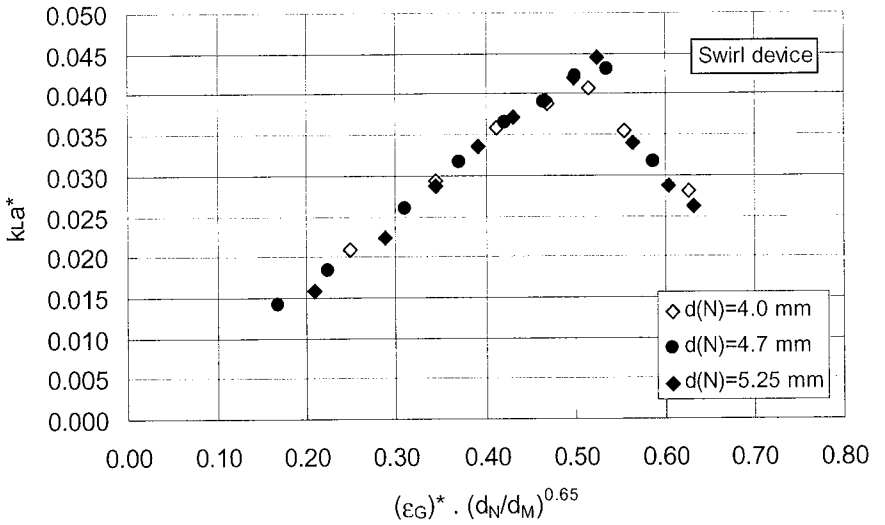

Fig. 5.8 (a) $(k_La)^*_{Ej} \approx$ versus $(\varepsilon_G)^* (d_N/d_M)^{0.65}$
(With swirl, L_M/d_M =10 and d_M = 12 mm, System: water/nitrogen)

Further it is seen that for all the ejectors studied, $(k_La)^*_{Ej}$ increases linearly with $(\varepsilon_G)^*$ in the bubble flow regime, whereas $k_La)^*_{Ej}$ decreases linearly with $(\varepsilon_G)^*$ in the so-called jet annular flow regime.

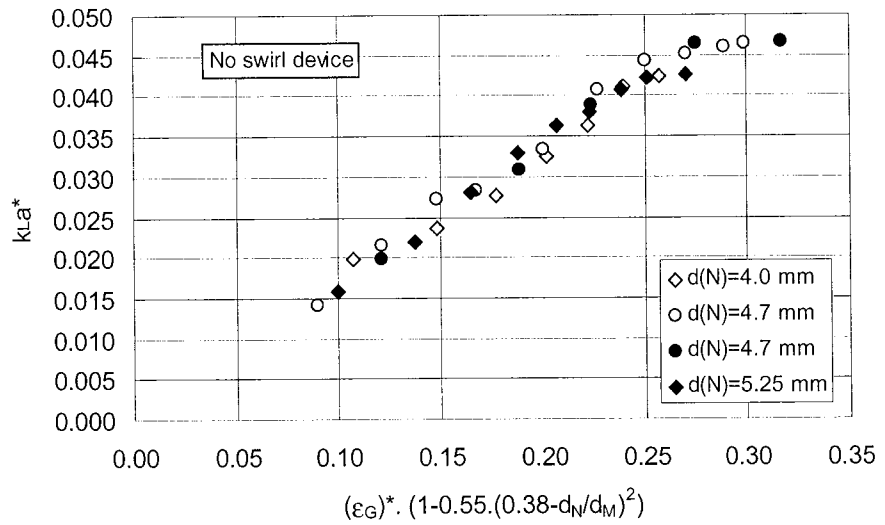

Fig. 5.8 (b) $(k_La)^*_{Ej} \approx$ versus $(\varepsilon_G)^* (1\text{-}0.55(0.38 - d_N/d_M)^2)$
(No swirl, L_M/d_M =10 and d_M = 12 mm, System: water/nitrogen)

5.5.1.3 Influence of the mixing tube length

According to the experiments of Dirix and Van de Wiele (1990), the mixing tube length has no influence on $(k_La)_{Ej}$. In their study the mixing tube length to diameter ratio (L_M/d_M) varied between 2 an 10. This observation is in disagreement with our experimental results as shown in Fig 5.9.

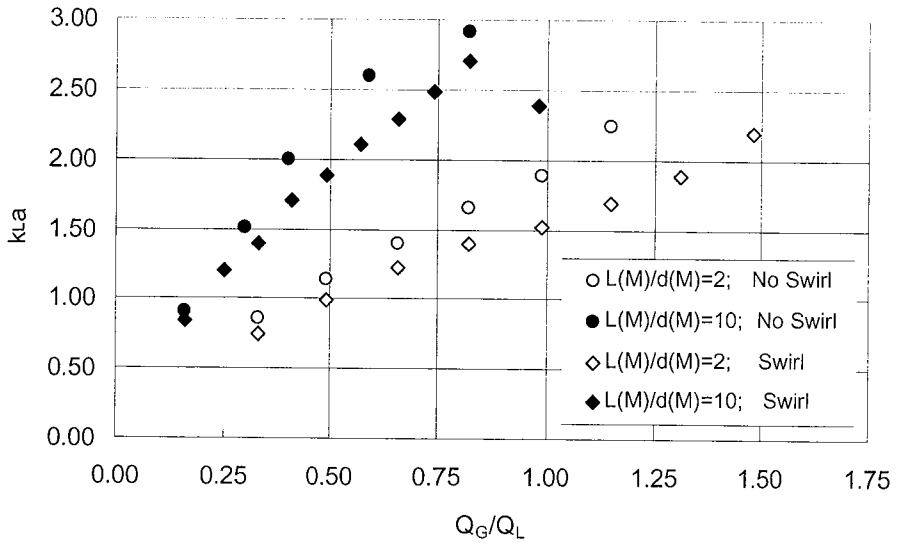

Fig. 5.9 Influence of the mixing tube length on $k_La)_{Ej}$ (Q_L=0.5 l/s, d_N=4.7 mm, System: water/nitrogen).

Fig. 5.9 clearly illustrates that the ejector with the longer mixing tube creates higher volumetric mass transfer coefficients compared to the ejector with a shorter mixing tube. Also, it is seen that when applying a swirl device, the flow transition point shifts to lower gas-liquid flow ratios for the longer mixing tube. As discussed in section 5.4, the reverse is true for an ejector without swirl device.

When $(k_La)^*_{Ej}$ is plotted versus $(\varepsilon_G)^*$, four individual curves are obtained, as shown in Fig. 5.10. This experimental observation indicates that each ejector configuration requires its own specific design correlation. The influence of the mixing tube length on $(k_La)_{Ej}$ can be explained from the local ejector hydrodynamics.

In the introductory chapter of this thesis a scheme of the local ejector hydrodynamics is shown, which shows the existence of two separate zones in the ejector, i.e. the mixing shock region and bubbly flow the remaining part of the ejector. In the mixing zone, the dispersion looks "milky", whereas below this zone a clear bubbly flow is observed. A schematic representation of the hydrodynamics observed is shown in Fig. 5.11.

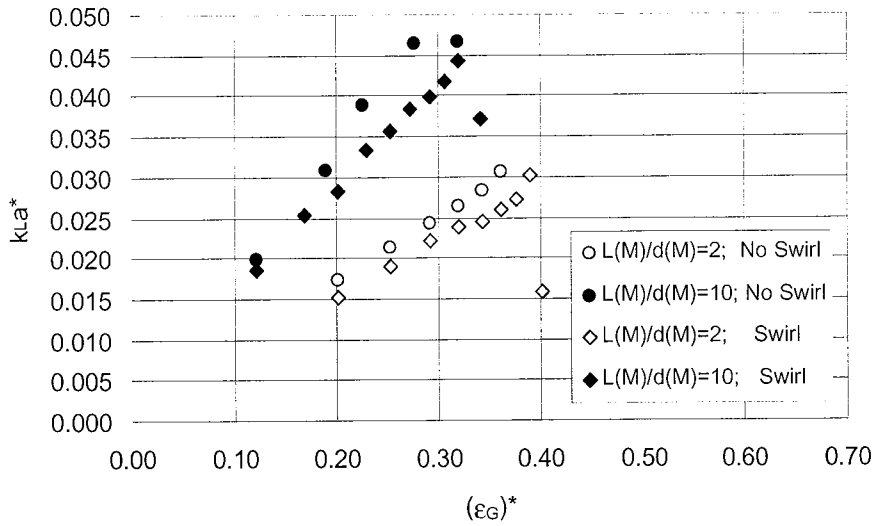

Fig. 5.10 Influence of the mixing tube length on $(k_La)^*Ej$.
(d_N=4.7 mm, System: Water/Nitrogen).

For the standard ejector (L_M/d_M =2), the mixing zone is located in the mixing tube and in a large volume of the diffuser. However, when L_M/d_M =10, the mixing zone is nearly completed in the mixing tube. This indicates that the initial dispersion volume (mixing zone volume) is influenced by the ejector configuration. From this visual observation it is concluded that the mixing zone volume of the ejector with an L_M/d_M ratio of 10 is smaller compared to the mixing zone volume of an ejector with a shorter mixing tube.

Assuming that the major amount of energy is dissipated within the mixing zone, the local energy dissipation rate in the mixing zone (ϵ_{MZ}) can be approximated by

$$\epsilon_{MZ} = \frac{(P_{Jet} - P_{Compres})}{\rho_M \cdot V_{MZ}} \qquad (5.20)$$

where V_{MZ} equals the mixing zone volume. Eq. (5.20) shows that the local energy dissipation rate in the ejector with the longer mixing tube is higher, since V_{MZ} is smaller. Since the initial dispersed bubble size is proportional to $(\epsilon_{MZ})^{-0.4}$, Eq. (5.4), the ejector with the longer mixing tube disperses smaller bubbles and hence gives higher k_La values. From this, it can be concluded that for proper designing and modelling of ejectors the local hydrodynamics have to be studied in more detail (as will be discussed in chapter 6).

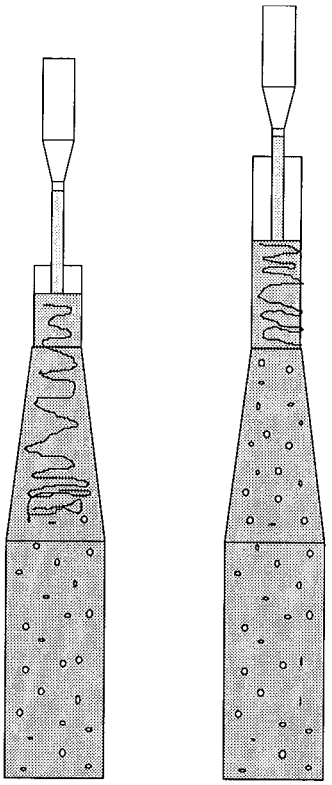

Fig. 5.11 Influence of the mixing tube length on the ejector hydrodynamics (jet velocity and gas-liquid flow ratio are identical).

5.5.2 Influence of scale

In order to study the influence of scale on the mass transfer performance of ejectors, an ejector with an L_M/d_M ratio of 2 was geometrically enlarged by a factor of 2. An overview of the experiments with these two ejectors is shown in Fig. 5.12.

The results presented in this figure show that the volumetric mass transfer coefficient is independent of the ejector size at the same energy input per unit volume. In addition, for the ejector without a swirl device no scale effect was found, both with respect to k_La and flow transition point. In contrast, for the ejector with a swirl device the flow transition point seemed to be influenced by scale, see section 5.4.1.4. However, In these experiments the swirl-number was not kept constant during the scale-up procedure. When the ejector is scaled up properly, with respect to the Sw-number, this scale dependency will probably vanish (Palmer and Musketh, 1984).

The following scale rules can be derived:
For a constant volumetric mass transfer coefficient in the ejector section, equal power-input per unit ejector volume and equal ejector dimensions are required for a proper scale-up of the ejector. These scale rules are valid for all the ejector configurations, whether a swirl

device is present in the upstream section of the nozzle or not. However, when using a swirl device, it has to be assured that during scale-up the Swirl-number is also kept constant. Otherwise, the flow transition point is affected by scale.

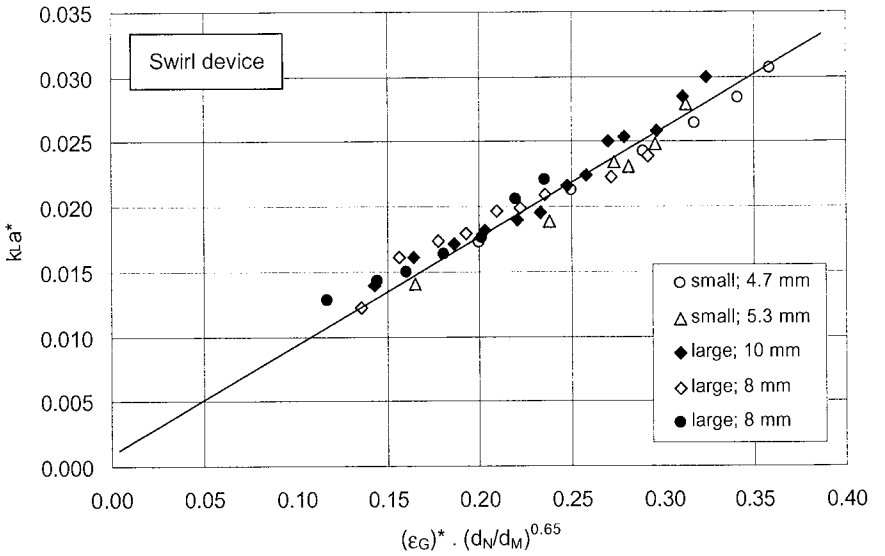

Fig. 5.12 Overview of experiments performed with the standard ejector and with an ejector geometrically scaled up by a factor of 2, both with swirl device in the nozzle (L_M/d_M = 2),

5.5.3 Influence of the gas density on mass transfer characteristics

Recently, it has been recognised that gas density has a significant influence on the mass transfer characteristics of gas-liquid contactors. Studies showed that the mass transfer characteristics the various gas-liquid reactors improved when higher density gases were used. This effect was attributed to a decrease in the bubble stability when applying higher density gases (as was demonstrated in Chapter 4). Therefore, also an influence of the gas density on $(k_La)_{Ej}$ is to be expected.

In order to illustrate this influence, experiments have been performed with a standard ejector (L_M/d_M = 2) with a swirl device in the upstream section of the nozzle. The gases used were helium, nitrogen and argon. The results of these experiments are shown in Fig. 5.13. This figure clearly demonstrates that the $(k_La)_{Ej}$-values in the bubble flow regime are systematically higher when higher density gases are used. The liquid side mass transfer coefficient is not affected by the gas phase used, since in all cases oxygen was desorbed from the water phase. Therefore, any change in the $(k_La)_{Ej}$-value must be due to a change in the specific gas-liquid interfacial area (a).

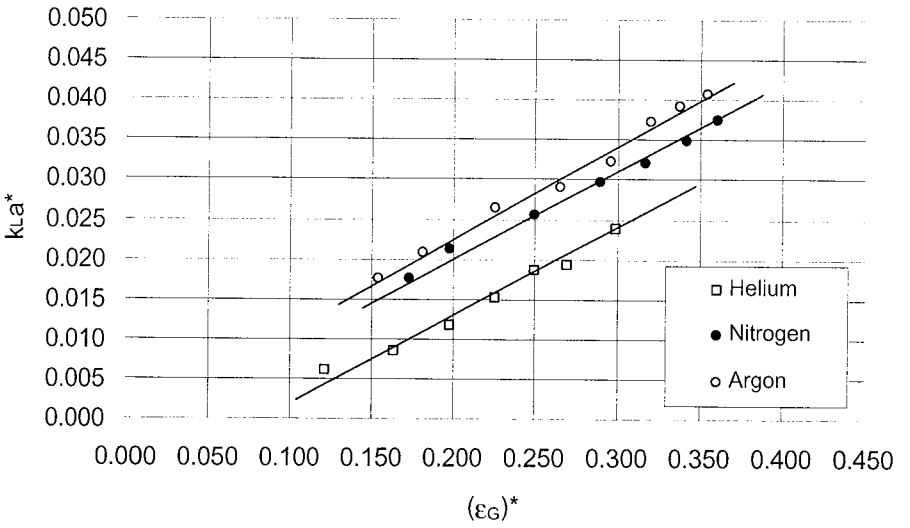

Fig. 5.13 Influence of the gas density on the volumetric mass transfer coefficient of a standard ejector.

In Chapter 4 it was demonstrated that the bubble diameter is proportional to $(\rho_G)^{-0.2}$. This indicates that a_{Ej} is proportional to $(\rho_G)^{0.2}$(and hence k_La). Eq. (5.8) appears to correlate the experimental data (of the bubble flow regime) very well, see Fig. 5.14. In this figure $(k_La)^*_{Ej}$, is plotted against $(\varepsilon_G)^*(\rho_G)^{0.2}$.

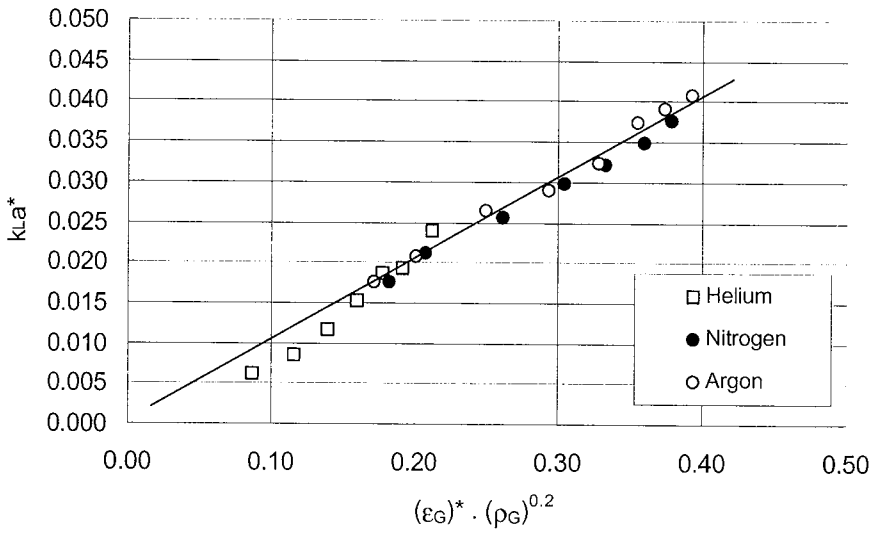

Fig. 5.14 $(k_La)^*_{Ej}$, versus $(\varepsilon_G)^*(\rho_G)^{0.2}$; Q_L =0.5 l/s, d_N =4.7 mm, L_M/d_M = 2 (Swirl device present).

These results show that Levich's theoretical exponent of 0.2 for the effect of the gas density is in agreement with our experimental observations.

5.6 DESIGN CORRELATIONS

In deriving design relations for the volumetric mass transfer coefficient of ejectors, as a basis Eqs. (5.8) and (5.11) have been used:

$$k_La = (\in_{Dis})^{0.65} \cdot \varepsilon_G \cdot \left(\frac{1+0.2\cdot\varepsilon_G}{1+\varepsilon_G}\right)^{1.2} \cdot \left(\frac{\rho_L^2\cdot\rho_G}{\sigma^3}\right)^{0.2} \cdot \zeta\left(\frac{d_N}{d_M}\right) \cdot \zeta\left(\frac{L_M}{d_M}\right) \quad (5.22)$$

where $\zeta\left(\frac{d_N}{d_M}\right)$ and $\zeta\left(\frac{L_M}{d_M}\right)$ include the geometrical effects of the nozzle to mixing tube diameter ratio and the mixing tube length to diameter ratio, respectively.

For the **ejector without swirl device** in the upstream section of the nozzle the data could be correlated as:

(5.23)

$$k_La = C_5 \cdot (\in_{Dis})^{0.65} \cdot \varepsilon_G \cdot \left(\frac{1+0.2\cdot\varepsilon_G}{1+\varepsilon_G}\right)^{1.2} \cdot \left(\frac{\rho_L^2\cdot\rho_G}{\sigma^3}\right)^{0.2} \cdot \left(\frac{L_M}{d_M}\right)^{0.42} \cdot \left\{1-0.55\left(0.38-\frac{d_N}{d_M}\right)^2\right\}$$

For the **ejector with swirl device** used in this study, the flow transition point could be correlated as:

$$\left(\frac{Q_G}{Q_L}\right)_{Trans} = C_8 \cdot \left(\frac{d_N}{d_M}\right) \cdot \left(\frac{L_M}{d_M}\right)^{-0.38} \quad (5.24)$$

The k_La-data obtained in the bubble flow regime could be correlated as:

$$k_La = C_6 \cdot (\in_{Dis})^{0.65} \cdot \varepsilon_G \cdot \left(\frac{1+0.2\cdot\varepsilon_G}{1+\varepsilon_G}\right)^{1.2} \cdot \left(\frac{\rho_L^2\cdot\rho_G}{\sigma^3}\right)^{0.2} \cdot \left(\frac{L_M}{d_M}\right)^{0.42} \cdot \left(\frac{d_N}{d_M}\right)^{0.65} \quad (5.25)$$

whereas the data in the jet-annular flow regime were correlated as:

$$k_La = C_7 \cdot (\in_{Dis})^{0.65} \cdot (1-\varepsilon_G) \cdot \left(\frac{d_N}{d_M}\right)^{0.65} \quad (5.26)$$

The predicted values of above mentioned design correlations are generally within 10 % accuracy of the measured values. **It has to be stressed that the predicted k_La-values**

are only valid for coalescing, non-viscous systems and for the geometrical ejector dimensions as used in this study.

5.7 CONCLUSIONS

From the present investigation it can be concluded that the ejector configuration has a significant effect on the mass transfer characteristics of ejectors. It was shown that:

(1) For a comparable volumetric mass transfer coefficient in the ejector section, both the power-input per unit ejector volume and the relative ejector dimensions should be the same for a proper scale-up of the ejector. These scale rules are both valid for ejector configurations, with or without a swirl device. However, when using a swirl device, it has to be assured that in scaling-up the Swirl-number is also kept constant. Otherwise, the flow transition point is affected by scale.

(2) A swirl device in the upstream section of the nozzle influences both the volumetric mass transfer coefficient and the hydrodynamics (flow regime) in the ejector. Without swirl device the highest $k_L a$-values are obtained.

(3) The mixing tube length influences the volumetric mass transfer rates. The $k_L a$-values increases when longer mixing tubes are used.

(4) When using a swirl device in the nozzle, the volumetric mass transfer coefficient of the ejector decreases when the nozzle to mixing tube diameter ratio is increased. When no swirl device is included, there seems to be an optimum d_N/d_M ratio of approximately 0.40.

(5) In the bubble flow regime the volumetric mass transfer coefficient increases when higher density gases are used. The results could be explained by using Levich's theory, i.e. when the gas density is increases, smaller bubbles are dispersed resulting in an increase of the $k_L a$-value.

(6) For a proper design and modelling of ejectors the local hydrodynamics have to be studied in more detail, i.e. the mixing zone region and the remaining volume of the ejector should be considered as two separate reactor units in series, as will be discussed in chapter 6.

NOTATION

a	specific gas-liquid contact area	m^2/m^3
d_B	bubble diameter	m
C_1	empirical constant	
C_G	oxygen concentration in the gas phase	mol/l
C_L	oxygen concentration in the liquid bulk	mol/l
$C_{L,i}$	oxygen concentration at G/L interface	mol/l
$C_{L,in}$	oxygen concentration at nozzle entrance	mol/l
$C_{L,out}$	oxygen concentration at ejector outlet	mol/l
d_S	Sauter mean bubble diameter	m
d_M	maximum stable bubble diameter	m
d_D	diffuser diameter	m
d_M	mixing tube diameter	m
d_N	nozzle diameter	m
D_L	diffusion coefficient in liquid phase	m^2/s
g	gravitational constant	m/s^2
He	Henry number ($C_G / C_{L,i}$)	
k_L	physical mass transfer coefficient	m/s
k_La	volumetric mass transfer coefficient	1/s
$(k_La)_{Ej}$	volumetric mass transfer coefficient of the ejector	1/s
$(k_La)^*_{Ej}$	mass transfer number (Eq. 5.16)	
l_s	swirl length	m
L_D	diffuser length	m
L_M	mixing tube length	m
$\Delta P_{G,Ej}$	pressure difference of the gas phase across the ejector	Pa
Q_G	volumetric gas flow rate	m^3/h
Q_L	volumetric liquid flow rate	m^3/h
r_N	radius of the nozzle	m
Sw	Swirl number (Eq. 5.15)	
U_N	jet velocity at the nozzle exit	m/s
U_{tan}	tangential velocity	m/s
V_{Ej}	effective ejector volume	m^3
$P_{\Delta P}$	Power required for gas compression	W
P_{Jet}	Power of discharging jet	W
ε_G	gas fraction	
$(\varepsilon_G)^*$	gas fraction defined by Eq. (5.17)	
$\in$	energy dissipation rate	W/kg

ν_L	kinematic liquid viscosity	m^2/s
μ_L	dynamic viscosity	Pa.s
ρ_L	liquid phase density	kg/m^3
ρ_G	gas density	kg/m^3
ρ_M	mixture density = ρ_L $(1-\varepsilon_G)$	kg/m^3
σ	surface tension	N/m
Θ	swirl angle	rad

Appendix A3:
Definition of a swirl number (Sw) of a liquid jet

The presence of a swirl device upstream of the ejector nozzle imparts a tangential velocity component to the liquid flow. This swirling characteristic of the liquid jet may be described with a Swirl number, defined as the ratio of tangential to axial velocity of the jet:

$$(A\ 3.1) \qquad Sw = \frac{r_N \cdot \omega_N}{u_{z,N}}$$

where r_N is the nozzle radius, ω_N the angular velocity at the nozzle and $u_{z,N}$ the axial velocity at the nozzle. Sw can be related to the swirl geometry and nozzle diameter. The following summarises the derivation for this relationship made by Palmer and Musketh (1984).

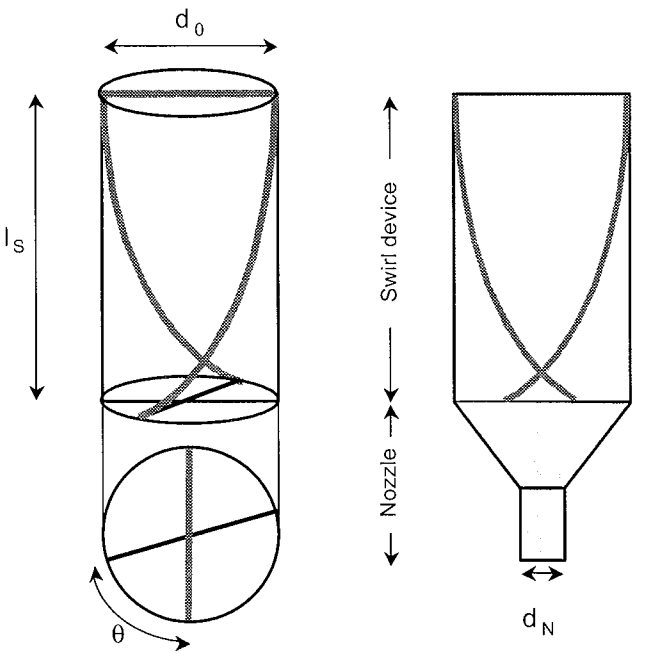

Fig. A 3.1 Geometrical parameters of Swirl device and connection to ejector nozzle.

If angular momentum is conserved about the pipe centre line when the swirl was carried from the swirl device to the nozzle outlet,

$$(A\ 3.2) \qquad r_N^2 \cdot \omega_N = r_0^2 \cdot \omega_0$$

where r_0 is the swirl radius, ω_0 the angular velocity in the swirl device.

The time that the liquid spends travelling along the swirl device can be expressed as:

$$t = \frac{l_S}{u_{z,0}} = \frac{\theta}{\omega_0} \qquad \text{(A 3.3)}$$

or

$$\omega_0 = \frac{\theta \cdot u_{z,0}}{l_S} \qquad \text{(A 3.4)}$$

Combining equations, (A-1), (A-2) and (A-4) gives:

$$Sw = \frac{r_N \cdot \theta}{l_S} \cdot \frac{r_0^2 \cdot u_{z,0}}{r_N^2 \cdot u_{z,N}} \qquad \text{(A 3.5)}$$

Since the second group equals to 1, Sw is given by:

$$Sw = \frac{r_N \cdot \theta}{l_S} \qquad \text{(A 3.5)}$$

Eq (A 3.5) shows that in a linear scale-up of the swirl device, the tangential velocity compared to the axial velocity remains constant. This indicates that for a proper scale-up of an ejector with swirl device in the nozzle, the swirl number has to be kept constant and the other dimensions of the ejector configuration.

Chapter 6
Prediction of the mass transfer characteristics of G/L ejectors
- A phenomenological model -

SUMMARY

The hydrodynamics and mass transfer characteristics of a straight tube ejector have been investigated both experimentally and theoretically. Both, from the experiments and the model calculations it was concluded that two different hydrodynamic zones exist in the ejector. In the first zone, the so-called "mixing shock" region, extremely high values of the volumetric mass transfer coefficient, k_La, are obtained. In the remaining part of the ejector volume a fine and homogeneous bubble flow appears in which the mass transfer rate is lower. Proper design and modelling of ejectors, therefore requires separate modelling of these two zones. A theoretical model is presented which describes the local mass transfer characteristics as a function of the jet velocity, the gas phase pressure drop across the ejector and some geometrical design parameters. Experimental data confirm the satisfactory agreement with the model.

6.1. INTRODUCTION

In Chapter 5 it has been demonstrated that the ejector configuration has a significant effect on the volumetric mass transfer coefficient. The observed phenomena, like the influence of the swirl device, the nozzle to mixing tube diameter ratio and the mixing tube length on the mass transfer characteristics could not be explained satisfactorily. However, it was observed that the mixing zone length was affected by some geometrical parameters.

The interpretation of mass transfer data of ejectors is usually based on the assumption that they behave as a single unit. In reality an ejector consists of two different hydrodynamic zones with distinct properties, i.e. a mixing shock and a bubble flow zone as is shown schematically in Fig. 6.1. This figure shows the local hydrodynamics and change in flow regime across the ejector.

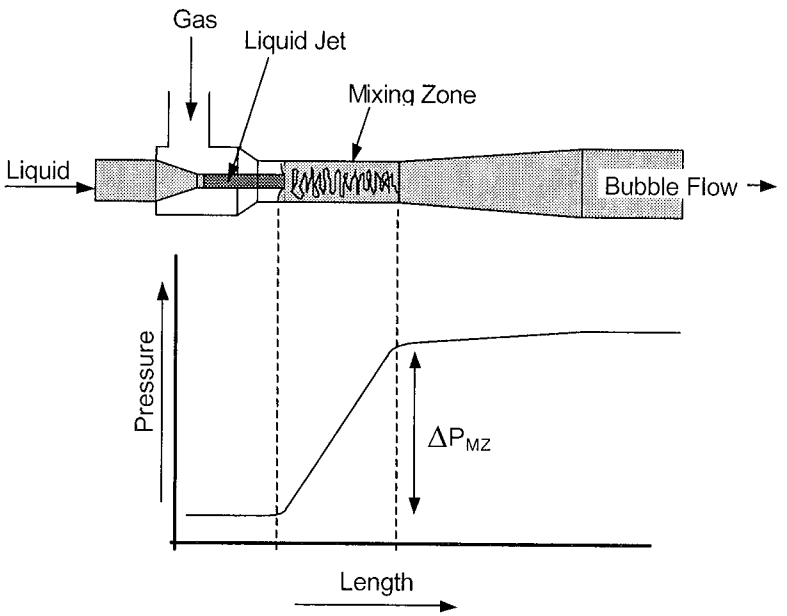

Fig. 6.1 Hydrodynamic conditions inside the ejector and the qualitative change of the pressure along the mixing tube and the diffuser of the ejector.

In the first zone the high velocity jet discharges into the mixing zone region, which is accompanied by a sudden pressure build-up ("mixing shock"). After this mixing zone both phases flow homogeneously through the remaining part of the ejector. It is expected that the difference in hydrodynamics of these two zones result in different local mass transfer characteristics. However, to our knowledge there are no literature data that confirm the above statements. This investigation presents an experimental study on the local mass

transfer characteristics of both zones in a straight tube ejector. A theoretical model has been developed which describes the experimental data quantitatively.

6.2 MODEL DEVELOPMENT

The development of a model predicting the local mass transfer characteristics of both zones is the main objective of this chapter. Firstly, relations have to be defined which predict the physical mass transfer coefficient and the specific gas-liquid contact area as function of both the physical properties and the energy dissipation rate. Secondly, expressions relating the energy dissipation rates to the system variables are required and finally a model has to be developed which predicts the volume of the mixing zone as function of the operating parameters. Each of these individual aspects of the model are discussed in the following sections separately.

6.2.1 Prediction of mass transfer parameters

The volumetric mass transfer coefficient k_La is composed of the specific gas liquid interfacial are ($a = 6\varepsilon_G/d_S$) and the physical mass transfer coefficient (k_L).

The specific interfacial area (a) can be calculated once the gas fraction (ε_G) and Sauter mean bubble diameter (d_S) are known. For the present it is assumed that bubbly flow exists in which small discrete bubbles move downward with nearly the same velocity as the liquid phase, as discussed in Chapter 5. Under these conditions the gas fraction is approximated by:

$$\varepsilon_G = \frac{Q_G}{Q_L + Q_G} \tag{6.1}$$

For predicting the Sauter bubble diameter, d_S, relations (5.4) and (5.3) will be used as discussed in Chapters 5:

$$d_S = 0.65 \cdot \left(\frac{We_C}{2}\right)^{0.6} \cdot \left(\frac{\sigma^3}{\rho_L^2 \cdot \rho_G}\right)^{0.2} \cdot (\in)^{-0.4} \cdot \left(\frac{1+\varepsilon_G}{1+0.2 \cdot \varepsilon_G}\right)^{1.2} \tag{6.2}$$

in which the critical Weber-number (We_C) equals to 1.1. This relation has been verified for dispersed phase fractions up to 40 %. Nevertheless, for the purpose of this study, Eq. (6.2) will be used up to dispersed phase fractions of approximately 62 %, where a maximum bubble packing" is reached.

The physical mass transfer coefficient (k_L) is obtained from the equation of Kawase and Moo-Young (1991), as stated in Chapter 5, i.e.

(6.3) $$k_L = 0.302 \cdot \sqrt{D_L} \cdot \left(\frac{\epsilon}{\nu_L}\right)^{0.25}$$

This equation was obtained from both experimental and theoretical studies. Application of Eq. (6.3) is most successful for gas-liquid dispersions in which the energy dissipation rate (ϵ) is homogeneously distributed over the entire flow field.

Once the local ϵ-values of both the mixing- and the bubble flow zone are known, the local k_L and a-values of both regions in the ejector can be estimated. The evaluation of the energy dissipation rates in both sections is discussed in the following section.

6.2.2 Prediction of energy dissipation rates

6.2.2.1 Mixing zone region

The average energy dissipation rate per unit mass (ϵ) within the mixing zone of an ejector can be calculated from the momentum and the energy balance across the mixing zone volume.

Following the detailed analysis of Cunningham and Dopkin (1974) and Evans (1990) for a liquid jet gas pump, and realising that the mixing zone corresponds to the throat section of such a pump, the pressure difference across the mixing zone (ΔP_{MZ}), due to the momentum transfer from the liquid to the gas phase is given by:

(6.4) $$\Delta P_{MZ} = \left(\frac{\rho_L \cdot U_N^2}{2}\right) \cdot \left\{ 2b - (2+k_{ML}) \cdot b^2 \cdot \left(1+\frac{\rho_G \cdot Q_G}{\rho_L \cdot Q_L}\right) \cdot \left(1+\frac{Q_G}{Q_L}\right) + \frac{2 \cdot \frac{\rho_G}{\rho_L} \cdot \left(\frac{Q_G}{Q_L}\right)^2 \cdot b^2}{1-b} \right\}$$

were b is the ratio of the cross-sectional area of the liquid jet to that of the mixing tube at the moment of impact (d_N^2/d_M^2) and k_{ML} the friction loss coefficient in the mixing zone.

From the energy balance the pressure difference across the mixing zone is calculated as (Cunningham and Dopkin, 1974):

(6.5) $$\Delta P_{MZ} = \left(\frac{\rho_L \cdot U_N^2}{2}\right) \cdot \left\{ 1 - b^2 \cdot \left(1+\frac{\rho_G \cdot Q_G}{\rho_L \cdot Q_L}\right) \cdot \left(1+\frac{Q_G}{Q_L}\right)^2 + 2 \cdot \frac{\rho_G}{\rho_L} \cdot \left(\frac{Q_G}{Q_L}\right)^3 \cdot \frac{b}{1-b} \right\} + - \frac{Q_G}{Q_L} P_1 \ln\left(\frac{P_2}{P_1}\right) - \rho_L \cdot \{(e_{S,MZ}) + (e_{S,ML})\}$$

where $e_{S,MZ}$ and $e_{S,ML}$ are the specific energy dissipation terms for "mixing" of both phases and friction mixing loss respectively. By recognising that the friction mixing loss equals to

$$\rho_L \cdot e_{S,ML} = \frac{\rho_L \cdot U_N^2}{2} \cdot k_{ML} \cdot b^2 \cdot \left(1+\frac{\rho_G \cdot Q_G}{\rho_L \cdot Q_L}\right) \cdot \left(1+\frac{Q_G}{Q_L}\right) \tag{6.6}$$

Equations (6.4) and (6.5) can be rearranged, to obtain an expression for the local specific energy dissipation $e_{S,MZ}$ for mixing of the gas and the liquid phase in the mixing zone. Further it has been assumed that both $\rho_G/\rho_L << 1$ and $k_{ML} << 1$:

$$(e_{S,MZ}) = \frac{U_N^2}{2} \cdot \left\{1-2b-b^2 \cdot \left(1+\frac{Q_G}{Q_L}\right)^2 + 2b^2 \cdot \left(1+\frac{Q_G}{Q_L}\right)\right\} - \frac{Q_G\, P_1}{\rho_L\, Q_L} \cdot \ln\left(\frac{P_2}{P_1}\right) \tag{6.7}$$

The energy dissipation rate per unit volume is obtained by multiplying Eq. (6.7) by the jet mass flow rate, $\rho_L Q_L$, and dividing by the mixing zone volume, V_{MZ}. This leads to:

$$\in_{MZ} = \frac{e_{S,MZ} \cdot \rho_L \cdot Q_L}{V_{MZ}} \tag{6.8}$$

Eq. (6.8) should give a reasonable approximation of the local energy dissipation rate within the mixing zone. This specific energy dissipation rate can be used to predict both the Sauter mean bubble diameter (Eq. 6.2) and the physical mass transfer coefficient (Eq. 6.3) created in the mixing zone.

6.2.2.2 Bubble flow zone

The specific energy dissipation rate of bubbly flow in straight tubes can be calculated by (Barnea, 1987):

$$\in_{BFZ} = \left|\frac{dP}{dz}\right| \cdot \left(\frac{U_L+U_G}{\rho_L}\right) \tag{6.9}$$

where

$$\frac{dP}{dz} = \frac{2f}{D_M} \cdot \rho_L \cdot (U_L+U_G)^2 \tag{6.10}$$

The friction factor f in Eq. (6.11) is given by

$$f = 0.078 \cdot (Re_M)^{-0.25} \tag{6.11}$$

where the Reynolds number is based on the mixing tube diameter (D_M), liquid physical properties and the total volumetric flow.

6.2.3 Prediction of mixing zone volume

The volume of the mixing zone can be determined by considering what happens to the entrained gas. Therefore, a scheme of the mixing zone is given in Fig. 6.2.

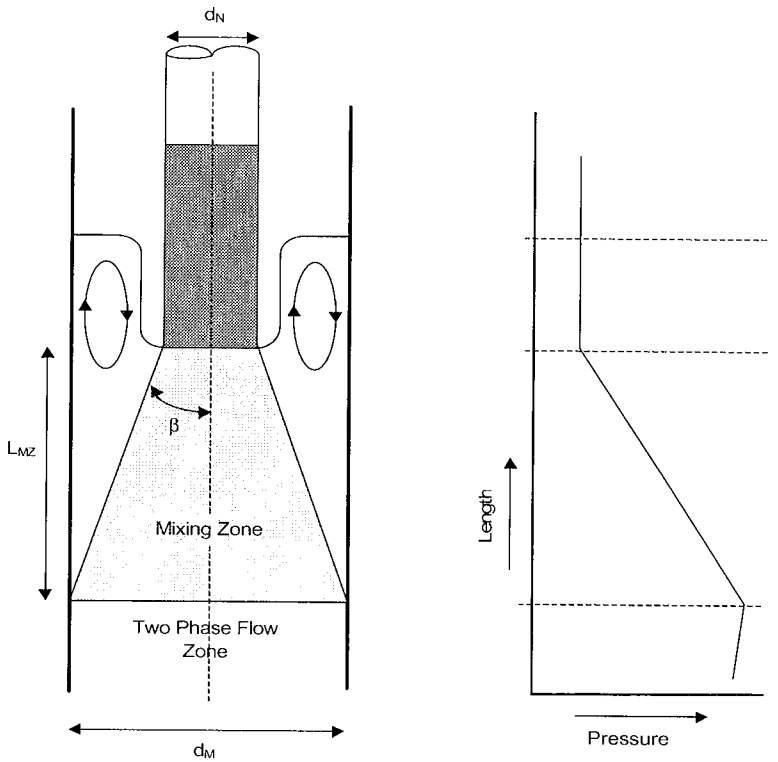

Fig. 6.2 Schematic representation of the mixing zone: Expansion of the two-phase submerged jet.

Where the high velocity jet discharges into the mixing zone, the resulting submerged jet will expand to occupy the entire cross-sectional area of the mixing tube (Ogawa et al, 1983 and Evans, 1990). Once the expanding submerged jet occupies the entire cross-sectional area of the mixing tube, the mixing shock is completed. It is assumed that the effective volume of the mixing zone equals the conical volume of the submerged two-phase jet as shown in Fig. 6.2. The effective mixing zone volume is given by:

$$V_{MZ} = \frac{\pi}{3} \cdot (R_M)^2 \cdot L_{MZ} \qquad (6.12)$$

The length of the mixing zone (L_{MZ}) can be calculated from the submerged jet angle and the tube radius, i.e.

$$L_{MZ} = \frac{R_M}{\tan(\beta)} \tag{6.13}$$

The submerged jet angle (β) can be obtained by considering the radial transfer of momentum from the jet to the re-circulating eddy (Evans, 1990).

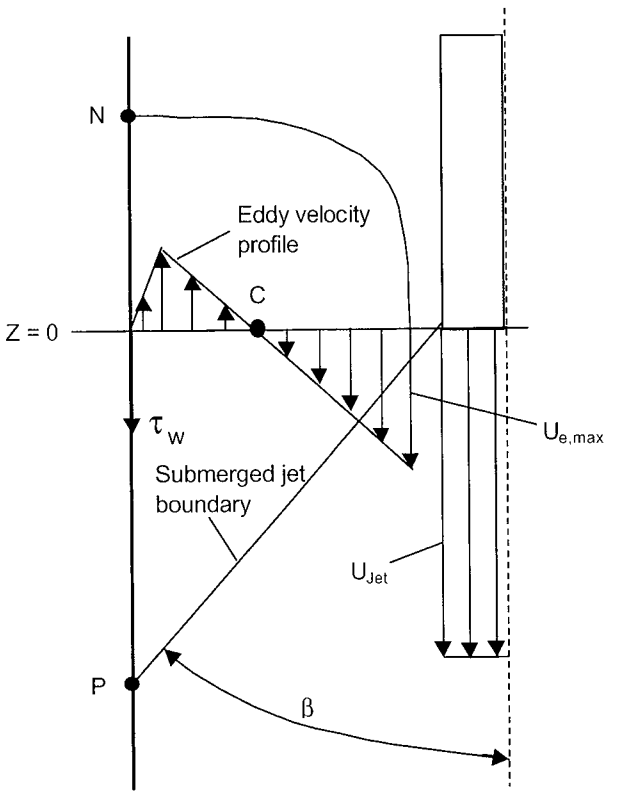

Fig. 6.3 Velocity profile of re-circulating eddy at z = 0 (Evans, 1990).

In Fig. 6.3 the existence of a shear stress τ_W acting in the direction opposite to the motion of the re-circulating eddy is shown. If this shear stress did not exist, $(M_e)_{\tau=0}$, the liquid at the surface of the re-circulating eddy would increase its velocity until no velocity gradient existed across the re-circulating eddy and submerged jet boundary. The re-circulating eddy angular momentum is then given by

$$(M_e)_{\tau=o} = 0.5 \cdot \rho_e \cdot Q_e \cdot (U_N - 0) \tag{6.14}$$

where Q_e is the re-circulating volumetric flow rate inside the eddy.

In reality, a shear stress acts along the mixing zone, $(M_e)_{\tau?0}$, resulting in a velocity difference between the re-circulating eddy and the jet at the origin of the submerged jet. In this case the re-circulating eddy angular momentum is given by

$$(M_e)_{\tau\neq o} = 0.5 \cdot \rho_e \cdot Q_e \cdot (U_{e,max} - 0) \tag{6.15}$$

The difference in momentum loss equals to

$$2\pi R_M L_{MZ} \cdot \tau_W = 0.5 \cdot \rho_e \cdot Q_e \cdot (U_N - U_{e,max}) \tag{6.16}$$

where 2" $R_M L_{MZ}$ equals the surface area of the mixing tube over which the shear stress acts. For fluids flowing through a cylindrical tube the shear stress is given by

$$\tau_W = \frac{R_M}{2} \cdot \frac{dP}{dz} \tag{6.17}$$

where dP/dz is the pressure gradient along the mixing zone length (L_{MZ}). If ΔP_{MZ} equals to the pressure difference across the mixing zone than

$$\tau_W = \frac{\tan(\beta)}{2} \cdot \Delta P_{MZ} \tag{6.18}$$

Substitution of Eq. (6.18) into Eq. (6.16) and rearranging gives an expression for the jet divergence angle, i.e.

$$\tan(\beta) = \frac{\rho_e \cdot Q_e \cdot (U_N - U_{e,max})}{2\pi R_M L_{MZ} (\Delta P_{MZ})} \tag{6.19}$$

An approximation of ΔP_{MZ} in the denominator of Eq. (6.19) can be obtained from the Euler number (Eu), which is the ratio between the pressure force and the inertial force of the system. If the inertial force is equivalent to the initial jet momentum, then the Euler-number for the plunging jet system is given by

$$Eu = \frac{2\pi R_M L_{MZ} (\Delta P_{MZ})}{M_J} \tag{6.20}$$

and the initial jet momentum M_J at the nozzle exit is equal to $0.5\rho_L Q_L U_N$.

The actual values of the mixing zone length and the pressure drop (as defined in Eq. (6.20) can be estimated by defining an overall mixing shock efficiency (η_{MZ}) , i.e.

$$\eta_{MIX} = \frac{\pi/4.\ d_J^2}{2\pi R_M L_{MZ}} = \left(\frac{\Delta P_{MZ}}{\frac{1}{2}.\rho_L U_N^2}\right)_{THEO} \cdot \left(\frac{\Delta P_{MZ}}{\frac{1}{2}.\rho_L U_N^2}\right)_{EXP} \tag{6.21}$$

which is the ratio of cross sectional area of the jet at the moment of impact and the surface area of the tube over which the shear stress acts. The overall mixing shock efficiency can be considered to be the product of the theoretical and the experimental efficiency. The theoretical efficiency can be considered as the pressure differential theoretically gained from the supplied jet power. The experimental efficiency equals to the experimental ΔP_{MZ} value related to the jet power. In fact, the overall mixing shock efficiency is comparable with the overall efficiency of compression pumps.

Substitution of Eqs. (6.20) and (6.21) in Eq. (6.19) and rearranging gives finally

$$\tan(\beta) = 4.\ \frac{\rho_M}{\rho_L}.\left(\frac{Q_e}{Q_L}\right).\left(\frac{U_N - U_{e,max}}{U_N}\right).\left(\frac{\Delta P_{MZ}}{\rho_L U_N^2}\right)_{THEO} \tag{6.22}$$

An estimate for $U_{e,max}$ can be obtained by assuming a solid body rotational velocity profile (Evans, 1990) in the circulating eddy as discussed in Chapter 2. A value of $U_{e,max}$ is:

$$U_{e,max} = \frac{4.\ Q_e}{\pi.\ R_M^2} \tag{6.23}$$

In order to obtain an expression for the flow rate within the circulation eddy, the results as obtained for confined jets have been used (Barchillon and Curtet, 1964 and Liu and Barkelow, 1986). The re-circulation flow, which is characterised by the mass flow rate in the re-circulating eddy was correlated by Curtet (1958) as

$$Q_{e,max} = Q_L.\left(\frac{0.37}{C_T} - 0.64\right).\left(\frac{\rho_L}{\rho_e}\right) \tag{6.24}$$

where C_T is the Crayer-Curtet number is given by Barchillon and Curtet (1964) as:

$$C_T = \frac{R_J}{\sqrt{R_M^2 - \frac{1}{2}.\ R_J^2}} \tag{6.25}$$

The final expression for predicting the submerged jet angle is obtained after substitution of Eq. (6.25) and (6.24) into Eq. (6.22):

$$\tan(\beta) = 4 \cdot \left(\frac{\Delta P_{MZ}}{\frac{1}{2} \cdot \rho_L U_N^2} \right)_{THEO} \cdot \left(\frac{0.37 \cdot \sqrt{R_M^2 - \frac{1}{2} R_J^2} - 0.64 \cdot R_J}{R_J} \right) \cdot \left(\frac{U_J - U_{e,max}}{U_J} \right) \quad (6.26)$$

The theoretical pressure difference across the mixing zone can be calculated with the momentum balance, assuming that the friction loss coefficient to zero. From Eq. (6.26) the submerged jet angle can be calculated and hence the volume of the mixing zone, Eq. (6.12).

6.3. EXPERIMENTAL SET-UP AND PROCEDURES

A scheme of the straight tube ejector used in the present investigation is shown in Fig. 6.4.

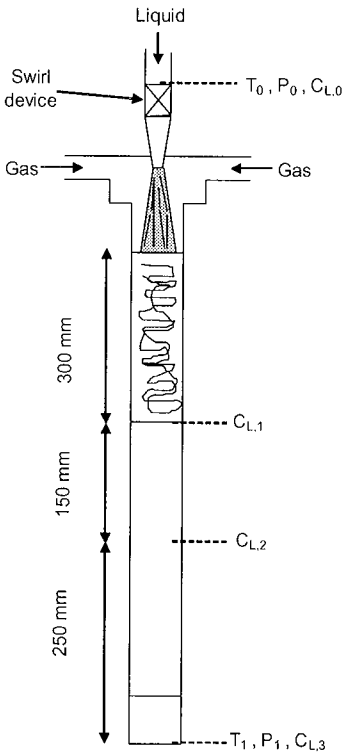

Fig. 6.4 Scheme of the straight tube ejector

The nozzle diameter was 11.9 mm and the ejector length and diameter were 700 mm and 29 mm, respectively.

As a model system the desorption of oxygen from water was used. The liquid (tap water) was pre-saturated with air in a large supply tank and than fed to the ejector. In order to

desorb the oxygen from the liquid, nitrogen gas was fed to the gas suction chamber of the ejector. The dissolved oxygen concentration was measured continuously at four different positions along the length of the ejector, as shown in Fig. 6.4. The effect of several parameters on the local mass transfer rates was investigated. The liquid supply varied from 1.8 to 2.2 ltr/s., while the gas/liquid flow ratio was varied between 0.3 and 1.6. Further, the influence of the swirl device on the volumetric mass transfer coefficient was investigated. All experiments were performed both with and without swirl device in the upstream section of the nozzle.

For the experimental procedure for calculating the $k_L a$-values from the experimental results, see Chapter 5.

6.4. EXPERIMENTAL RESULTS

6.4.1 Submerged jet angle

In order to check the validity of Eq. (6.26) for calculating the two-phase submerged jet angle, experimental data of Cunningham and Dopkin (1974) and Evans (1990) have been used.

Cunningham and Dopkin (1974) measured the pressure profiles across liquid jet gas pumps. In the throat section of such a pump, also a mixing shock is present. From the measured mixing shock lengths and the diameter of the mixing tube, the submerged jet angle could be calculated from their experiments. Evans (1990) studied plunging liquid jet "bubble columns". The lengths of the mixing zones were determined experimentally from axial pressure profiles along the wall of the columns. The results of Evans (1990) were re-examined and only experiments 2, 5, 8, 11, 14, 17, 32, 41 and 64 have been used. This selection was necessary, since in the other experiments the boundary condition of equal gas and liquid phase down flow velocities in the bubble flow zone of the column was not fulfilled, indicating that Eq. (6.1) can not be used. Fig. 6.5 shows a parity plot of the predicted and experimentally determined submerged jet angles of Evans (1990) and Cunningham and Dopkin (1974). This figure shows that Eq. (6.26) is in good agreement with the experimental data of both authors.

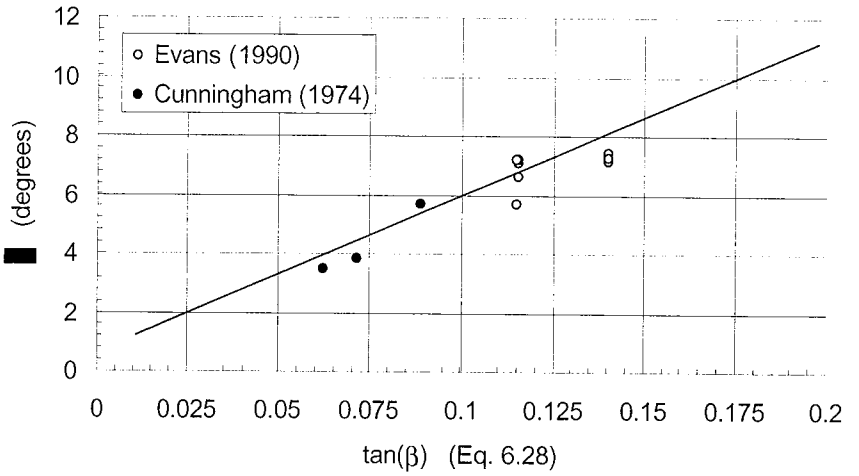

Fig. 6.5 Comparison between measured and predicted jet angle values

From these results it can be concluded that with the aid of Eq. (6.26) it is possible to make a real good estimate of the mixing zone length as a function of some geometrical and operating parameters of ejectors.

6.4.2 Mass transfer in the different sections of the ejector

The influence of the gas-liquid flow ratio and the jet velocity on the local k_La-values of both the mixing and bubble flow zone are shown in Figs. 6.6 (a) and (b), for two different liquid flow rates. The data were obtained with a swirl device in the nozzle. Both figures show that the local k_La -values of the mixing zone are higher than those of the bubble flow zone. Further, the mixing and the bubbly flow zone seem to have a maximum in the volumetric mass transfer rates at a gas-liquid flow ratio of approximately 0.8 and 1.4, respectively. The curves are the values predicted by the theoretical model developed (as will be discussed in the next section). The experimental results show that very high k_La-values are created in both sections of the ejector. Since most energy is dissipated in the mixing zone, it is understandable that the highest k_La-values are measured in this mixing zone.

In Chapter 5 it was demonstrated that at comparable power input, the presence of a swirl device in the upstream section of the nozzle results in lower k_La-values in comparison to an ejector without swirl device. In the same chapter it was argued that the swirl device results in increased mixing zone volumes, compared to the ejector without swirl device. This indicates that the ejector without swirl device is more effective.

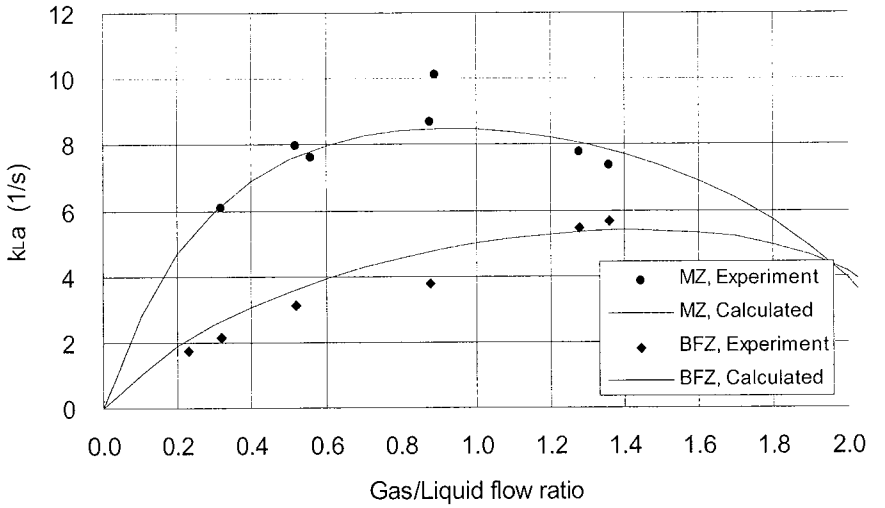

Fig. 6.6(a) Influence Q_G/Q_L on k_La in the mixing zone and in the two phase flow zone
Q_L = 1.8 l/s (swirl device present in the upstream section of the nozzle)

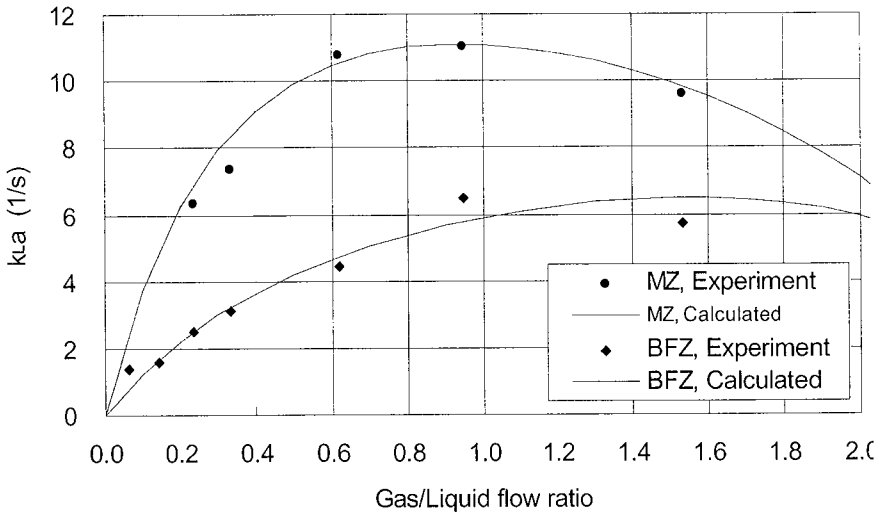

Fig. 6.6(b) Influence Q_G/Q_L on k_La in the mixing zone and in the two phase flow zone
Q_L = 2.2 l/s (swirl device present in the upstream section of the nozzle)

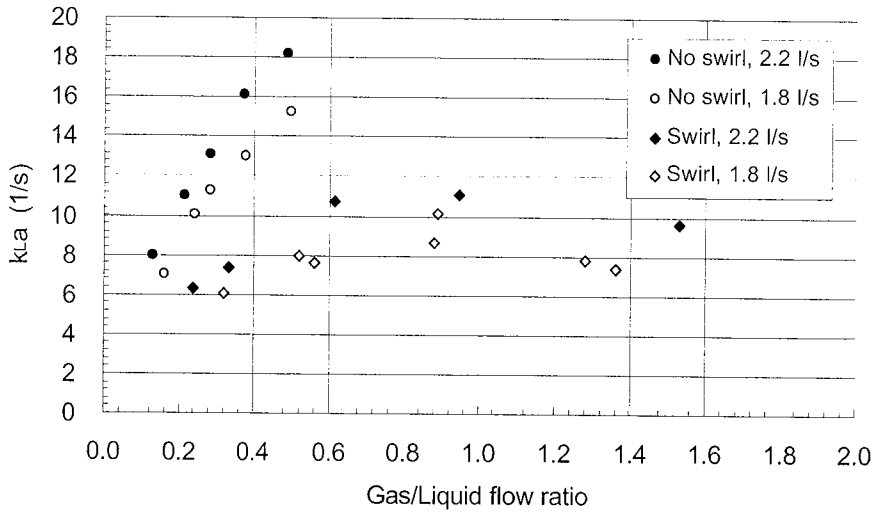

Fig. 6.7 Effect of a swirl device on the local $k_L a$-value in the mixing zone

The influence of a swirl device on the local volumetric mass transfer coefficient in the mixing zone $(k_L a)_{MZ}$ is shown in Fig. 6.7. The explanation of these results will be discussed below.

6.5 MODEL CALCULATIONS AND DISCUSSION

6.5.1 Model calculations vs. experimental results

The main problem for applying our model to predict the experimental results is a lack of information of the actual jet diameter at the position of impact. For a start, it is assumed that the fluid can be considered as a coalescence-inhibiting medium. If so, the bubble size distribution in the mixing shock region and in the remaining volume of the ejector is the same.

When applying a swirl device, the location of the mixing zone is nearly independent of the gas-liquid flow ratio as was shown in Chapter 5. In this case, the jet diameter at the plunging point is also nearly constant. The experimental results shown in Fig. 6.6 (a) and (b) were fitted by applying jet diameters of approximately 15.6 mm and 16.2 mm for the liquid flow rates of 1.8 and 2.2 l/s, respectively. The diagram shows that the agreement between the predicted and the measured values is quite close, for both the mixing zone and the two-phase flow region. From this it can be concluded that the model is able to predict the experimental data quantitatively, once the actual jet diameters are known.

Our assumption that the bubbles, as created in the mixing zone, enter the bubble flow zone and do not coalesce apparently is justified from the agreement between the predicted and experimental values of Figs. 6.6. This virtually absence of bubble coalescence is surprising in view of the widely reported observation that water is a coalescence promoting fluid. The probability that bubbles do coalesce is influenced by the degree of turbulence, as was shown by Chesters (1991). According to this study, bubbles do not coalesce if their approach/collision velocity is sufficiently large. Coalescence of bubbles occurs only if the interaction time (t_i) exceeds the coalescence time (t_C), i.e. the time required for the film to drain to its critical value and to break-up. This is supported by experimental observations of Kirkpatrick and Locket (1974) who showed that bubbles rising in water to a free surface, where these bubbles had a high approach velocity, bounced several times before coalescence occurred. According to Chesters and Hofmann (1982) the ratio of both times is given by

$$\frac{t_C}{t_i} = \sqrt{\frac{4 \cdot \rho_L \cdot U^2 d_B}{\sigma}} \qquad (6.27)$$

If t_C/t_i is larger than unity, bubbles bounce without coalescing. An order of magnitude calculation showed that for the present experiments the Weber-values in the bubble flow zone were always larger than 2, indicating that the bubbles present in this region can not coalesce. Hence, the assumption of negligible bubble coalescence in the ejector section is justified, as long as the turbulence level of the flow field is sufficiently large.

6.5.2 Influence of d_J/d_M on the mass transfer rate

In Chapter 5.5.1.2 it was experimentally verified that the nozzle to mixing tube diameter ratio had an influence on the mass transfer coefficient of the ejector. For no swirl device present, the experiments have shown that there exists an optimum d_N/d_M-ratio of 0.38-0.40. Model calculations show that d_J/d_M has a significant effect on the local energy dissipation rate within the mixing shock region (V_{Mz}). The influence of the d_J/d_M ratio on the calculated values of the mixing zone length, the specific energy dissipation, energy dissipation rate and the mass transfer characteristics ($k_L$and a) are shown in Figs. 6.8 (a) and (b).

Figure 6.8 A and B show that d_J/d_M has a significant effect on the local energy dissipation rate and consequently on the local $k_L$and a-values in the mixing zone. Further, it is seen that there exists an optimum value at a d_J/d_M -ratio of approximately 0.40, which is in agreement with the experimental observations of Chapter 5.5.1.2. These model calculations show that the actual d_J/d_M -ratio at the plunging point is of crucial importance

for the local k_La-values in the mixing zone and consequently also for of the overall mass transfer characteristics/ performance of ejectors.

Another illustration of the influence of d_J/d_M on the local mass transfer characteristics of the mixing zone is shown by the experimental results with and without a swirl device, as presented in Fig. 6.7. This figure shows that the ejector without a swirl device creates k_La-values which are approximately twice as high as with a swirl device, although the d_N/d_M-ratio and the overall power input to the ejector are similar. The reason is that the swirl device forces the jet to disintegrate relatively fast. Thus with a swirl device the actual jet diameter at the point of impact is wider in comparison to the jet without a swirl device. The d_N/d_M ratio used in the experiments was 0.41. Thus, for no swirl device, the d_J/d_M-ratio at the plunging point is only slightly higher than 0.41, whereas with a swirl device the d_J/d_M-ratio at the plunging point is much larger than 0.41, resulting in a decrease of the local k_La-value in the mixing zone (see Fig. 6.8 (b)). The main conclusion to be drawn from both the theoretical and the experimental observations is, that the ratio of the actual jet to mixing tube diameter is of crucial importance for the local volumetric mass transfer coefficient in the mixing zone.

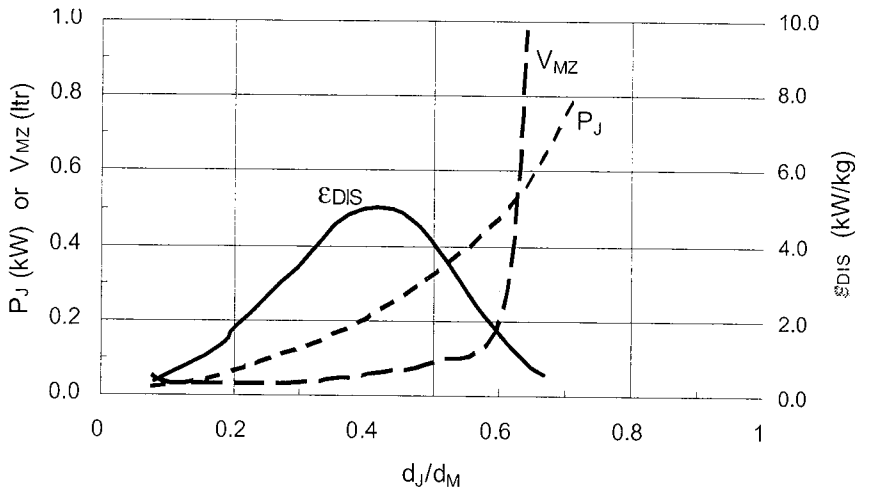

6.8(a) Influence of the d_J/d_M ratio on the calculated values of the mixing zone volume, the specific energy dissipation and the energy dissipation rate

This indicates that the mass transfer performance of ejectors should not be related to ejector dimensions like d_N/d_M, as is the custom in all-existing literature, but must be related to the actual jet diameter at the plunging point.

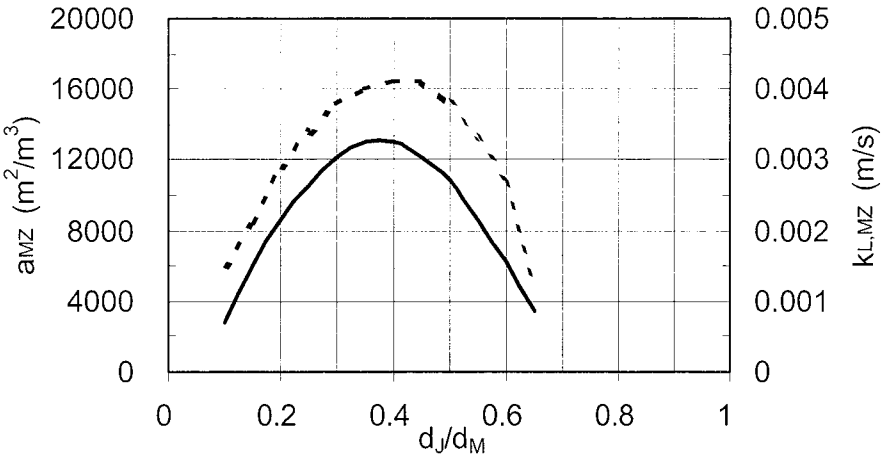

Fig. 6.8(b) Influence of the d_J/d_M ratio on the calculated values the local mass transfer characteristics (k_L and a) in the mixing zone.

6.5.3 Influence of the mixing tube length on the mass transfer rate

In Chapter 5.5.1.3 it was shown that the mass transfer characteristics of ejectors improved when longer mixing tubes were used. It was observed, that for a longer mixing tube (L_M/d_M=10), the mixing shock was nearly completed within the mixing tube of the ejector.

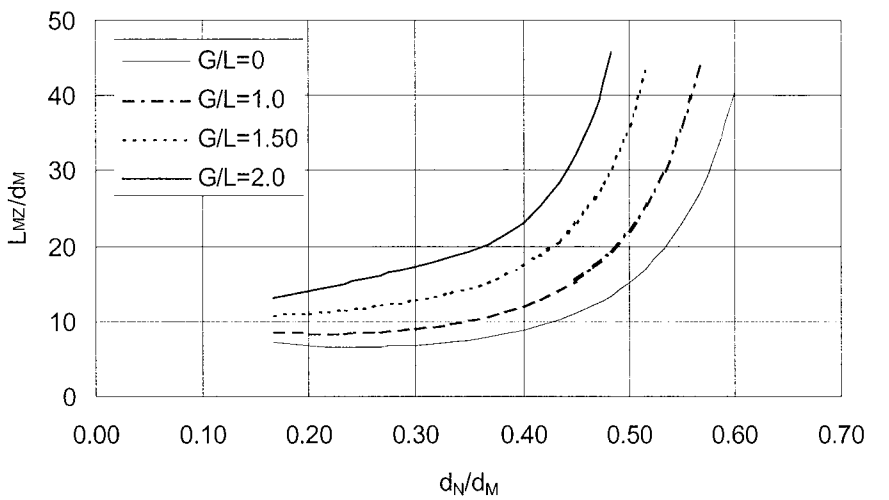

Fig. 6.9 Influence of d_N/d_M and Q_G/Q_L on the calculated L_M/d_M-ratio.

The influence of d_N/d_M and Q_G/Q_L on the calculated mixing zone length to mixing tube diameter ratio (L_{MZ}/d_M) is shown in Fig. 6.9. It shows that the L_{MZ}/d_M increases with

increasing d_N/d_M and Q_G/Q_L . The increase in mixing zone length with Q_G/Q_L is obvious since ΔP_{MZ} is a function of Q_G/Q_L, as shown in Chapter 3. Combining Eqs. (6.13) and (6.22) shows $L_{MZ} \approx (\Delta P_{MZ})^{-1}$.

From Fig. 6.9 it follows that for straight tube ejectors or Henzler types of ejectors (with diffuser), the optimum L_M/d_M-ratio is approx. 20 when using a d_N/d_M ratio between 0.3 and 0.4. Under these conditions the mixing zone region is completed within the mixing tube of the ejector, provided Q_G/Q_L is in the range between 1.5 and 2.

6.5.4 Effective mixing zone contribution

In Fig. 6.10, the effective contribution of the mixing zone section, $(V_{MZ}/V_{EJ})\cdot(k_La)_{MZ}$, to the overall k_La-value of the ejector is shown. The curves shown are the predicted values from the model. It shows that the effective mixing zone contribution is approximately 40 %.

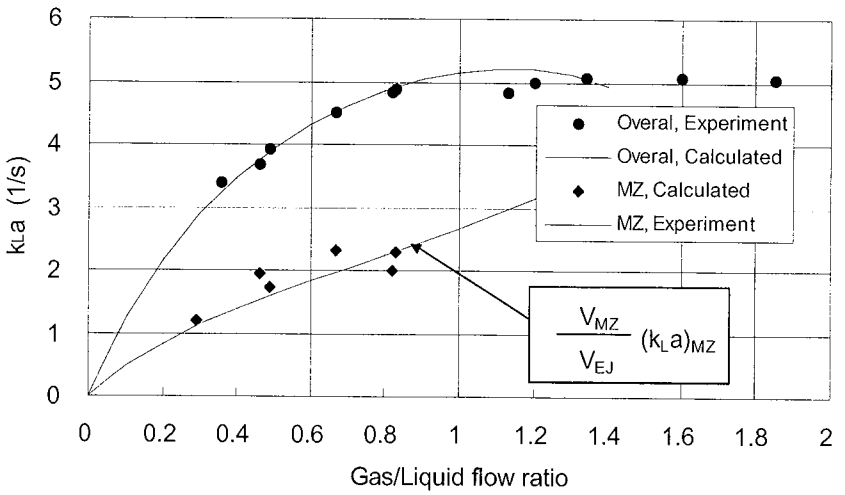

Fig. 6.10 Effective contribution of the mixing zone section to the overall k_La value of the straight tube ejector

From these observations it follows that for a proper design and modelling of gas-liquid ejectors, the mixing zone and the two-phase flow zone should be modelled as two different units in series. The overall k_La-value of the ejector is given by

$$(k_La)_{EJ} = \frac{V_{MZ}}{V_{MZ} + V_{BFZ}} \cdot (k_La)_{MZ} + \frac{V_{BFZ}}{V_{MZ} + V_{BFZ}} \cdot (k_La)_{BFZ} \tag{6.28}$$

indicating that the volume ratio of both zones has a significant effect on the overall mass transfer characteristics of ejectors. In the (scarce) literature only overall k_La-values of

ejectors have been reported for variety of ejector geometries (various d_N/d_M, L_M/d_M, straight tube ejectors or ejectors with diffusers, nozzles with and without swirl device, etc.), indicating that the volume ratio of both zones varied significantly. Given the variety of ejector configurations used, it is not surprising that the constants of the k_La correlations proposed in the open literature do not agree, because of this lumping of the mixing and two phase flow zone mass transfer rates.

6.6 CONCLUSIONS

The experiments showed that it is essential to consider the mixing zone and the bubble flow zone in ejectors as a system of two separate units in series, each requiring separate modelling. Further, the phenomena occurring in ejectors should be related to the actual jet diameter at the impact position (d_J/d_M), instead of the ejector configuration (d_N/d_M). In the literature overall k_La-values of ejectors are reported only, for a variety of ejector geometries (various d_N/d_M, L_M/d_M, straight tube ejectors or ejectors with diffusers, nozzles with and without swirl device, et.), indicating that the volume ratio of both zones varied significantly. Given this variety of ejector configurations used, it is not surprising that the constants of the k_La correlations proposed in the open literature do not agree, since the mixing and the two phase flow zone mass transfer rates were lumped together.

For designing straight tube ejectors or Henzler type of ejectors (with diffuser), the optimum L_M/d_M-ratio is approx. 20 when using a d_N/d_M ratio smaller or equal to 0.4. Under these conditions, the mixing zone region is completed within the mixing tube of the ejector. With respect to maximum mass transfer the optimum d_J/d_M ratio is between 0.38 and 0.42.

From the experimental results it is also concluded that the use of a swirl device has several advantageous results, i.e. stabilisation of the mixing zone position and improvement of the maximum gas suction rates. However, it was also shown that ejectors with a swirl device create lower k_La-values, relative to nozzles without swirl device.

NOTATION

a	specific interfacial area	(m^2/m^3)
b	area ratio $(d_N/d_M)^2$	(-)
C_X	constant in Eq. 6.3	(-)
C_T	Crayer-Curtet number (Eq. 6.21)	(-)
D_L	diffusion coefficient	(m^2/s)
d_S	Sauter bubble diameter	(m)
d_J	liquid jet diameter	(m)
d_M	mixing tube diameter	(m)
d_N	nozzle diameter	(m)
e	specific energy dissipation term in Eq. (6.5)	(m^2/s^2)
Eu	Euler number	(-)
f	friction factor	(-)
k_L	mass transfer coefficient	(m/s)
k_{ML}	friction loss coefficient in mixing zone	
L_M	mixing tube length	(m)
L_{MZ}	mixing zone length	(m)
P	pressure	(Pa)
P_1	pressure before mixing shock	(Pa)
P_2	pressure after mixing shock	(Pa)
ΔP_{MZ}	pressure difference across mixing zone	(Pa)
Q_e	volumetric flow rate inside re-circulating eddy	(m^3/s)
Q_G	volumetric gas flow rate	(m^3/s)
Q_L	volumetric liquid flow rate	(m^3/s)
Re	Reynolds number	
R_M	mixing tube radius	(m)
t_i	interaction time of bubbles	(s)
t_C	coalescence time of bubbles	(s)
U_e	velocity of re-circulating eddy	(m/s)
U_G	superficial gas velocity	(m/s)
U_J	actual jet velocity	(m/s)
U_L	superficial liquid velocity	(m/s)
U_N	jet velocity at nozzle exit	(m/s)
V_{MZ}	mixing zone volume	(m^3)
V_{BFZ}	bubble flow zone volume	(m^3)
We	Weber number	(-)
z	length	(m)
β	angle	
$\in$	energy dissipation rate	(W/kg)

ε_G	gas fraction	
ν_L	kinematic liquid viscosity	m^2/s
ρ_G	gas density	kg/m^3
ρ_L	liquid phase density	kg/m^3
σ	surface tension	N/m
τ	turbulent stresses	N/m^2

References

Barchillon M. and Curtet R. (1964),
Journ. Basic Eng., Vol. 86, 777-787

Barnea T. (1987),
Int. J. Multhiphase Flow, 13, 1-13

Bhat, P.A., Mitra A.K. and Roy, A.N. (1972),
Can. J. Chem. Eng., 50, 313-317.

Bhutada, S.R. and Pangarkar, V.G. (1989),
Chem. Eng. Sci., 10, 2384-2387.

Bin A.K. (1988),
VDI Forschungsheft, 648, 1-36

Bin A.K. (1988),
Chem. Eng. Sci., 43, 379-389

Biswas, M.N., Mitra, A.K. and Roy, A.N. (1975)
2th Symposium on jet pumps & ejectors and gas lift techniques,
March 24th-26th, E3 27-42.

Brahim, A.B., Prevost, M. and Bugarel, R. (1984),
Int. J. Multiphase Flow, 10, 79-94.

Bracco et al. (1982)
Trans ASME, Vol. 89, pp 62-97

Brown and Pitt (1972)
Chem. Eng. Sci., 27, 577-583

Calabrese R.V., Chang T.P.K. and Dang P.T. (1986)
AIChEJ, 32, 657-666

Changfeng X., Renjie L. and Gance D. (1991),
Chem. React. Eng. Technol., 7, 143-149

Cramers P.H.M.R., van Dierendonck L.L. and Beenackers A.A.C.M. (1992),
Chem. Eng. Sci., 47, 2251-2256.

Cramers P.H.M.R., Beenackers A.A.C.M. and van Dierendonck L.L. (1992),
Chem. Eng. Sci., 47, 3557-3564.

Cramers P.H.M.R., Leuteritz G., van Dierendonck L.L. and Beenackers A.A.C.M. (1993),
Chem. Eng. J., 53, 67-73.

Cramers P.H.M.R., Duveen R.F, .Beenackers A.A.C.M. and van Dierendonck L.L. (1994),
Catalysis in Multiphase Reactors European Symposium, Lyon, France, 7-9 December, Paper C-III-4.

Cramers P.H.M.R., Beenackers A.A.C.M. and Dierendonck van L.L. (1996),
The 5th World Congress of Chemical Engineering, San Diego, ASU, July 14-18, Vol. 3, 202-207.

Cramers P.H.M.R. and Beenackers A.A.C.M. (2001),
Chem. Eng. J., 3770, 1-11

Cunningham R.G. (1974),
Trans ASME – J. Fluids Engng, 96 (3), 203-215

Cunningham R.G. and Dopking R.J. (1974),
Trans ASME – J. Fluids Engng, 96 (3), 216-226

Curtet R. and Ricou F.P. (1964)
J. Basic Eng., 86, 735-742

Davies and Mitra (1966)
Chem. Eng. J., 36, 141-154

Deckwer, W.D. and Schumpe, A. (1987),
Int. Chem. Eng., 27, 405-422.

Deckwer, W.D. and Schumpe, A. (1993),
Chem. Eng. Sci., 48, 889-911.

Dierendonck van L.L., Meindersma G.W. and Leuteritz G.M. (1988),
6th European Conference on Mixing, Pavia, Italy, 24-26 May, 287-295

Dirix C.A.M.C. and Wiele van der K. (1990),
Chem. Eng. Sci., 45(8), 2333-2340.

Dutta N.N. and Raghavan K.V: (1987),
Chem. Eng. J., 36, 111-121

Engel M.O. (1963),
Proc. Instn. Mech. Engrs., 177 (13), 347-362

Evans G.M. (1990),
PhD-Thesis, University of Newcastle, N.S.W.

Greenwood T.S. (1986),
Chemistry and Industry, Feb. 3th

Havelka P., Linek V., Sinulke J., Zahradnik J. And Fialova M. (1997),
Chem. Eng. Sci., 52 (11) , 1701-1713

Havelka P., Linek V., Sinulke J., Zahradnik J. And Fialova M. (2000),
Chem. Eng. Sci., 55 , 535-549

Hesketh R.P., Etchells A.W. and Russel T.W.F., (1987)
AIChE Journal, 33(4), 663-667

Henzler, H.J. (1981),
VT < Verfahrenstechnik >>, 15, 738-749.

Hikita, H., Asai, S., Tnigawa, K., Segawa, K. and Kitao, M. (1980),
Chem. Eng. J., 20, 59-67.

Hikita, H., Asai, S., Tnigawa, K., Segawa, K. and Kitao, M. (1981),
Chem. Eng. J., 21, 61-69.

Hinze J.O. (1955),
AIChE Journal, 1(3), 289-295

Jekat, H. (1975),
PhD-thesis, Munchen, Germany.

Jekat H. and Pilhofer T. (1975)
VT Verfahrenstechnik, Vol. 11, 572-577

Kastner L.J. and Spooner J.R. (1950),
Proc. Instn. Mech. Engrs., 162 (2), 149-166

Kawase Y. and Moo-Young M. (1990)
Chem. Eng. J., 43, B19-B41

Kumagai M. And Endoh K. (1982)
J. Chem. Eng. Japan, 15, 427-433

Kumagai M. And Endoh K. (1983)
J. Chem. Eng. Japan, 16, 74-75

Kumagai M. And Endoh K. (1983)
J. Chem. Eng. Japan, 16, 357-363

Laats M.K. and Frishman, (1971)
Fluid Dyn., 8, 304-320

Leuteritz G.M., Reimann P. and Vergères P. (1976),
Hydrocarbon Processing, 99-100

Levich V.G. (1962),
Physicochemical Hydrodynamics, Englewood Cliffs, Prentice Hall, New York

Lewis D.A. and Davidson J.F. (1982)
Trans. Inst. Chem. Eng., 60, 283-291

Lin T.J. (1963),
Ph.D. Thesis, Wayne State University, Detroit, Michigan, United States

Lin T.J. and Donnely H.G. (1966),
AIChE J, Vol. 12, 563-571

Liu C. and Barkelew C.H. (1986)
AIChE J, Vol. 32, 1813-1820

Malone R.J. (1982),
Chem. Eng. Prog., 76 (6), 53-59

McCarthy M.J. (1972),
PhD-Thesis, University of Newcastle, N.S.W.

McCarthy M.J. and Molloy N.A. (1974),
Chem. Eng. J., 7, 1-20

McKeogh E.J. and Ervine D.A. (1981),
Chem. Eng. Sci., Vol. 36, 1161-1172

Nagel O., Kürten H., Hegner B. and Sinn R. (1970),
Chem. Ing. Techn., 42 (7), 474-479

Nagel O., Kürten H., Hegner B. and Sinn R. (1970),
Chem. Ing. Techn., 42 (14), 921-926

Nagel O., Kürten H. and Sinn R. (1972),
Chem. Ing. Techn., 44 (6), 367-373

Nagel O., Kürten H. and Sinn R. (1972),
Chem. Ing. Techn., 44 (14), 899-903

Nagel O., Kürten H. and Sinn R. (1973),
Chem. Ing. Techn., 45 (14), 913-920

Nagel O., Kürten H. and Sinn R. (1976),
Chem. Ing. Techn., 48 (6), 513-519

Ogawa s., Yamaguchi H., Tone S. and Otake T., (1982),
J. Chem. Eng. Japan, 15 (6), 469-474

Ogawa s., Yamaguchi H., Tone S. and Otake T., (1983),
J. Chem. Eng. Japan, 16 (5), 419-425

Ohkawa A., Shiokawa Y., Sakai N. and Endoh K. (1985)
J. Chem. Eng. Japan, 18, 172-174

Ohkawa A., Shiokawa Y., Sakai N. and Imai H. (1985)
J. Chem. Eng. Japan, 18, 466-469

Ohkawa A., Kusabiraki D., Kawai Y., Sakai N. and Endoh. (1986)
Chem. Eng. Sci., 41, 2347-2361

Ohkawa A., Kawai Y., Kusabiraki D., Sakai N. and Endoh. (1987)
J. Chem. Eng. Japan, 20, 99-101

Otake T., Tone S., Kuboi R., Takahashi T. and Nakap R. (1981),
Int. Chem. Eng., 21 (1), pp 72-80

Ozturk, S.S., Schumpe, A. and Deckwer, W.D. (1987),
AIChE J., 33, 1473-1480.

Palmer M. and Musketh M. (1984)
Proc. Second Int. Conf. on Mult. Phase Flow, 16(4), 327-333

Radharkrishnan and Mitra (1984)
Can. J. Chem. Eng., April, 170-178

Ranz W.E. (1958),
Can. J. Chem. Eng., August, 175-181

Reitz R.D. and Bracco F.V. (1982),
Phys. Fluids, Vol. 25, No. 10, 1730-1742

Reitz R.D. and Bracco F.V. (1986),
Encyclopedia of Fluid Mechanics, Vol. 3, 233-249

Rylek M. and Zahradnik J. (1984),
Collection Czechosloval Chem. Commun. , 49, 1939-1948

Sene K.J. (1988),
Chem. Eng. Sci., Vol. 43, 2615-2623

Sheridan A.T. (1966),
Nature, 209, 799-800

Sridhar, T. and Potter, O.E. (1980),
Chem. Eng. Sci., 25, 683-695.

Sridhar, T. and Potter, O.E. (1980),
Ind. Eng. Chem. Fundam, 19, 21-26.

Taylor G.I. (1940),
The Scientific Papers, Vol. 3, 244-254

van de Sande E. (1974),
PhD-Thesis, University of Delft, Netherlands

van de Sande E. and Smith J.M. (1973),
Chem. Eng. Sci., Vol. 28, 1161-1168

van de Sande E. and Smith J.M. (1976),
Chem. Eng. Sci., Vol. 31, 219-224

Walter J.F. and Blanch H.W. (1986)
Chem. Eng. J., 32, B7-B17

Wammes, W.J.A. and Westerterp, K.R. (1990),
Chem. Eng. Sci., 45, 2247-2254.

Wilkinson, P.M. and van Dierendonck, L.L., (1990),
Chem. Eng. Sci., 45, 2309-2315.

Wilkinson, P.M. (1991),
PhD-thesis, University of Groningen, The Netherlands.

Witte J.H. (1969)
J. Fluid Mech., 36 (4), 639-655

Wong C.W., Yeh M.C. and Cgang C.L. (1985)
J. Chin.I.Ch.E., 16(4), 327-335

Wu K.J., Su C.C., Steinberger R.L., Santavicca D.A. and Bracco F.V. (1983),
Trans ASME, Vol. 105, 406-413

Zahradnik J., Kastanek F., Kratchovil J. and Rylek M. (1982),
Collect. Czech. Chem. Commun. , 47, 1939-1949

Zahradnik J. and Kratchovil J. and Rylek M. (1985),
Collect. Czech. Chem. Commun. , 50, 2535-2544

Zahradnik J. and Kratchovil J. and Rylek M. (1991),
Collect. Czech. Chem. Commun. , 56, 619-635

Zhang S.H., Yu S.C. and Su Y.F. (1985)
Can J. Chem. Eng, 63, 212-226

Zhu M.Z., Hannon J. and Green A. (1992),
Chem. Eng. Sci., 47, 2847-2852

Dankwoord

Aan de tot standkoming van dit proefschrift (gedurende 4 jaar onderzoek bij het DSM Research laboratorium te Geleen in samenwerking met Buss AG in Zwitzerland)) hebben velen (van Groningen tot Geleen en Basel) bijdragen geleverd, die ik gaarne wil bedanken. Een aantal van hen wil ik hier met name noemen.

Mijn grote waardering geldt wijlen Prof. Laurent van Dierendonck en wijlen Prof. Ton Beenackers voor het in mij gestelde vertrouwen en voor de wijze waarop beiden mijn onderzoek hebben begeleid en de ruime mate van zelfstandigheid waarmee ik binnen DSM Research laboratorium en Buss AG aan het onderzoek heb mogen werken. Veel dank ben ik aan hun verschuldigd. De kritische en stimulerende discussies met zowel Laurent als Ton heb ik zeer gewaardeerd. Helaas hebben zowel Laurent als Ton de uiteindelijke versie van dit proefschrift niet meer mogen meemaken. Desalnietemin zullen de "insiders" de schrijfstijl van zowel Laurent en Ton in dit proefschrift terugvinden.
Veel dank ben ik ook verschuldigd aan Prof. Leon Janssen voor het in mij gestelde vertrouwen en voor de laatste suggesties en de snelle manier waarop hij mijn proefschrift heeft afgerond.

Peter Wilkinson, mijn collega promovendus binnen het DSM Research laboratorium, ben ik zeer erkentelijk voor zijn algehele steun tijdens het onderzoek.De stimulerende discussies met hem heb ik zeer gewaardeerd.

Tevens wil ik Leo Smit, Ton Bongers, Gert Clement en Stan Mutsers bedanken voor de waardevolle ondersteuning vanuit de zijde van DSM research. Gunther Leuteritz en Daniel Hariri wil ik bedanken voor de waardevolle ondersteuning vanuit de zijde van de toenmalige Buss AG.

Een zeer belangrijke bijdrage aan dit proefschrift hebben de studenten geleverd die hun afstudeerwerk op onderdelen van het onderzoek hebben uitgevoerd. Mijn erkentelijkheid gaat uit naar Miklas Dronkers, Gertjan Hartholt, Sander Riedstra, Cees Bleek, Menko Plaggenborg, Hans van der Valk en Peter Wolfs. Ook zij hebben met hun afstudeeronderzoek uitgevoerd bij DSM een grote bijdrage geleverd..

Tenslotte wil ik mijn kinderen Stan & Mitch en Diana en mijn ouders bedanken voor hun algemene steun "langs de lijn" en het stimuleren tot het voltooien van dit proefschrift.

Dankwoord

Aan de tot standkoming van dit proefschrift (gedurende 4 jaar onderzoek bij het DSM Research laboratorium te Geleen in samenwerking met Buss AG in Zwitzerland)) hebben velen (van Groningen tot Geleen en Basel) bijdragen geleverd, die ik gaarne wil bedanken. Een aantal van hen wil ik hier met name noemen.

Mijn grote waardering geldt wijlen Prof. Laurent van Dierendonck en wijlen Prof. Ton Beenackers voor het in mij gestelde vertrouwen en voor de wijze waarop beiden mijn onderzoek hebben begeleid en de ruime mate van zelfstandigheid waarmee ik binnen DSM Research laboratorium en Buss AG aan het onderzoek heb mogen werken. Veel dank ben ik aan hun verschuldigd. De kritische en stimulerende discussies met zowel Laurent als Ton heb ik zeer gewaardeerd. Helaas hebben zowel Laurent als Ton de uiteindelijke versie van dit proefschrift niet meer mogen meemaken. Desalnietemin zullen de "insiders" de schrijfstijl van zowel Laurent en Ton in dit proefschrift terugvinden.
Veel dank ben ik ook verschuldigd aan Prof. Leon Janssen voor het in mij gestelde vertrouwen en voor de laatste suggesties en de snelle manier waarop hij mijn proefschrift heeft afgerond.

Peter Wilkinson, mijn collega promovendus binnen het DSM Research laboratorium, ben ik zeer erkentelijk voor zijn algehele steun tijdens het onderzoek.De stimulerende discussies met hem heb ik zeer gewaardeerd.

Tevens wil ik Leo Smit, Ton Bongers, Gert Clement en Stan Mutsers bedanken voor de waardevolle ondersteuning vanuit de zijde van DSM research. Gunther Leuteritz en Daniel Hariri wil ik bedanken voor de waardevolle ondersteuning vanuit de zijde van de toenmalige Buss AG.

Een zeer belangrijke bijdrage aan dit proefschrift hebben de studenten geleverd die hun afstudeerwerk op onderdelen van het onderzoek hebben uitgevoerd. Mijn erkentelijkheid gaat uit naar Miklas Dronkers, Gertjan Hartholt, Sander Riedstra, Cees Bleek, Menko Plaggenborg, Hans van der Valk en Peter Wolfs. Ook zij hebben met hun afstudeeronderzoek uitgevoerd bij DSM een grote bijdrage geleverd..

Tenslotte wil ik mijn kinderen Stan & Mitch en Diana en mijn ouders bedanken voor hun algemene steun "langs de lijn" en het stimuleren tot het voltooien van dit proefschrift.